MAY 1959 VOLUME 4 (1959) No. 4

GREGG M. SINCLAIR LIBRARY
UNIVERSITY OF HAWAII
8-7-63

NUCLEAR INSTRUMENTS & METHODS

A JOURNAL ON ACCELERATORS, INSTRUMENTATION AND TECHNIQUES IN NUCLEAR PHYSICS

EDITOR: K. SIEGBAHN - UPPSALA

CONTENTS

E. GATTI and V. SVELTO, Theory of time resolution in scintillation counters 189
W. MÜLLER und J. REMBSER, Überlegungen zum Bau eines Wendellinearbeschleunigers für Protonen 202
TAGE SUNDSTRÖM and SVEN SVENNERSTEDT, An experimental study of the linear pinch stability 213
U. FACCHINI, E. GATTI and F. PELLEGRINI, A new method for track angle measurement in a gridded ionization chamber 221
G. W. HUTCHINSON, W. H. WELLS AND D. H. WHITE, Fast scaling circuits 228
P. S. DUBBELDAM, C. C. JONKER and F. J. HEEMSKERK, Measurement of the polarization of D–D neutrons by a solenoid 234
K. RAMAVATARAM and D. I. PORAT, Measurement of surface density of thin foils 239
J. SANDSTAD, Regularizing action of scalers (Letter to the Editor) 243
Erratum 244
Book review 244

NORTH-HOLLAND PUBLISHING COMPANY - AMSTERDAM

NUCLEAR INSTRUMENTS AND METHODS

A journal on accelerators, instrumentation and techniques in nuclear physics

EDITOR: K. SIEGBAHN, UPPSALA

EDITORIAL BOARD:

J. B. ADAMS (CERN)
F. A. ALSINA (Buenos Aires)
E. AMALDI (Rome)
H. L. ANDERSON (Chicago)
K. T. BAINBRIDGE (Cambridge, Mass.)
C. J. BAKKER (CERN)
P. R. BELL (Oak Ridge)
R. E. BELL (Montreal)
A. BERTHELOT (Saclay)
H. BRINKMAN (Groningen)
S. DE BENEDETTI (Pittsburgh)
M. DE HEMPTINNE (Louvain)
A. DE-SHALIT (Rehovoth)
M. DEUTSCH (Cambridge, Mass.)
S. DU TOIT (Pretoria)
B. S. DŽELEPOV (Leningrad)
W. GENTNER (CERN)
P. C. GUGELOT (Amsterdam)
H. HALBAN (Paris)
O. HAXEL (Heidelberg)
P. HUBER (Basel)
D. J. HUGHES (Brookhaven)
S. KIKUCHI (Tokyo)
J. KOCH (Copenhagen)
M. S. KOZODAEV (Moscow)
S. LIVINGSTON (Cambridge, Mass.)
E. M. MCMILLAN (Berkeley)
M. G. MEŠČERJAKOV (Moscow)
P. B. MOON (Birmingham)
M. L. OLIPHANT (Canberra)
W. PAUL (Bonn)
A. S. RAO (Bombay)
G. SALVINI (Rome)
P. SAVIĆ (Belgrade)
P. SCHERRER (Zürich)
CH. SCHMELZER (CERN)
H. W. B. SKINNER (Liverpool)
R. TANGEN (Oslo)
D. TAYLOR (Harwell)
V. I. VEKSLER (Moscow)
O. WERNHOLM (Stockholm)
G. VON DARDEL (CERN)
R. R. WILSON (Cornell)
S. D. WINTER (Saclay)

INSTRUCTIONS FOR CONTRIBUTORS

Contributions may be sent to the Editor, Professor K. Siegbahn, Institute of Physics, University of Uppsala, Sweden, either directly or through the intermediation of one of the members of the Editorial Board. Contributions may be written in English, French or German but should always, except for very short papers, be supplied with a brief abstract in English. Figures should be in inked original drawings or glossy prints and they should be sufficiently large. Contributors should make sure that important details in drawings and photographs will show up clearly in the diminished copy used by the publisher.

Books for review should be sent to Professor Siegbahn.

Objective and descriptive material on endeavours and product developments from the industry for the section "Spotlight on Industry" should be sent directly to the publishers, North-Holland Publishing Company, P.O. Box 103, Amsterdam.

Nuclear Instruments and Methods is published monthly. The subscription price of a volume of 360 pages is $ 17.00 (130 s), postage free.

Subscriptions should be sent to the publishers, North-Holland Publishing Company, P.O.Box 103, Amsterdam or to any subscription-agent.

No part of this issue may be reproduced in any form, by print, photoprint, microfilm or any other means without written permission from the publisher. Reprints, photoprints or microfilms are obtainable at cost from the publisher.

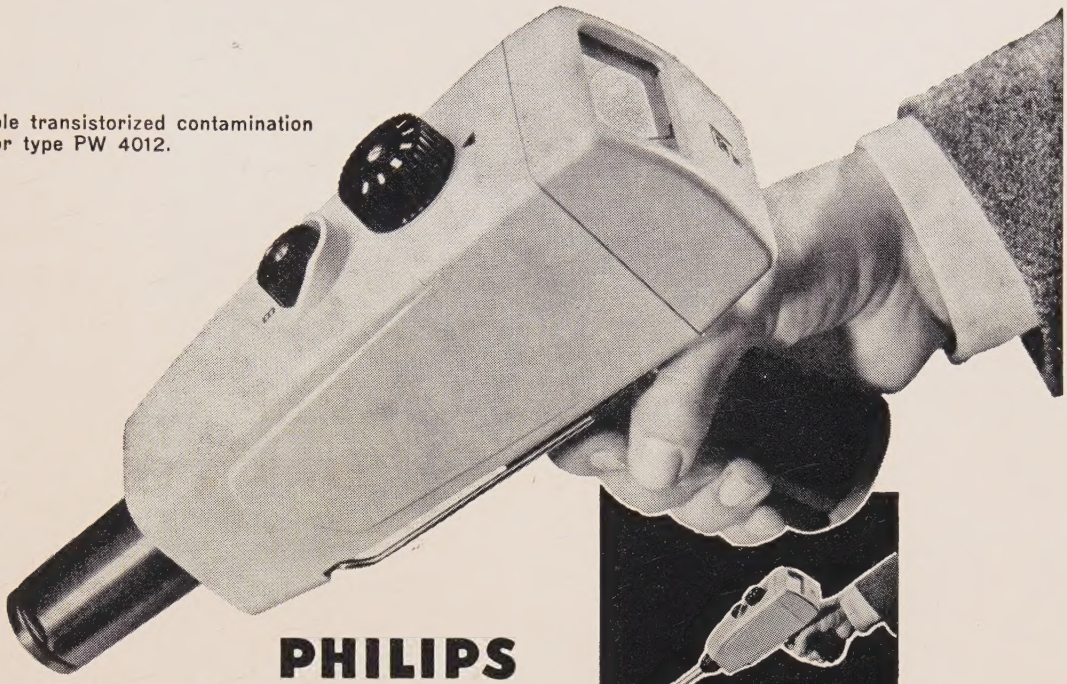

Portable transistorized contamination monitor type PW 4012.

PHILIPS

equipment for Nuclear Physics and Atomic Energy

This rugged, watertight and tropicallized battery-operated instrument incorporating the Philips G.M. counter tube type 18503 has been designed for the detection and measurement of radio-activity in such applications as:

- General radiation intensity checks in isotope laboratories, around isotope containers etc.
- Contamination checks of benches and apparatus.
- Radiation exposure measurements of personnel working with isotopes or X-rays.

It incorporates the following features:

- Three measuring ranges resp. 0-1, 0-10 and 0-100 mr/h (Ra γ).
- Compensation for voltage drop during battery life ensures maintenance of accuracy.
- Provision to insert probe extension.
- Beta sensitive G.M. tubes 18504 (2-3 mgr/cm^2) and 18505 (1.5-2 mgr/cm^2) can be used as well.
- Large, easy readable and shock-proof measuring instrument.

PW 4012
with probe extension.

- Synchro-cyclotrons for various final energies.
- Cockcroft-Walton accelerators.
- Generators for very high d.c. voltages.
- Linear electron accelerators.
- Reactor control instrumentation
- Radiation measuring and detection equipment.
- Civil defence instruments.
- Area monitoring instrumentation.
- Geiger counter tubes.
- Photomultipliers.
- Radio-active isotopes.
- Air & gas liquefiers.

PHILIPS

Nuclear Equipment

For further information please apply to:

N.V. PHILIPS' GLOEILAMPENFABRIEKEN,
Scientific Equipment Department, Eindhoven-Holland
RESEARCH & CONTROL INSTRUMENTS LTD.,
Instrument House, 207/215, King's Cross Road, London WC 1

PHILIPS

NDO

These names make NUCLEAR POWER

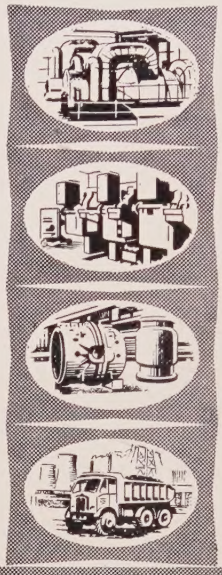

C. A. PARSONS & COMPANY LTD.

A. REYROLLE & COMPANY LTD.

HEAD, WRIGHTSON & COMPANY LTD.

SIR ROBERT McALPINE & SONS LTD.

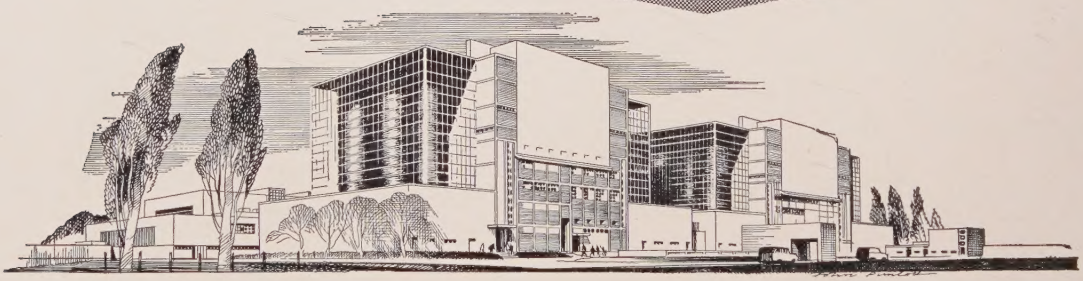

Bradwell, Essex, has leapt into fame as the site of the first commercial nuclear power station in the world to be built by N.P.P.C. Eight names make The Nuclear Power Plant Company Limited. N.P.P.C. thus combines the resources of eight specialist companies whose individual skills are co-ordinated to form a unified team capable of undertaking the construction of complete nuclear power stations throughout the world.

Bradwell nuclear power station will have a guaranteed output of 300 Megawatts. It is being built by The Nuclear Power Plant Co. Ltd. for the Central Electricity Generating Board.

WHESSOE LTD.

STRACHAN & HENSHAW LTD.

ALEX. FINDLAY & COMPANY LTD.

CLARKE, CHAPMAN & COMPANY LTD.

A Greater Britain through Nuclear Power

NPPC

THE NUCLEAR POWER PLANT COMPANY LIMITED · BOOTHS HALL · KNUTSFORD · CHESHIRE · ENGLAND

TGA NP3/

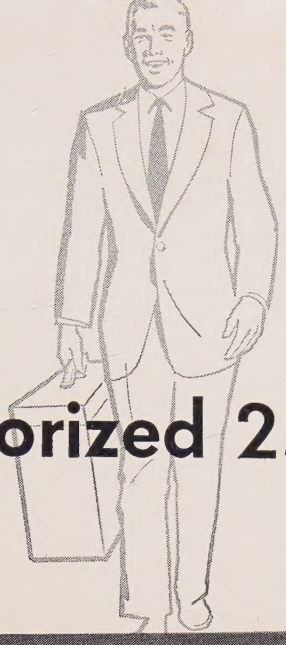

- *only 8¾" high*
- *uses interchangeable plug-in logic units*
- *provides complete versatility and portability*

. . . A Transistorized 256-Channel Pulse Analyzer

MODEL CN-110
256-CHANNEL ANALYZER
WITH PLUG-IN MODEL 210
PULSE HEIGHT ANALYZER UNIT

THE BASIC CN-110 IS THE MEMORY containing all the elements for complete magnetic core data storage — memory current drive, cycle control binaries, address and arithmetic binaries, power supplies, etc.

PLUG-IN LOGIC UNITS make several different analyzers available in the time it takes to interchange units. Standard plug-in units are available for Pulse Height Analysis, Time of Flight Measurements, Count as a Function of Time; units for special programs can be built to order.

CARRY THE SYSTEM TO THE OPERATION — the completely transistorized Model CN-110 weighs only *40* lbs. (including logic unit), and is only *8¾"* high. It is easily carried by one person to any location. With auxiliary readout system, total weight is approximately 100 lbs. — over 1500 lbs. less than equivalent systems using vacuum tubes.

NO COOLING PROBLEMS — the complete use of transistors in the Model CN-110 reduces heat dissipation — air conditioning or bulky blowers are not required; total power less than 10 watts.

MANY TYPES OF READOUT may be used — analog . . . binary . . . octal and decimal. Data can be recorded on strip chart or X-Y recorders . . . printed paper tape . . . magnetic computer tape . . . punched paper tape . . . punched cards. The Model 220 *Decimal Converter,* available as an accessory, is designed specifically for use with the CN-110. It includes a paper tape printer which prints channel number and count number on the same line (with 3-space separation). During the counting period, the Model 220 also functions as a live time indicator and automatic dead time corrector.

/rite for complete data on the Model N-110 and standard plug-in logic units. For etails on custom logic units and data eadout programmers, outline your specific equirements.

TMC **TECHNICAL MEASUREMENT CORPORATION**

441 WASHINGTON AVE., NORTH HAVEN, CONN.

Société d'Applications Industrielles de la Physique
S. A. I. P.
38, rue Gabriel Crié - MALAKOFF (Seine)

NUCLEAR PHYSICS

50-CHANNEL KICKSORTER "SA 50"

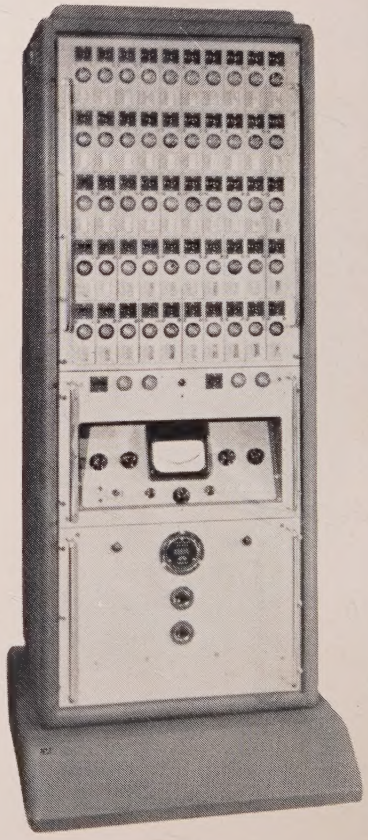

- Resolution: 1 millisecond.
- Maximum counting rate 10,000 c/sec. At high counting rates, the dead time correction is well defined throughout, and the spectrum will not undergo any deformation.
- Indication on a 1 : 10 scale, with interchangeable scales.
- For the integration, the graduation is in hundreds; for the last channel, graduation is in thousands.
- Release circuit for coincidence measurements of spectra.

OTHER PRODUCTS:

Single-channel kicksorters
Scalers
Scintillation spectrometers
Proportional counters
Circulation counters
Pressurised ionisation chambers
Linear amplifiers
Vibrating condensator type D.C. amplifiers
Automatic sampling dispensers.

AGENTS:

BELGIUM:	DRUA, 205 Avenue Van Volxem, BRUSSELS
DENMARK:	LANGEBAEK & SON, Trondhjemsgade 9, COPENHAGEN
NETHERLANDS:	ENRAF-EVERSHED, Van Leeuwenhoeksingel 69, DELFT
ITALY:	AMPERE, Via Felice Casati 8, MILAN
FINLAND:	ISOTEKNO, 13 A Mikontaku, HELSINKI
JAPAN:	RIKEI TRADING C°, Kosato Building, 12-4 Chome Shiba Tamura-Cho Minato-Ku, TOKYO
SWITZERLAND:	A. MAGAT, 28, rue de Vermont, GENEVA
U.S.A.:	LEVIANT, 239 Broadway, N.Y. 7., NEW YORK

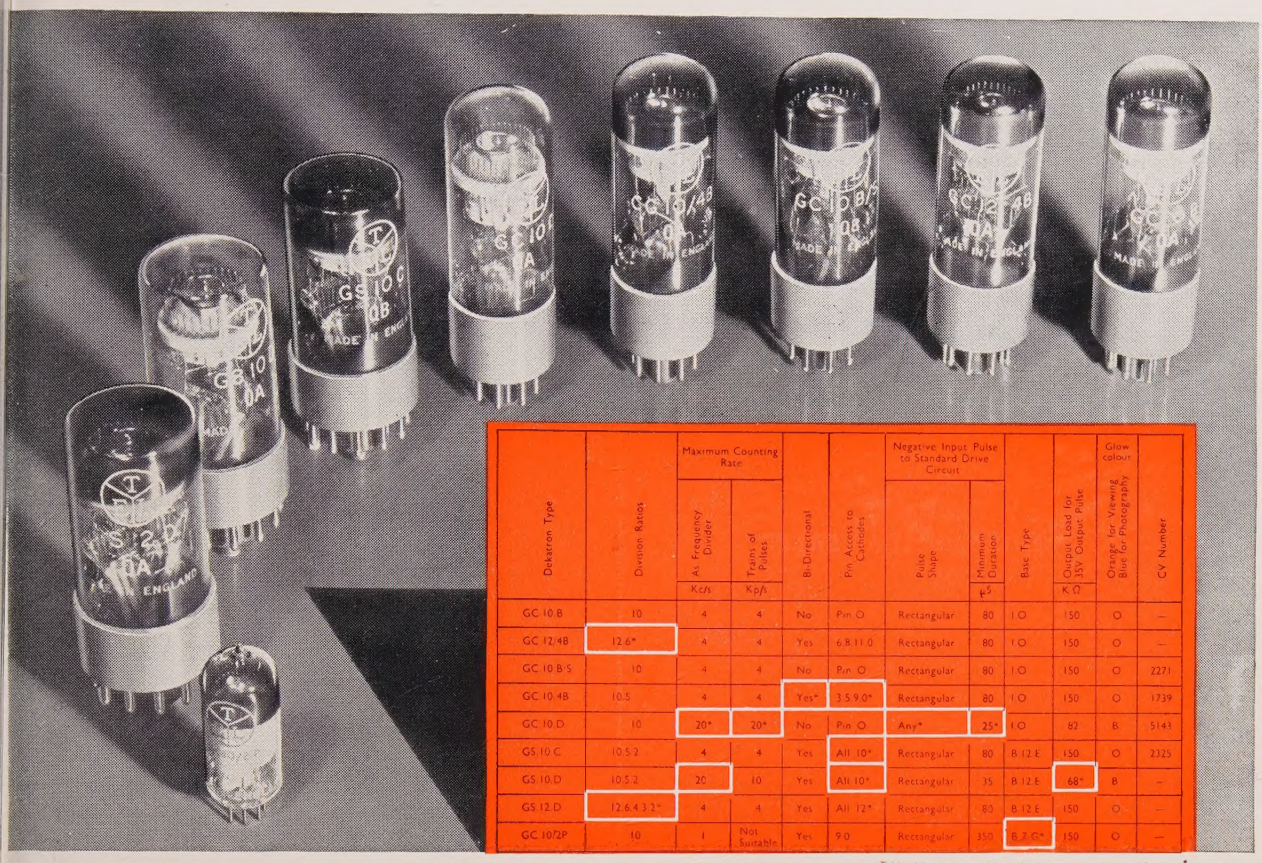

Dekatron Type	Division Ratios	Maximum Counting Rate: As Frequency Divider (K c/s)	Maximum Counting Rate: Trains of Pulses (K p/s)	Bi-Directional	Pin Access to Cathodes	Negative Input Pulse to Standard Drive Circuit: Pulse Shape	Negative Input Pulse to Standard Drive Circuit: Minimum Duration (μ sec)	Base Type	Output Load for 35V Output Pulse (K Ω)	Glow colour: Orange for Viewing, Blue for Photography	CV Number
GC 10.B	10	4	4	No	Pin O	Rectangular	80	1 O	150	O	—
GC 12/4B	12.6*	4	4	Yes	6.8.11.0	Rectangular	80	1 O	150	O	—
GC 10.B/S	10	4	4	No	Pin O	Rectangular	80	1 O	150	O	2271
GC 10.4B	10.5	4	4	Yes*	3.5.9.0*	Rectangular	80	1 O	150	O	1739
GC 10.D	10	20*	20*	No	Pin O	Any*	25*	1 O	82	B	5143
GS 10.C	10.5.2	4	4	Yes	All 10*	Rectangular	80	B 12 E	150	O	2325
GS 10.D	10.5.2	20	10	Yes	All 10*	Rectangular	35	B 12 E	68*	B	—
GS 12.D	12.6.4.3.2*	4	4	Yes	All 12*	Rectangular	80	B 12 E	150	O	—
GC 10/2P	10	1	Not Suitable	Yes	9.0	Rectangular	350	B 7 G*	150	O	—

Table showing comparative characteristics and special features.*

DEKATRONS

The most comprehensive range of glow-transfer scaling tubes in the world

FEATURES INCLUDED IN THIS RANGE

- BI-DIRECTIONAL COUNTING ◀
- SPEEDS UP TO 20,000 COUNTS PER SEC. ◀
- ONLY RANGE TO INCLUDE 10 OR 12 CATHODE TUBES ◀
- ACCESS TO ONE, FOUR OR ALL CATHODES ◀
- NO SHAPING OF INPUT WAVEFORM NECESSARY ◀

Described as the most significant advance in the technique of slow and medium speed counting during the last decade, Dekatron scaling tubes have logged hundreds of thousands of unfailing working hours. Leading manufacturers of counting, timing and measuring instruments prefer these reliable tubes because they allow simplified circuitry, replace a number of thermionic tubes, operate at low current, dissipate negligible heat and are moderately priced.
Available in decade and duo-decade types, the Dekatron is the original and the leading counting tube for superior performance.
Are *you* taking full advantage of the economy, long life and versatility of these cold-cathode scaling tubes?

If you would like more information please write to:—

THE TECHNICAL SERVICES DEPT.,
TUBE DIVISION
BEESTON · NOTTINGHAM · ENGLAND

ETELCO

DEKATRON IS AN ETELCO TRADE MARK

ETELCO LIMITED, HEAD OFFICE: 22 LINCOLNS INN FIELDS LONDON, W.C.2. Telephone: HOLborn 6936

E115AR/93AR

ORIGINATORS AND SOLE MANUFACTURERS OF DEKATRON SCALING TUBES

INTERNATIONAL

advertise

YOUR NUCLEAR PRODUCTS IN

sell

YOUR NUCLEAR PRODUCTS

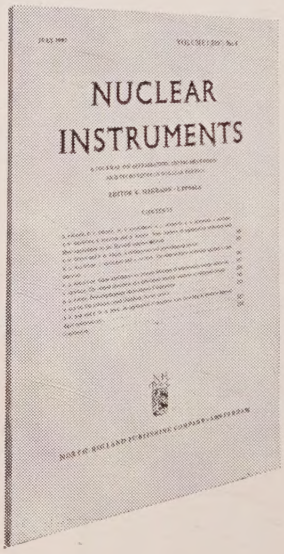

reap

YOUR NUCLEAR SALES
REWARDS

world wide

KEY NUCLEAR MANAGEMENT
NUCLEAR SCIENTISTS
NUCLEAR ENGINEERS
NUCLEAR PRODUCTION
PERSONNEL

SUBSCRIBE TO

you reach

THE WHOLE
NUCLEAR SALES WORLD IN

Entirely international in scope Nuclear Instruments and Methods is the one nuclear scientific journal that has an established subscription clientele throughout the whole world-where-ever nuclear men are at work—they want your nuclear products—they need your nuclear products—advertise in Nuclear Instruments and tell them WHAT – HOW – WHERE they can get your nuclear products

GO INTERNATIONAL WITH YOUR SALES PROGRAM TODAY WRITE

WILLIAM F. BAARS - ADVERTISING MANAGER NORTH-HOLLAND PUBLISHING COMPANY

P.O. BOX 103 – AMSTERDAM, HOLLAND

INTERNATIONAL

Announcing the Eldorado 4100

A Fast, Stable Pulse Height Analyzer

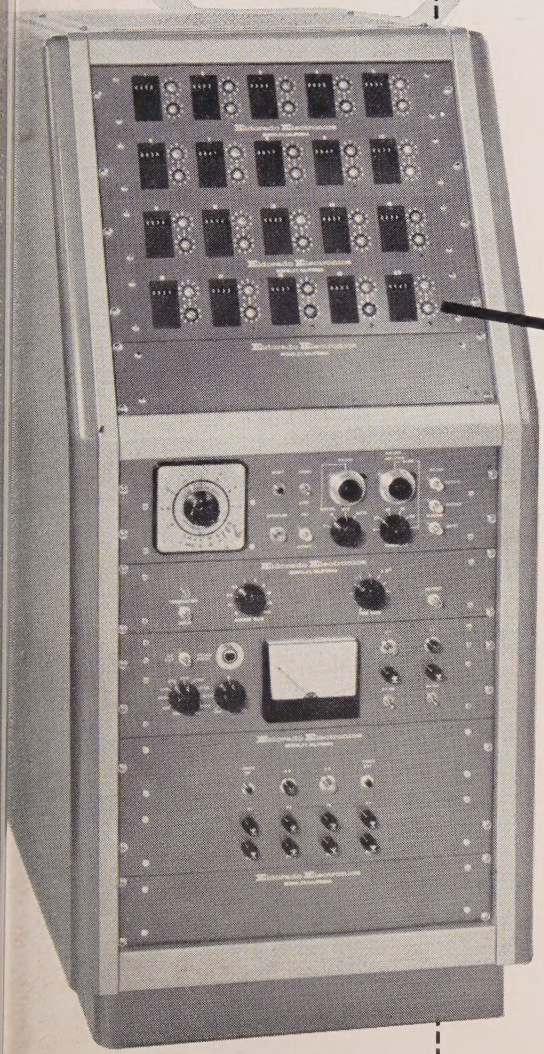

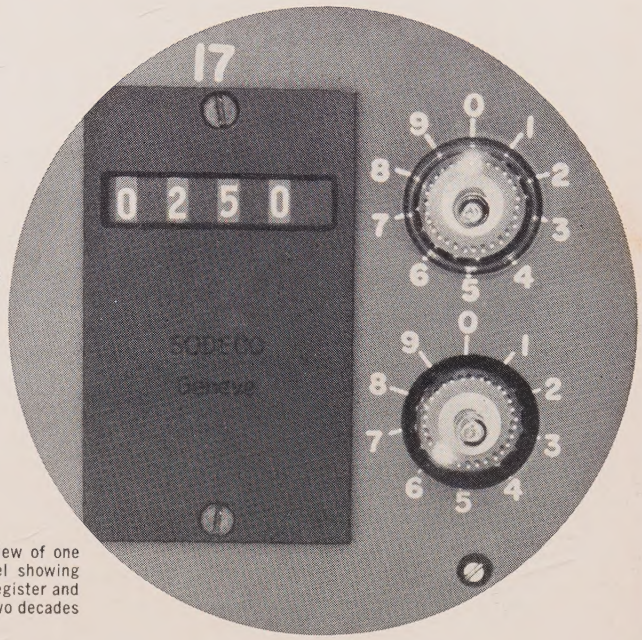

Full size view of one channel showing register and two decades

How Fast?

- ✻ Double pulse resolution better than 0.5 microseconds
- ✻ Dead time less than 0.1 microseconds
- ✻ Average counting rates greater than 10^5 counts per second without baseline distortion or use of temporary storage

How Stable?

- ✻ Channel width less than 1% drift per week
- ✻ Baseline less than 0.1% shift per week
- ✻ Channel triggering level unaffected by changes in input pulse width

For complete details, call your nearby Eldorado Engineering representative or write Dept. H3

ow in production, with 30 day delivery, the 100 is priced at $8950 f.o.b. Berkeley, Cali- rnia. Shown with optional LA-600 Linear mplifier and optional High Voltage ower Supply PS-530

RIEF SPECIFICATIONS

NUMBER OF CHANNELS	20
CHANNEL WIDTH	1.0V NOMINAL
SCALER CAPACITY	10^6 COUNTS/CHANNEL
INDOW AMPLIFIER INPUT	20V NOMINAL
WINDOW POSITION RANGE	5-105V

Eldorado Electronics

2821 TENTH STREET · BERKELEY 10, CALIFORNIA

Phone THornwall 1-4613

NORTH-HOLLAND BOOKS

ELECTROMAGNETIC ISOTOPE SEPARATORS AND APPLICATIONS OF ELECTROMAGNETICALLY ENRICHED ISOTOPES

By J. KOCH *(Editor)*,

R. H. V. M. DAWTON, M. L. SMITH and W. WALCHER

6 x 9″ xii + 314 pp. 156 illus. 53 s.

"This is a very welcome book on a subject which had its beginnings 24 years back, which has grown to undreamt of proportions during and after the war, and of which this is the first comprehensive monograph. It is written by a team of experts with first-hand experience in electromagnetic separators... it tells in a masterly way the fascinating "success story" of a physical instrument which has grown into a giant". (D. GABOR in *British Journal of Applied Physics*)

Sole Agency for U.S.A.:
Interscience Publishers Inc. New York
NORTH-HOLLAND PUBLISHING COMPANY
AMSTERDAM

FOR SCINTILLATION & PROPORTIONAL COUNTING
Non-overloading Linear Amplifiers
MODELS 108 and 108 p

* GAIN–40,000, continuously variable
* RISE TIME–0.2 microsecond
* ACCEPTS + AND — PULSES

Tremendous Dynamic Range
EXCEEDS 1,000,000 (0.1 mV to 100 V)

Excellent linearity for small pulses in the presence of tremendous overloads that paralyze other amplifiers.
Model 108 P includes precision trigger type Pulse-Height Selector.

Model 413 Mercury relay precision sliding Pulser

The **one** pulser that fills **every need** of the Nuclear Physics Laboratory
0 to 100 Volts

10 full scale ranges from 1 mV to 100 volts
Fast rise and exponential decay of 1, 3, 10. 30, and 100 microsec simulate pulses from scintillation, proportional and Geiger counters.
Incorporates both manual control and precision motor drive.
The ideal instrument for precise calibration and test of pulse-height analyzers and other nuclear instrumentation.

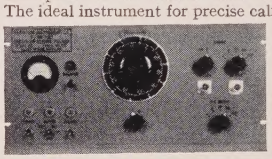

Window widths are determined AUTOMATICALLY, 10 × more ACCURATELY, 40 × FASTER than with conventional pulsers.

Model 108 Amplifier . . . . . $ **545.00**
Model 108 P Amplifier (includes pulse-height selector) $ **595.00**
Model 413 Precision Sliding Pulser . . . . . $ **630.00**
Prices f.o.b. Silver Spring. Md.

RADIATION INSTRUMENT CO.
P.O. BOX 733 SILVERSPRING, MARYLAND, U.S.A.

NORTH-HOLLAND BOOKS

Just out

Analytical and Canonical Formalism in Physics

by

ANDRÉ MERCIER

Head of the Department of Theoretical Physics, University of Berne

6 × 9″ VIII + 222 pages Guilders 20.00 (40 s.)

THE CONTENTS

i LAGRANGIAN FORMALISM
ii LAGRANGIAN DENSITY
iii CANONICAL FORMALISM
iv CANONICAL FORM OF ELECTRODYNAMICS
v HAMILTONIAN DENSITIES
vi TRANSFORMATIONS
vii CANONICAL FORMALISM WITH VANISHING JACOBIAN DETERMINANT

Sole Agency for U.S.A.: Interscience Publishers Inc. – New York

NORTH-HOLLAND PUBLISHING COMPANY — AMSTERDAM

RIDL *presents* . . . MODEL 50-9 X-RAY SCINTILLATION SPECTROMETER

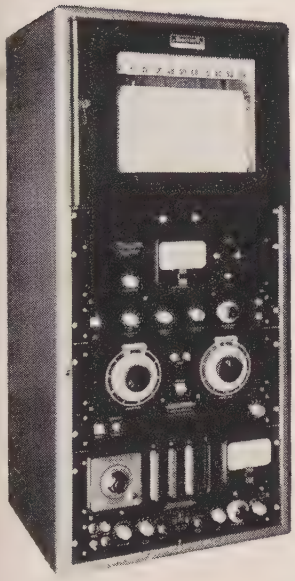

Now - for researchers who want the best, RIDL presents the all new Model 50-9 X-Ray Scintillation Spectrometer consisting of:

- Model 10-2 X-Ray Scintillation Counter
- Model 33-1 Single Channel Analyzer
- Model 35-5 Count Rate Meter
- Model 49-12 Scaler
- Two Second Brown ElectroniK Recorder

This system has been specifically designed for work in X-Ray detection and measurements and offers unexcelled performance and dependability.

The Model 10-7 is an optimum design, low noise, high speed counter especially suited for these applications. As shown in the above spectogram, the 6 KEV Barium L X-Ray from Cs^{137} is clearly resolved by this unit. The 10-7 may be obtained with mounting flanges for attachment to standard X-Ray Diffraction Systems. The unit includes a gain of 10 preamplifier, a selected photomultiplier tube and a specially fabricated, thin NaI (Tl) X-Ray crystal.

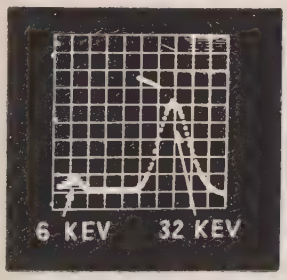

Use of the 50-9 offers greater facilities for research into areas such as measurements of X-Ray absorption coefficients, studies of crystalline structure, etc.

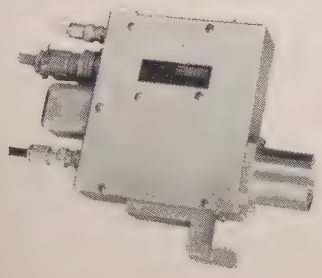

The Model 50-9 is just one of the many excellent instrument systems manufactured by RIDL. REMEMBER, whatever your instrumentation problem may be, RIDL has the solution. Our staff is always available to answer your inquiries. Write to Dept. RDS for complete information.

SEE US AT BOOTH NO. 707 AT THE ATOM-FAIR

RIDL INC.

Radiation Instrument Development Laboratory, Inc.

5737 South Halsted Street, Chicago 21, Illinois USA TRiangle 3-2345

Representatives in major cities

Versatile Research Accelerator

3-Mev Model K *Van de Graaff*

This powerful multi-particle accelerator — proved in the field — is the basic tool for a broad program of fundamental or applied radiation research.

Now in use for:

- Nuclear physics
- Radiation processing
- Polymerization
- Radiation chemistry
- Reactor engineering
- Sterilization
- Radiation damage
- Biology
- Particle injection
- Radiography

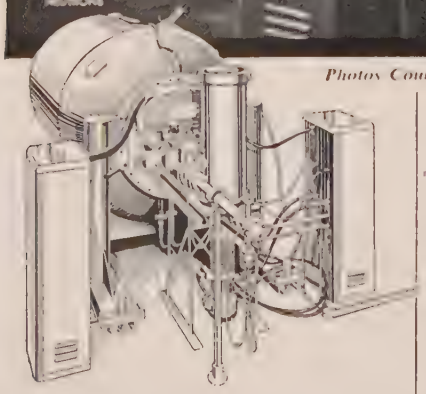

Photos Courtesy of Gulf Research and Development Company

The 3-Mev, Model K Van de Graaff can be furnished for horizontal installation as illustrated above.

ELECTRONS:
1 microampere to 1 milliampere. (Use of maximum current requires beam scanning).

X-RAYS:
900 R per minute at one meter. (Equivalent to 20,000 curies of Cobalt-60).

POSITIVE IONS:
10 to 200 microamperes.

NEUTRONS:
6×10^{11} neutrons per second.

Both voltage and current output are stable, precisely controlled, and continuously variable.

HIGH VOLTAGE ENGINEERING CORPORATION
BURLINGTON MASSACHUSETTS

HIGH VOLTAGE SERVICING CO. LTD.
60 Carpenter's Wood Drive
Chorley Wood, Rickmansworth, Herts ,Engl
Telephone Field End 7431

NUCLEAR INSTRUMENTS AND METHODS 4 (1959) 189–201; NORTH-HOLLAND PUBLISHING CO.

THEORY OF TIME RESOLUTION IN SCINTILLATION COUNTERS

E. GATTI† and V. SVELTO

C.I.S.E. *Laboratories, Milano*

Received 8 April 1959

Four methods of handling the output pulse current of a scintillation counter, for extracting time information, have been theoretically compared. Final graphs are given for the time resolution, which can be obtained with the four methods, as a function of parameters that describe the multiplier phototube and the scintillator.

1. Introduction

Recently a theory was developed by one of the Authors and other co-workers[1]) to ascertain the accuracy limits in the measurement of time intervals defined by scintillation counter pulses.

Recently we completed the theory by introducing a more approximate picture of the behaviour of the multiplier phototube†† and comparing four methods for using the output current pulses for time definition.

For reading without continuous reference to the previous work[1]), the whole theory is again given (briefly except for the new contributions).

We have to estimate the accuracy with which we can evaluate the time position of the interaction between a charged particle and the sensitive element of a scintillation counter. For this purpose, the chain of the processes leading to the detection of a particle is given below[2]):

1. Slowdown in the scintillator and excitation of optically active states, or direct emission of photons by Čerenkov effect.

2. Decay of the excited states and consequent emission of light.

3. Collection of light.

4. Emission of photoelectrons by the photocathode of the phototube.

5. Formation of the electronic cascade (avalanche).

6. Processing of the output current pulse of the phototube, by means of a suitable electronic instrument.

We shall overlook the details of processes 1, 2, 3, and take into account only their effect through the photocathode illumination function $I(t)$ which may be considered as a continuous function of time (a justified approximation as far as the photoelectron emission is concerned) in view of the low photoelectronic yield of 5–10%.

The illumination function $I(t)$ can be normalized as follows:

$$\int_0^\infty I(t)\,\mathrm{d}t = R$$

where R is the average number of electrons emitted as a consequence of a scintillation.

It is assumed that the photoelectron emission following a given illumination obeys the Poisson distribution, and so to Q electrons emitted in average we attribute the variance

$$Q\,(1 + \bar{r}\varepsilon_{rr}{}^2)$$

where $\bar{r}$ is the mean yield and $\varepsilon_{rr}{}^2$ is the relative variance of the photocathode yield (see Appendix I).

2. Multiplier Features

The essential properties of the electron multiplier are taken into account by representing

† Politecnico of Milano and C.I.S.E.

†† In this work we have followed, as far as possible, the standard terms related to phototubes as reported in the "counting note" CC5-8 of the Lawrence Radiation Laboratory, Berkeley.

[1]) S. Colombo, E. Gatti and M. Pignanelli, Nuovo Cimento 5 (1957) 1739.

[2]) E. Baldinger and W. Franzen, Advances in Electronics and Electron physics, Vol. 8 (1956) p. 255.

the response S.E.R. (Single Electron Response) to a photoelectron emitted by the photocathode with the following expression:

$$U(t) = A\, f(t,\lambda,h) = A\, \frac{\lambda_0}{\lambda} f\left[\frac{\lambda_0}{\lambda}(t - b) + h + b\right] \quad (1)$$

where A is the current amplification of the multiplier phototube with average value $\underline{A}$ and relative root-mean square error ε_A.

The variance $\varepsilon_A{}^2$ refers to the amplification A of individual photoelectrons (mainly due to fluctuation in multiplication at the first dynode) and is assumed[3,4] equal to:

$$\varepsilon_A{}^2 = \frac{1}{g - 1} \quad (2)$$

where g is the secondary emission factor, considered equal for all dynodes. Poisson statistics are used, which seems a reasonable assumption the accelerating voltage between dynodes, being of the order of 150 V[5]).

The function $f(t, \lambda, h)$ characterizes the S.E.R. and it is normalized thus:

$$\int_0^\infty f(t,\lambda,h)\, \mathrm{d}t = 1 \ ;$$

λ is the pulse width defined as the second moment of S.E.R.

$$\lambda^2 = \int_0^\infty (t - b)^2 f(t,\lambda,h)\, \mathrm{d}t$$

where b is the centroid of the S.E.R. It can be assumed that this width has the mean value:

$$\lambda_0{}^2 = (n - 1)\, \varepsilon_{\mathrm{dd}}{}^2 \quad (3)$$

where n is the number of dynodes including the collector, and $\varepsilon_{\mathrm{dd}}$ the root-mean square deviation of the delay time between two successive dynodes. λ has a relative variance (see Appendix II):

$$\varepsilon_{\lambda,\mathrm{r}}{}^2 = \frac{1}{(g - 1)\,(n - 1)^2}\left(1 + \frac{3}{2g}\right) \quad (3_a)$$

h is a statistical variable, having time dimension, with an average value 0 and a r.m.s. error $\varepsilon_{\mathrm{ph}}$. This variable accounts for the device time spread, and is the standard deviation of the time interval between the instant of emission of one photoelectron and the instant in which the centroid of the S.E.R. arrives at the output. The following variance (Appendix III) can be attributed to h:

$$\varepsilon_{\mathrm{ph}}{}^2 = \varepsilon_{\mathrm{cd}}{}^2 + \frac{\varepsilon_{\mathrm{dd}}{}^2}{g - 1}\left(1 + \frac{2}{g}\right) \quad (4)$$

where $\varepsilon_{\mathrm{cd}}$ is the cathode time spread, that is the standard deviation of the delay time of a photoelectron between the cathode and first dynode, and accounts for different delay times of electrons due to different initial velocities and different starting points.

In short, the phototube response to a photoelectron has been described with a standard wave shape S.E.R. containing three statistical parameters:

1. the multiplier factor A having relative variance $\varepsilon_A{}^2$;
2. the displacement term h having variance $\varepsilon_{\mathrm{ph}}{}^2$;
3. the pulse width λ having variance $\varepsilon_\lambda{}^2$.

Moreover, no non-linearity due to space charge saturation has been considered, nor has a spread in time decay of light from different points of the scintillator.

3. Pulse Processing

Now let us introduce four ways of processing the output pulse of the multiplier phototube, each of which involving a distinct definition of the occurrence time of an event, as "seen" by the timing instrument.

3.1.

In a first method (A), we suppose (see fig. 1), that the output current of the phototube $i(t)$ is integrated on the input capacity of an electronic sharp cut-off tube and that the relationship between the input voltage and the anode current i_{a} of the tube is linear until the cut-off is reached.

The anode current is applied to a high Q resonant circuit having a period larger than t_{f}, which is the time necessary to bring the tube to cut-off through the accumulation of a charge $C(t_{\mathrm{f}})$.

[3]) J. Sharpe, Nuclear Radiation Detectors (London, 1955), p. 105.

[4]) G. A. Morton, Proceedings Geneva Conference, Vol. **14** (1955) p. 255.

[5]) A. Van der Ziel, Noise (Prentice Hall, New York) p. 113.

For $t < t_i$, the current signal at the anode is

$$i_a(t) = K \int_0^t i(t)\, dt$$

while for $t > t_i$ the signal is a constant $KC(t_i)$.

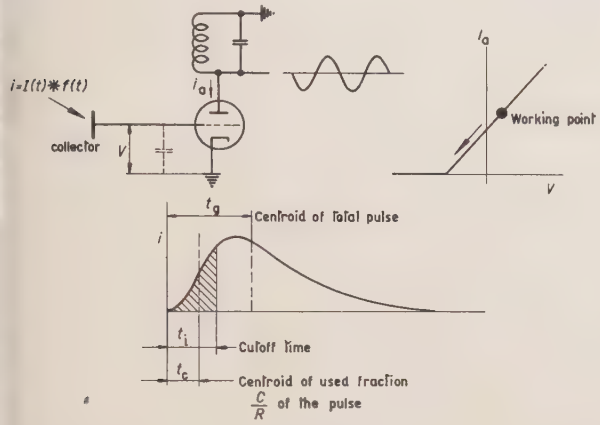

Fig. 1. Scheme for illustrating methods A, C, D of pulse processing.

If $i_a(t)$ is this function and $i_a(p)$ its Laplace transform, the voltage at the terminals of the resonant circuit is:

$$V(p) = Z(p) \cdot i_a(p) = Z(p) \cdot \frac{1}{p} \cdot \bar{i}\,(p) \qquad (5)$$

where $\bar{i}(p)$ is the transform of $\bar{i}(t)$ that is of $i(t)$ considered $= 0$ for $t > t_i$ and $Z(p)$ is the impedance of the resonant circuit.

From equation (5) it can be concluded that, except for a constant, the phase of the oscillation $V(t)$, which is equal to $\arg V(j\omega)$ is equal to $\arg \bar{i}(j\omega)$.

If we suppose that the instrument is sensitive to the oscillation phase considered at an instant t_0 given by an external time reference, we see that it will register the arrival of the pulse $i(t)$ at a time μ equal to:

$$\mu = \frac{1}{\omega} \arg \bar{i}\,(j\omega)\,. \qquad (6)$$

If, for the time being, $\bar{i}(p)$ is so normalized that

$$\int_0^\infty \bar{i}\, dt = 1$$

$\bar{i}(p)$ can be written as follows:

$$\bar{i}\,(p) = 1 - p \int_0^\infty t \cdot \bar{i}\,(t) \cdot dt + \tfrac{1}{2} p^2 \int_0^\infty t^2 \cdot \bar{i}\,(t) \cdot dt - \cdots . \qquad (7)$$

Moreover, if the period corresponding to the angular frequency ω of the resonant circuit is long with respect to the pulse width, it can be concluded from (7) that:

$$\arg \bar{i}\,(j\omega) = \omega \int_0^\infty t \cdot \bar{i}\,(t) \cdot dt\,. \qquad (8)$$

Therefore, the "machine time" is the centroid of current pulse $i(t)$. For such a method the problem is therefore reduced to that of determining the variance of the centroid of the current pulse $\bar{i}(t)$ following a scintillation. It was assumed that the phase is measurable with negligible error; this was experimentally proved. This method of working will be called briefly "fractional pulse centroid".

3.2.

We shall further deal with the case where cut-off charge $C(t_i)$ is never reached. This method (C) of working will be called "linear" and, in that case, instead of $\bar{i}(t)$, the whole pulse $i(t)$ will be used for the purpose of measurement. "Machine time" is the centroid of the whole pulse.

3.3.

A third case (D), in which the operation is again linear, but the oscillating circuit period not very long in comparison with the scintillation light pulse, has been examined; we shall call this method "non ballistic linear". The "machine time" is defined by (6).

3.4.

In another method (B) the "machine time" is defined as the time at which a definite charge C is collected at the output of the phototube. This theory was previously developed by several authors[6,7,8]), but they neglected the effect of width λ of the S.E.R.

The four introduced definitions of the "machine time" permit the straightforward deduction of the variances of the machine time from

[6]) R. Post and L. J. Schiff, Phys. Rev. **80** (1950) 1113.
[7]) G. Minton, Jour. Res. NBS **57** (1956) 119.
[8]) L. Beghian, G. Kegel and R. Scharemberg, Rev. Sci. Instr. **29** (1958) 753.

the statistical properties of photoelectron emission and electronic multiplication, account being also taken of the finite width λ of the S.E.R. and its statistical fluctuation.

It is important to take λ into account: in fact it is to be noted that the output due to one scintillation is the convolution of the illumination law $I(t)$ and the S.E.R. $f(t)$, that is the convolution of two pulses of comparable width (respectively τ and λ) in the case of fast scintillators. It is therefore meaningless to conceive the developed charge at the output as due to successive distinct contributions of the successively emitted photoelectrons. For instance in the "non linear" method the cut-off charge is reached with the contributions, with different weights, of the first, second, etc., photoelectron; these weights decrease to zero, passing from the first to the last photoelectron which contributes to the cut-off charge.

4. Resolution in the Case of Non Linear Working

"Machine time" is the centroid of used pulse fraction. A general law of illumination $I(t)$ of the photocathode was considered, while a response $U(t) = Af(t,\lambda,h)$ was considered for the phototube.

In the absence of statistical fluctuation $\underline{i}(t)$ would be given by:

$$\underline{i}(t) = I(t) * f(t) . \tag{9}$$

A statistical fluctuation corresponding either to ΔK electrons emitted in addition to the average, in the time between σ and $\sigma + \Delta\sigma$ or to an amplification $A(1 + \Delta K)$ relatively greater by ΔK than the average one for a certain electron emitted at time σ, brings the current to:

$$i(t) = I(t) * f(t) + \Delta K\, f(t - \sigma) \tag{10}$$

where with $f(t)$ it is denoted $f(t,\lambda,h)$ for $\lambda = \lambda_0$, $h = 0$.

The disturbance (considering ΔK to be positive for the sake of reasoning) has a double effect on the "machine variable" (for a more detailed deduction, reference is to be made to[1]): a direct effect due to the displacement of the centroid resulting from the presence of the disturbance current which, between σ and t_i, is different from zero, and an indirect effect due to the displacement of the cut-off time t_i; t_i is reached earlier because the charge $C(t_i)$ necessary to the cut-off is also reached by the contribution of the charge due to the disturbance current in the time interval between σ and t_i.

In fact, for the variance of the centroid due to the statistics of the emission and spread of the current gain A, we obtain by means of the procedure reported in[1]:

$$\varepsilon^2_{c,\mathrm{em},A} = (1 + \bar{r}\varepsilon_{rr}^2 + \varepsilon_A^2)\, \frac{\left[\int_0^{t_i} \mathrm{d}t \int_0^t f(t)\, \mathrm{d}t\right]^2 * I(t_i)}{\left[\int_0^{t_i} \underline{i}(t)\, \mathrm{d}t\right]^2} . \tag{11}$$

By a similar calculation[1], the variance of the centroid due to the fluctuation in the mean transit characterized by the variance ε_{ph}^2, is:

$$\varepsilon^2_{c,ph} = \varepsilon_{ph}^2\, \frac{\left[\int_0^{t_i} f(t)\, \mathrm{d}t\right]^2 * I(t_i)}{\left[\int_0^{t_i} \underline{i}(t)\, \mathrm{d}t\right]^2} . \tag{12}$$

The variance of λ adds the following contribution (Appendix IV):

$$\varepsilon^2_{c,\lambda} = \varepsilon_\lambda^2\, \frac{\left[\int_0^{t_i} (t - b)\, f(t)\, \mathrm{d}t\right]^2 * I(t_i)}{\left[\int_0^{t_i} \underline{i}(t)\, \mathrm{d}t\right]^2} \tag{13}$$

and finally, by summing up the variance due to the various effects considered we obtain:

$$\varepsilon_c^2 = \varepsilon^2_{c,\mathrm{em},A} + \varepsilon^2_{c,ph} + \varepsilon^2_{c,\lambda} . \tag{14}$$

By means of (14) ε_c^2 is expressed as a function of t_i, but for the purpose of experimental comparison, ε_c^2 must be expressed in terms of $C(t_i)$, that is the charge necessary for the cut-off.

C is a function of t_i and its average value is:

$$C(t_i) = \int_0^{t_i} [I(t) * f(t)]\, \mathrm{d}t . \tag{15}$$

Between (14) and (15), t_i can be eliminated and ε_c^2 can be expressed as a function of $C(t_i)$.

We assumed in the numerical calculation an illumination

$$I(t) = \frac{R}{\tau} \exp\left(-\frac{t}{\tau}\right) \tag{16}$$

and a phototube response

$$f(t) = \frac{\sqrt{m+1}}{\lambda \cdot m!} \left(\sqrt{m+1}\, \frac{t}{\lambda}\right)^m \exp\left(-\sqrt{m+1}\, \frac{t}{\lambda}\right)$$

with $m = 8$. (17)

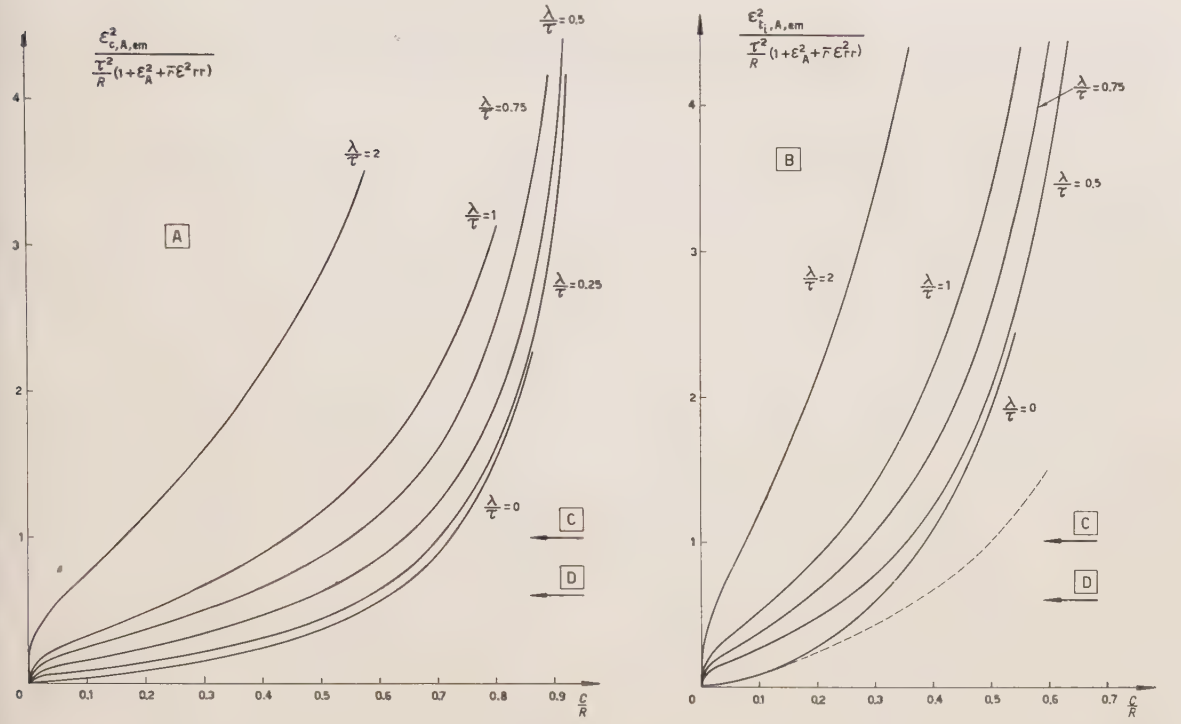

Fig. 2. "Machine time" variance due to statistical fluctuations in photoelectron emission, spread in photoelectric yield, spread in the current gain.

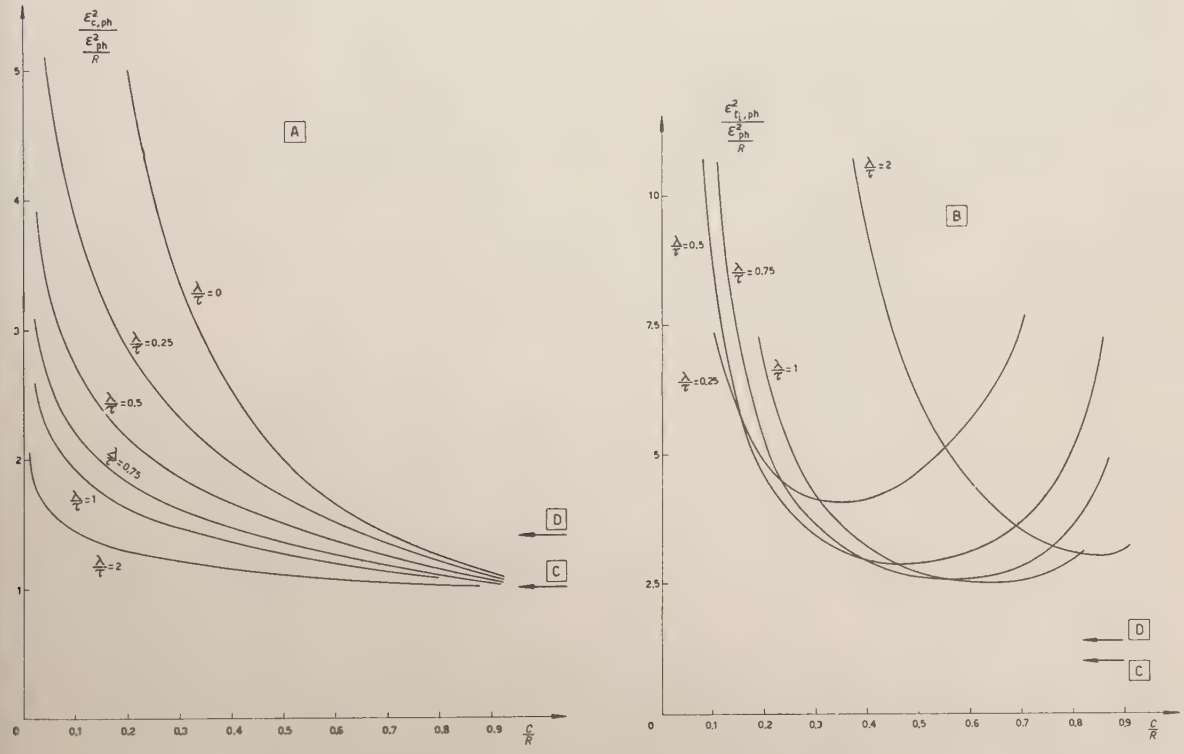

Fig. 3. "Machine time" variance due to spread in the device delay time.

The three contributions (11), (12), (13) to the variance are shown in the graphs A (figs. 2, 3, 4).

In the fig. 7, (15) is reported for our case.

We expect that (11) is not correct for the approximation made in deducing it, when the charge C collected to the time t_i is caused by the contribution of a few photoelectron pulses.

therefore cannot be drawn in a graph with the relative variables C/R and

$$\frac{\varepsilon^2_{c,\mathrm{em},A}}{\frac{\tau^2}{R}(1+\bar{r}\varepsilon_{rr}^2+\varepsilon_A^2)}$$

adopted.

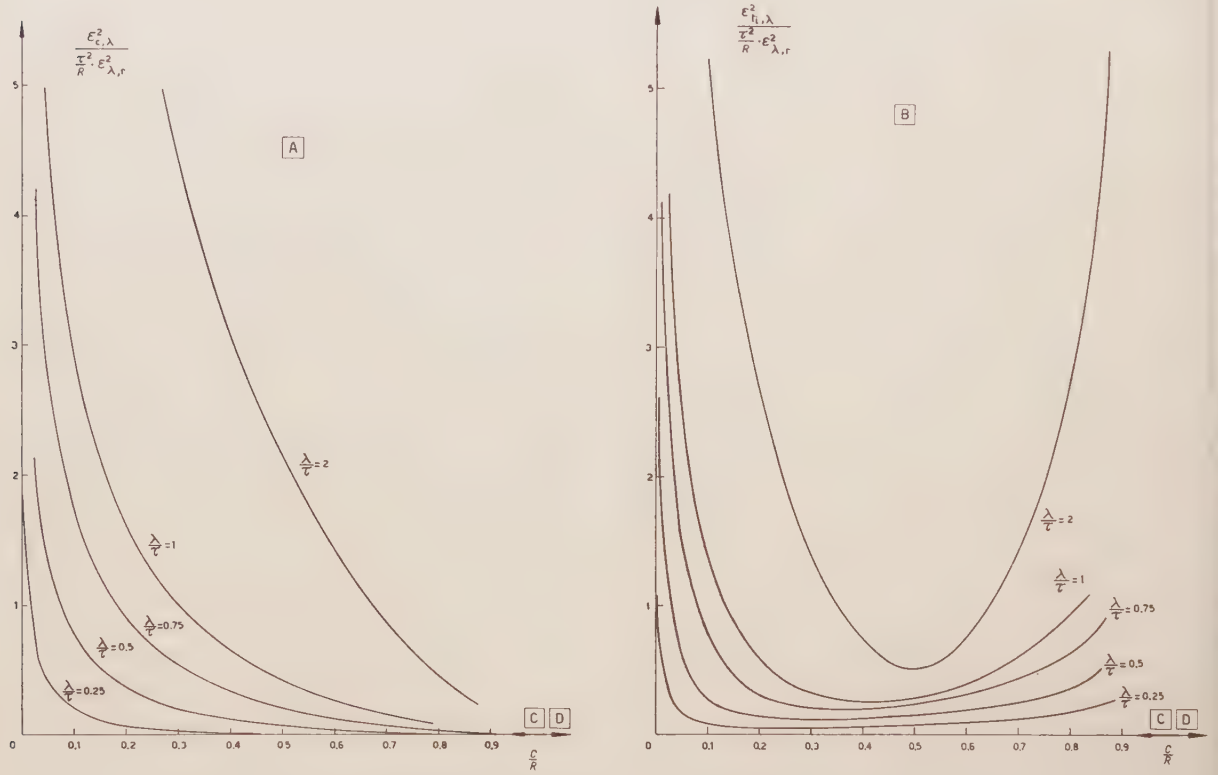

Fig. 4. "Machine time" variance due to spread in the S.E.R. width λ.

In fact for $\lambda = 0$ and constant illumination $I = R/\tau$, (11) gives:

$$(1+\bar{r}\varepsilon_{rr}^2+\varepsilon_A^2)\frac{1}{3}\frac{\tau^2}{R}\frac{C}{R}$$

to compare with:

$$(1+\bar{r}\varepsilon_{rr}^2+\varepsilon_A^2)\frac{1}{3}\frac{\tau^2}{R}\frac{C}{R}\left[1+\frac{3}{2C}+\frac{1}{2C^2}\right]$$

which represents the exact solution for $\lambda = 0$ and constant illumination[1]).

We can utilize this exact solution to correct (11); it should be noted that this correction cannot be shown in the graphs of fig. 2, inasmuch as the correction is dependent on C and

For $\lambda = 0$, (12) gives:

$$\varepsilon^2_{c,\mathrm{ph}} = \varepsilon^2_{\mathrm{ph}}/C$$

which is evidently the correct limit.

Finally, for $\lambda = 0$, (13), as expected gives no contribution.

5. Resolution for t_i as "machine time"

The calculation of the variance of time t_i in which a definite charge C is collected follows directly from formulas 2.6 and 3.3. of paper[1]) and (IV-4) of Appendix IV respectively, by summing up the variances caused by each illumination contribution $I(\sigma)\,\mathrm{d}\sigma$:

$$\varepsilon_{t_i}^2 = \frac{\int_0^{t_i} I(\sigma)\,\mathrm{d}\sigma \left\{ (1 + \bar{r}\varepsilon_{rr}^2 + \varepsilon_A^2) \left(\int_0^{t_i} f(t-\sigma)\,\mathrm{d}t \right)^2 + \varepsilon_{ph}^2 (f(t-\sigma))^2 + \varepsilon_\lambda^2 ((t-\sigma-b)\, f(t-\sigma))^2 \right\}}{[(It_i) * f(t_i)]^2}$$

or

$$\varepsilon_{t_i}^2 = I(t_i) * \frac{(1 + \bar{r}\varepsilon_{rr}^2 + \varepsilon_A^2) \left[\int_0^{t_i} f(t)\,\mathrm{d}t \right]^2 + \varepsilon_{ph}^2 [f(t_i)]^2 + \varepsilon_\lambda^2 [(t_i - b)\, f(t_i)]^2}{[I(t_i) * f(t_i)]^2} . \tag{18}$$

The first of the three terms of (18) gives for $\lambda = 0$:

$$(1 + \bar{r}\varepsilon_{rr}^2 + \varepsilon_A^2) \frac{\tau^2}{R} \frac{C/R}{(1 - C/R)^2} \tag{19}$$

which we can compare to the variance calculated by Post and Shiff[6]) for the occurrence time of the Cth photoelectron (for $\lambda = 0$, the collected charge C and the Cth photoelectron are equivalent concepts) which, with our symbols, becomes:

$$(1 + \bar{r}\varepsilon_{rr}^2 + \varepsilon_A^2) \frac{\tau^2}{R} \frac{C}{R} \left(1 + \frac{2(C+1)}{R} + \cdots \right).$$

The second of the three terms of (18) has no meaning with respect to $\lambda = 0$ and simple physical considerations show that in such a case the limit should have the value ε_{ph}^2.

At such limit is arrived at through formula (18), if rather than $\lambda = 0$ we consider a pulse width λ so chosen that at the interdiction time the pulse amplitude due to a photoelectron is equal to the mean current (this hypothesis is contained in the arguments which lead to the expression (18)).

As expected the third term of (18) gives no contribution for $\lambda = 0$.

6. Resolution in the Case of Ballistic Linear Working

In the case of "ballistic linear working" in which the total pulse of the current from the phototube is impressed on the oscillating circuit, possibly by means of a linear amplifier though not necessary very fast, the calculations are very simple because there is no more need to introduce the "response" $f(t)$ of the phototube with finite width, and it is enough to consider a response $A\delta(t + h)$ with h affected by a variance ε_{ph}^2 and A by a variance ε_A^2.

Moreover, a disturbance, in the form of an additional electron emitted between σ and $\sigma + \Delta\sigma$ for example does no more than displace the centroid by its very presence.

For details of the calculations, we refer to[1]).

ε_c^2 is given by:

$$\varepsilon_c^2 = \frac{1}{R} \left[(1 + \bar{r}\varepsilon_{rr}^2 + \varepsilon_A^2) \frac{1}{R} \int_0^\infty (\sigma - t_b)^2 I(\sigma)\,\mathrm{d}\sigma + \varepsilon_{ph}^2 \right] \tag{20}$$

and in accordance with the hypothesis of an illumination law given by

$$I(t) = \frac{R}{\tau} \exp\left(-\frac{t}{\tau} \right)$$

we obtain:

$$\varepsilon_c^2 = \frac{\varepsilon_{ph}^2 + \tau^2 (1 + \bar{r}\varepsilon_{rr}^2 + \varepsilon_A^2)}{R} . \tag{21}$$

7. Resolution in the Case of "non Ballistic Linear Working"

We call "non ballistic linear working" the case where the period T of the resonant circuit is not very long with respect to the duration of the light pulse. In this case the "machine variable" is defined with reference to (6) by;

$$\mu = \frac{1}{\omega} \arg i(j\omega) .$$

In Appendix V the variance was calculated, and we obtain (whatever S.E.R. may be):

$$\varepsilon_c^2 = \frac{\tau^2}{R} (1 + \bar{r}\varepsilon_{rr}^2 + \varepsilon_A^2) \frac{1 + 2\omega^2\tau^2}{1 + 4\,\omega^2\tau^2} + \frac{\varepsilon_{ph}^2}{R} \left(1 + \frac{2\,\omega^4\tau^4}{1 + 4\,\omega^2\tau^2} \right). \tag{22}$$

The results are formally the same as obtained in[1]), but they are again dealt with in Appendix V, where the useless hypothesis of $\lambda \ll T$ is discarded.

8. Conclusions

In figs. 2, 3 and 4 are shown the contributions to the variance of machine time respectively due to:

1. Statistical fluctuation in the photoelectron emission, spread in the photoelectric yield of different points of the photocathode, spread in the current gain of the phototube.

2. Statistical fluctuation in the device delay time.

3. Statistical fluctuation of the S.E.R. width λ. The curves refer to the cases in which the "machine time" is the:

$$\frac{\tau}{\varepsilon_{ph}} = 2 \quad \text{for instance} \quad \begin{cases} \tau = 10^{-9}\ \text{sec} \\ \varepsilon_{ph} = 5 \times 10^{-10}\ \text{sec} \end{cases}$$

and so figs. 5 and 6 were obtained.

The figures show that the minimum variance is reached with method A. The minima are very wide and their value does not change appreciably with λ.

The method B leads to greater variances.

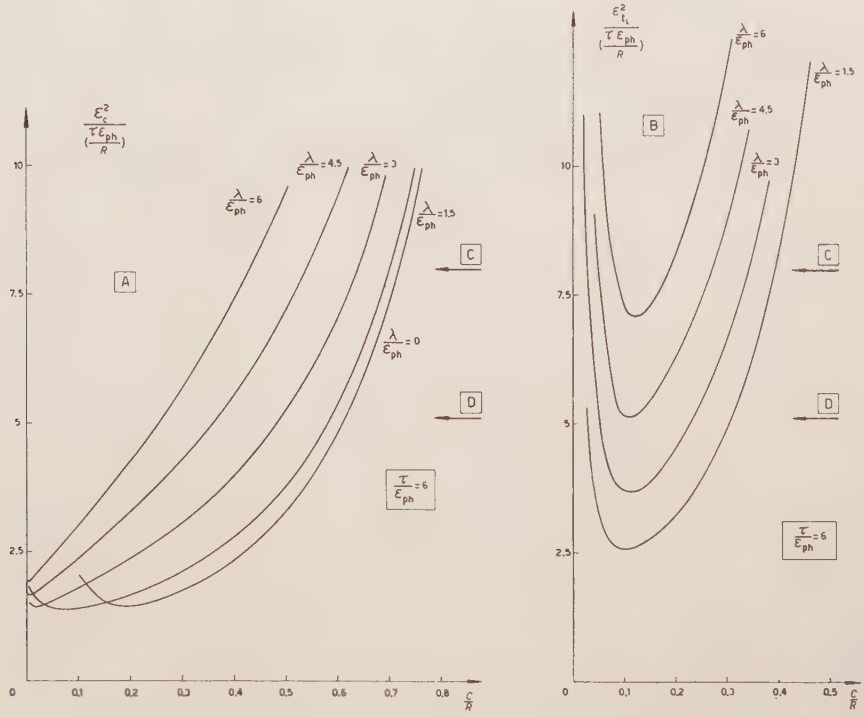

Fig. 5. Total "machine time" variance for the fixed parameter $\tau/\varepsilon_{ph} = 6$.

(A) Centroid of the used pulse fraction (centroid non linear).

(B) Time in which a definite charge C is collected.

(C) Centroid of the total pulse (ballistic linear).

(D) As defined in the non ballistic linear method with $\omega\tau = 1$.

We have added contributions 1, 2, 3 taking into account the weights corresponding to the choice of the values:

$$\frac{\tau}{\varepsilon_{ph}} = 6 \quad \text{for instance} \quad \begin{cases} \tau = 3 \times 10^{-9}\ \text{sec} \\ \varepsilon_{ph} = 5 \times 10^{-10}\ \text{sec}. \end{cases}$$

The minima are more dependent on λ and are very narrow against C/R.

Among the linear methods, the non ballistic (the value $\omega\tau = 1$ was considered) is better than the ballistic. The linear methods are inferior to the non linear ones, particularly for high τ/ε_{ph}.

For small τ/ε_{ph} (fast scintillators, Čerenkov counters) linear methods are advisable.

In the non linear methods, the "machine time" depends on C/R (which is not the case in the linear methods) and then, for a fixed value of C, on R, that is on the pulse amplitudes (see also fig. 7).

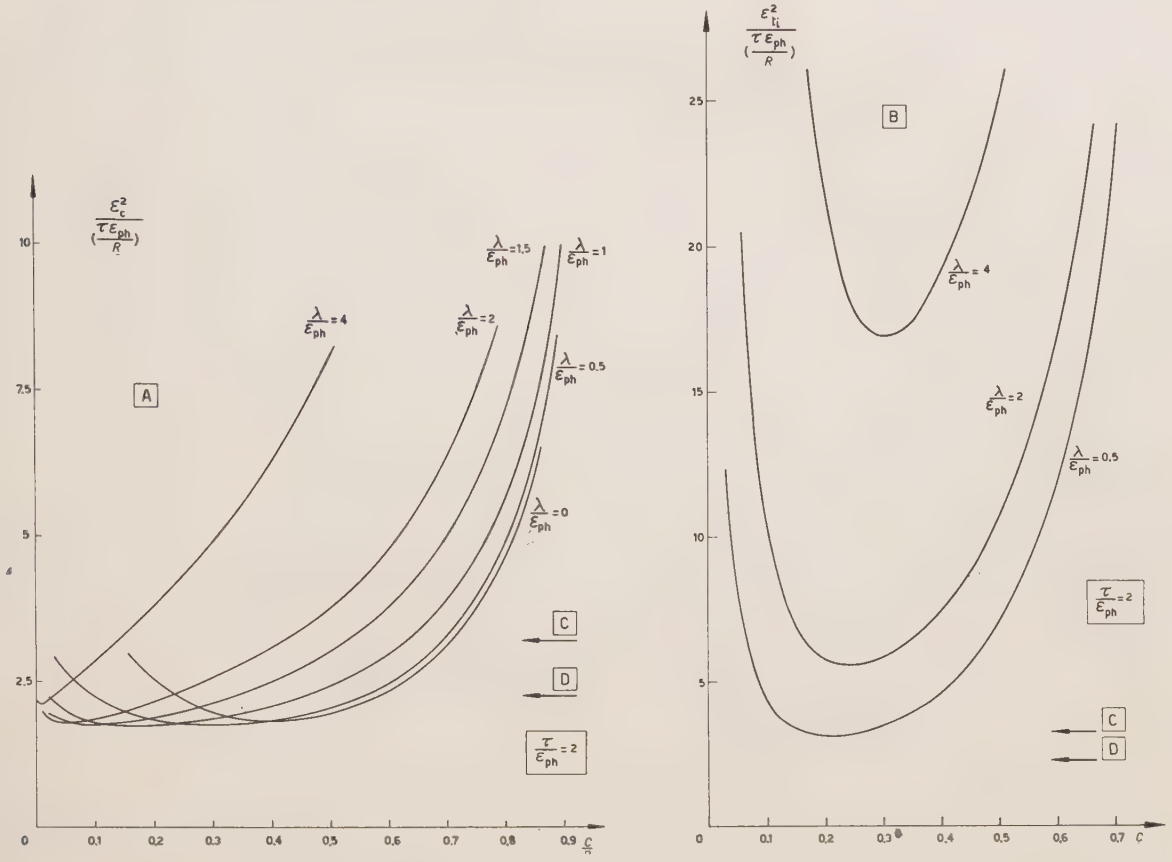

Fig. 6. Total "machine time" variance for the fixed parameter $\tau/\varepsilon_{ph} = 2$.

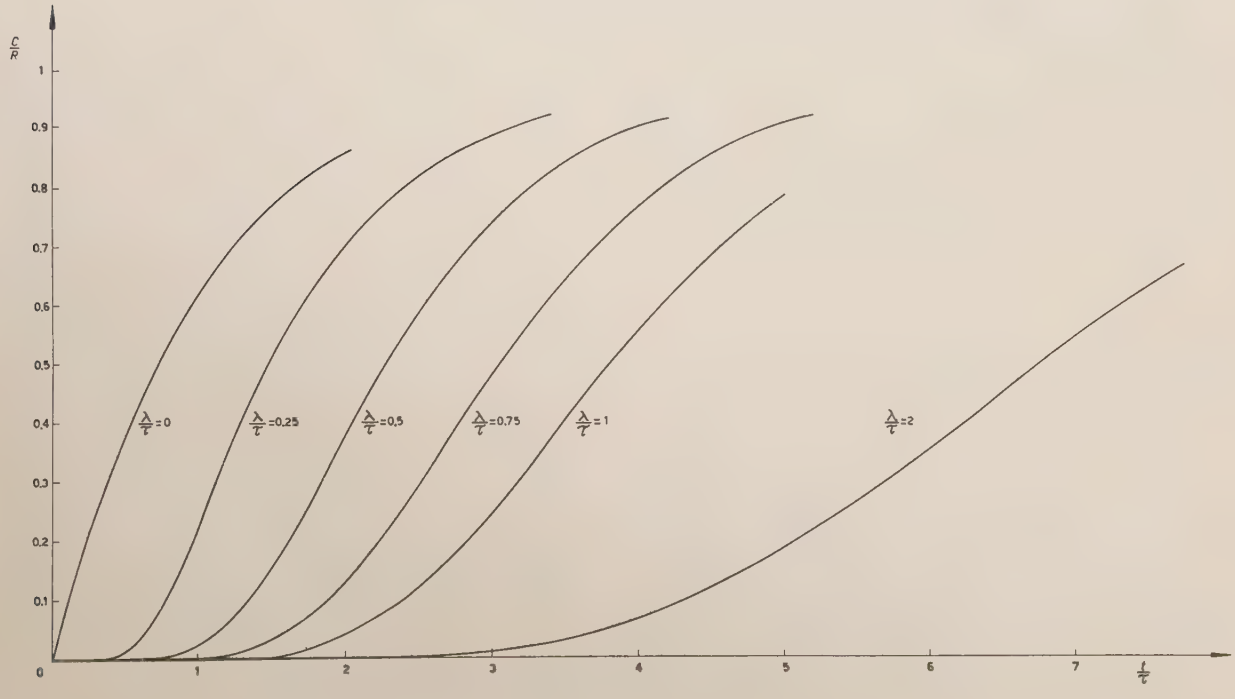

Fig. 7. Average value of C/R as a function of t/τ.

Therefore, this dependence calls for a selection of a limited amplitude range for the accepted pulses, or for some correction device involving the pulse height. The dependence of the machine time on R is more sensitive in case B than in case A, and, of course, it becomes more important as the S.E.R. width increases.

Morton has recently developed a device which eliminates this systematic dependence[9]).

In this device the machine time is the time in which a fixed fraction of the total charge R (emitted in each event) is collected. The "machine time" variance is equal to that of method B as far as contributions 2 and 3 are concerned; contribution 1 on the contrary, differs appreciably only for rather large values of C/R (much larger than the values for which the total curves of figs. 5 and 6 give the minimum variance).

We calculated the first contribution only for $\lambda = 0$ in Appendix VI. The corresponding curve is shown in dotted line in fig. 2B.

We can conclude that, except for the removal of the amplitude dependence, the minimum variances of this method are equal to the minimum variances of method B.

In the experimental works[10-13]) developed in our laboratory we adopted the linear method with $\omega\tau = 0.4$.

Prompt coincidence curves give a width of line $W_{\frac{1}{2}} = 6 \times 10^{-10}$ sec by a pulse selection corresponding to an energy between 0.8 and 1 MeV in the two measurement channels.

The theoretical value is calculated as follows:

$$W_{\frac{1}{2}} = 2.36\, \varepsilon \sqrt{2}$$

where ε is the variance of the machine time of a single channel given by (22). Assuming in our case

$$\tau = 3 \times 10^{-9} \text{ sec}; \quad \varepsilon_{ph} = 5 \times 10^{-10} \text{ sec}; \quad R = 350.$$

$W_{\frac{1}{2}}$ results to be 5.6×10^{-10} sec, which is in good agreement with the experimental value.

Experiments on the non linear method A are now being planned, in which the dependence on the amplitude R is corrected, after the time amplitude conversion, with a correcting signal based on the amplitude of pulses in both channels.

9. Acknowledgement

The skillful help of Dr. L. Lunelli and Dr. A. Ghirardi of the "Centro Calcoli Numerici" of the Politecnico of Milano for the numerical computation with an electronic computer is greatly acknowledged.

Appendix I

Let us consider a great number of events, constituted by "jets" of F photons on the photocathode, and let us devide these events into classes characterized by the same incidence points of the photoelectrons on the photocathode.

The mean number of the emitted photoelectrons, obtained from the events of each class and from all the classes, is $\bar{r}F = \bar{\bar{Q}}$, where $\bar{r}$ is the mean photocathode yield.

The mean value of the events of a class is:

$$\bar{Q} = r_1 + r_2 + \cdots r_F$$

where r_1, r_2, r_F are the photoelectric yields of the particular points 1, 2... F of the photocathode, which define the considered class.

We have:

$$\bar{Q} - \bar{\bar{Q}} = \Delta\bar{Q} = \sum_{i=1}^{F} \mathrm{d}r_i; \qquad \mathrm{d}r_i = r_i - \bar{r}.$$

The variance of $\bar{Q}$ (considering a sufficiently great number of classes) is:

$$\varepsilon_{\bar{Q}}^2 = F\varepsilon_r^2$$

where ε_r^2 is the variance of r.

[9]) G. A. Morton, The Scintillation Counter (Proceedings of the "Colloque International sur l'électronique nucléaire", Paris, Sept. 1958).

[10]) C. Cottini and E. Gatti, Nuovo Cimento 4 (1956) 1550.

[11]) C. Cottini and E. Gatti, Nuclear Instruments 2 (1958) 88.

[12]) C. Cottini, E. Gatti and F. Vaghi, Nanosecond Vernier time analyzer (Proc. of "Colloque Intérnational sur l'éléctronique nucléaire", Paris Sept. 1958).

[13]) C. Cottini, E. Gatti, V. Svelto and F. Vaghi, Time sorting of nanosecond pulses (Proc. of the "Second Symposium on advances in fast pulse techniques for nuclear counting", Lawrence Radiation Laboratory, Berkeley February 1959).

The variance in number Q of electrons emitted in a "jet" is obtained by adding the variance $\overline{Q}$ arising from the Poisson statistics and the variance $F\varepsilon_r^2$ of the mean number $\overline{Q}$.

$$\varepsilon_Q^2 = \overline{Q} + F\varepsilon_r^2 = \overline{Q}\left(1 + \frac{\varepsilon_r^2}{\overline{r}}\right) = \overline{Q}\,(1 + \overline{r}\,\varepsilon_{rr}^2)$$

where ε_{rr}^2 is the relative variance of r.

Appendix II

Let us consider two successive dynodes of the phototube and a group of m electrons starting at the same instant from the first dynode.

(We can imagine that these m electrons are originated by the multiplication of a single electron on the considered first dynode.)

We shall calculate in what follows the width λ_A and its variance $\varepsilon_{\lambda_A}^2$ for the pulse constituted by the group of m electrons arriving at the second dynode; then, the width λ_B and its variance $\varepsilon_{\lambda_B}^2$ for the pulse starting from the second dynode (the starting pulse is constituted by the mg secondary electrons).

The pulse width in A is defined as:

$$\lambda_A^2 = \varepsilon_{dd}^2 = \frac{\sum_{i=1}^{m} x_i^2}{m} \qquad \text{(II-1)}$$

where x_i is the arrival time of the ith electron in respect to the mean arrival time.

Differentiating (II-1):

$$2\lambda_A\,d\lambda_A = \frac{2\sum_{i=1}^{m} x_i\,dx_i}{m}$$

from which (ε_{dd}^2 being the variance of x_i) we obtain:

$$\varepsilon_{\lambda_A}^2 = \frac{\varepsilon_{dd}^2}{m}. \qquad \text{(II-2)}$$

The pulse width in B is:

$$\lambda_B^2 = \frac{\sum_{i=1}^{m} g_i x_i^2}{\sum_{i=1}^{m} g_i} \qquad \text{(II-3)}$$

and in average $\lambda_A^2 = \lambda_B^2$, g_i and x_i being uncorrelated variables.

Differentiating (II-3) with respect to g_i and x_i, we obtain:

$$2\lambda_B\,d\lambda_B = \frac{\sum_{i=1}^{m} x_i^2\,dg_i}{\sum_{i=1}^{m} g_i} - \frac{\sum_{i=1}^{m} g_i x_i^2 \cdot \sum_{i=1}^{m} dg_i}{\left[\sum_{i=1}^{m} g_i\right]^2} + \frac{2\sum_{i=1}^{m} g_i x_i\,dx_i}{\sum_{i=1}^{m} g_i}$$

substituting the mean value mg for $\sum_{i=1}^{m} g_i$ and with reference to (II-3):

$$d\lambda_B = \frac{\sum_{k=1}^{m} (x_k^2 - \lambda_B^2)\,dg_k}{2\lambda_B\,mg} + \frac{\sum_{i=1}^{m} g_i x_i\,dx_i}{\lambda_B\,mg}.$$

Consequently the variances are (ε_g^2 is indicated as the g variance):

$$\varepsilon_{\lambda_B}^2 = \frac{\sum_{k=1}^{m} (x_k^2 - \lambda_B^2)^2\,\varepsilon_g^2}{4\lambda_B^2 m^2 g^2} + \frac{\sum_{i=1}^{m} g_i^2 x_i^2}{\lambda_B^2 m^2 g^2}\,\varepsilon_{dd}^2. \qquad \text{(II-4)}$$

We shall now calculate the mean value of the first summation, assuming for $P(x)$ a gaussian distribution normalized to m with a variance $\varepsilon_{dd}^2 = \lambda_B^2$.

For the second summation we have:

$$\sum_{i=1}^{m} g_i^2 x_i^2 = m\varepsilon_{dd}^2\,(g^2 + \varepsilon_g^2)$$

and finally

$$\varepsilon_{\lambda_B}^2 = \frac{\varepsilon_{dd}^2}{m}\left[1 + \tfrac{3}{2}\frac{\varepsilon_g^2}{g^2}\right] = \frac{\varepsilon_{dd}^2}{m}\left[1 + \frac{3}{2g}\right] \qquad \text{(II-5)}$$

if $\varepsilon_g^2 = g$.

We can now calculate the pulse width and its variance at the output of the phototube.

As the multiplication process does not change the pulse width ($\lambda_A^2 = \lambda_B^2$), we have as a total width:

$$\lambda^2 = \sum_{i=2}^{n} \lambda_i^2 = (n-1)\,\varepsilon_{dd}^2. \qquad \text{(II-6)}$$

Let us calculate the variance of λ.

Differentiating (II-6):

$$\lambda\,d\lambda = \sum_{i=2}^{n} \lambda_i\,d\lambda_i$$

consequently the variances are:

$$\lambda^2\varepsilon_\lambda^2 = \sum_{i=2}^{n} \lambda_i^2\varepsilon_{\lambda_i}^2.$$

Recalling (II-5) we have

$$\lambda^2\varepsilon_\lambda^2 = \varepsilon_{dd}^2 \sum_{i=2}^{n} \varepsilon_{\lambda_i}^2 = \varepsilon_{dd}^4\left[1 + \frac{3}{2g}\right]\sum_{i=2}^{n} \frac{1}{m_i} =$$

$$= \frac{\varepsilon_{dd}^4}{g-1}\left[1 + \frac{3}{2g}\right]$$

being in average $m_2 = g$; $m_3 = g^2 \ldots$ and summing the geometric progression.

So that we have, recalling the (II-6) the relative variance:

$$\varepsilon_{\lambda,r}^2 = \frac{\varepsilon_\lambda^2}{\lambda^2} \cdot \frac{1}{(g-1)(n-1)^2}\left[1 + \frac{3}{2g}\right]. \quad \text{(II-7)}$$

Appendix III

The variance of h is calculated, following the pattern of Appendix II for $\varepsilon\lambda^2$.

The variance of x is:

$$\varepsilon_{dd}^2 = \frac{\sum_{i=1}^{m} x_i^2}{m}.$$

The centroid of the starting pulse is:

$$x_B = \frac{\sum_{i=1}^{m} g_i x_i}{\sum_{i=1}^{m} g_i} = \frac{g\sum_{i=1}^{m} x_i + \sum_{i=1}^{m} \Delta g_i x_i}{\sum_{i=1}^{m} g_i} \quad \text{(III-1)}$$

where $g_i = g + \Delta g_i$.

Differentiating and considering that the numerator of (III-1) is zero in average, we have:

$$dx_B = \frac{\sum_{i=1}^{m} g_i \sum_{i=1}^{m} x_i \, d\Delta g_i}{\left(\sum_{i=1}^{m} g_i\right)^2} + \frac{g\sum_{i=1}^{m} dx_i + \sum_{i=1}^{m} \Delta g_i \cdot dx_i}{\sum_{i=1}^{m} g_i}.$$

Then, passing to the variance and substituting the mean values for the summation we have:

$$\varepsilon_B^2 = \frac{\varepsilon_{dd}^2}{m}\left(1 + \frac{2\varepsilon_g^2}{g^2}\right) = \frac{\varepsilon_{dd}^2}{m}\left(1 + \frac{2}{g}\right)$$

and then for the whole phototube, the device time spread squared is:

$$\varepsilon_{ph}^2 = \varepsilon_{cd}^2 + \frac{\varepsilon_{dd}^2}{g-1}\left(1 + \frac{2}{g}\right). \quad \text{(III-2)}$$

Appendix IV

The average value of the current output pulse of the phototube is:

$$\underline{i}(t) = f(t) * I(t).$$

If we suppose that the shape of current due to one photoelectron emitted at the time σ in consequence of a light quantity $I(\sigma)\Delta\sigma$ (where $\Delta\sigma$ is chosen in order to obtain $I(\sigma)\Delta\sigma = 1$) is:

$$\frac{\lambda_0}{\lambda} f\left[\frac{\lambda_0}{\lambda}(t-b) + b\right]$$

rather than the average shape $f(t)$, then the current is:

$$i(t) = \underline{i}(t) - f(t-\sigma) + \frac{\lambda_0}{\lambda} f\left[\frac{\lambda_0}{\lambda}(t-b) + b\right] \quad \text{(IV-1)}$$

or differentiating with respect to λ and introducing $\Delta\lambda = \lambda - \lambda_0$:

$$i(t) = \underline{i}(t) - \frac{\Delta\lambda}{\lambda_0}\left[f(t-\sigma) + (t-\sigma-b)\frac{df(t-\sigma)}{d(t-\sigma)}\right]. \quad \text{(IV-2)}$$

The charge $C(t)$ becomes:

$$C(t) = \underline{C}(t) - \frac{\Delta\lambda}{\lambda_0}(t-\sigma-b) f(t-\sigma). \quad \text{(IV-3)}$$

By this equation, we can calculate the variation Δt_i of t_i with regard to $\underline{t_i}$, arising from the considered width variation:

$$\Delta t_i + \frac{\Delta\lambda}{\lambda_0}\frac{(t-\sigma-b) f(t-\sigma)}{\underline{i}(t_i)}. \quad \text{(IV)-4}$$

By the definition of t_c and by eq. (IV-4) as in Appendix II of [1]), we find:

$$\Delta t_c = -\frac{\Delta\lambda}{\lambda_0}\frac{\int_\sigma^{t_i}(t-\sigma-b) f(t-\sigma)\,dt}{\int_0^{t_i}[f(t) * I(t)]\,dt}. \quad \text{(IV-5)}$$

$\Delta\lambda/\lambda_0$ is the statistical variable accounting for a fluctuation in average pulse width λ_0 whose variance is

$$\varepsilon_{\lambda,r}^2 = \frac{1}{(n-1)^2(g-1)}\left(1 + \frac{3}{2g}\right);$$

hence by adding the contributions due to each photoelectron in the time interval $0 - t_i$, we have:

$$\varepsilon_{c,\lambda}^2 = \varepsilon_\lambda^2 \frac{I(t_i) * \left[\int_0^{t_i}(t-b) f(t)\,dt\right]^2}{\left[\int_0^{t_i}(I(t_i) * f(t))\,dt\right]^2}. \quad \text{(IV-6)}$$

Appendix V

First we shall calculate the "machine time" variance due to emission statistics and to gain fluctuations, then the variances due to transit time fluctuations. Since the contribution given to total current by each photoelectron is $f(t-\sigma)$ and as the scintillation is $I(t) = (R/\tau)\exp(-t/\tau)$, the mean current and the perturbed current are respectively:

$$\underline{i}(t) = I(t) * f(t) \qquad \text{(V-1)}$$

$$i(t) = \underline{i}(t) + \Delta K\, f(t - \sigma) \qquad \text{(V-2)}$$

where ΔK is a perturbation at time σ.

The Laplace transform of (V-1) and (V-2) are:

$$\underline{i}(p) = I(p)\, f(p) \qquad \text{(V-3)}$$

$$i(p) = I(p)\, f(p) + \Delta K\, f(p) \exp(-\sigma p) =$$

$$= f(p)\, \{I(p) + \Delta K \exp(-\sigma p)\}\,. \qquad \text{(V-4)}$$

If μ here is the "machine time", from (6) we obtain:

$$\omega\mu = \arg i(j\omega)\,.$$

Substituting $j\omega$ for p in (V-3) and (V-4) we find

$$\omega\,\underline{\mu} = \arg \underline{i}(j\omega) = \arg I(j\omega) + \arg f(j\omega) \qquad \text{(V-5)}$$

$$\omega\mu = \arg i(j\omega) = \arg f(j\omega) +$$

$$+ \arg \{I(j\omega) + \Delta K \exp(-j\omega\sigma)\} \qquad \text{(V-6)}$$

where $\underline{\mu}$ is the mean value of μ.

By subtracting eq. (V-5) from (V-6) we obtain for $\Delta\mu = \mu - \underline{\mu}$

$$\Delta\mu = \frac{\arg \{I(j\omega) + \Delta K \exp(-j\omega\sigma)\} - \arg I(j\omega)}{\omega}.$$

It is to be noted that this expression does not involve the S.E.R. $f(j\omega)$. Now introducing:

$$I(j\omega) = \frac{R}{1 + j\omega\tau}$$

we obtain:

$$\Delta\mu = \frac{\omega\tau \cos \omega\sigma - \sin \omega\sigma}{\omega R}\, \Delta K$$

whence, assuming as in a previous paper[1]), that $(1 + \omega^2\tau^2) \ll R$,

$$\varepsilon^2_{\mu,\mathrm{em},A} = (1 + \overline{\nu}\, \varepsilon_{rr}^2 + \varepsilon_A^2)\, \frac{\tau^2}{R}\, \frac{1 + 2\omega^2\tau^2}{1 + 4\omega^2\tau^2}\,.$$

Similarly the "machine time" variance due to $\varepsilon_{\mathrm{ph}}$ is independent of the S.E.R. width and is given by:

$$\varepsilon^2_{\mu,\mathrm{ph}} = \frac{\varepsilon_{\mathrm{ph}}^2}{R}\left(1 + \frac{2\omega^4\tau^4}{1 + 4\omega^2\tau^2}\right)$$

it being assumed that

$$\omega\,(1 + \omega^2\tau^2) \ll \frac{R}{\varepsilon_{\mathrm{ph}}}\,.$$

Appendix VI

We can define the "machine time" as the time t_i in which a fixed fraction $\gamma = C/R$ of the total charge R, emitted in a single event, is collected.

It has to be noted that if R were not affected by statistical fluctuations, this method would be equivalent to that for which the "machine time" is the time at which a definite charge C is collected.

Let us calculate the variance due to the emission statistics and gain fluctuation, in the case of S.E.R. width $\lambda = 0$, and considering also the fluctuations of R.

As in Appendix II of the previous work[1]) we have:

$$\underline{i}(t) = \delta(t) * I(t) \qquad \text{(VI-1)}$$

$$i(t) = \underline{i}(t) + \Delta K\, \delta(t - \sigma)\,. \qquad \text{(VI-2)}$$

By definition of "machine time" t_i we have:

$$\int_0^{t_i} i(t)\, \mathrm{d}t = \gamma \int_0^{\infty} i(t)\, \mathrm{d}t$$

and considering (VI-2)

$$\int_0^{t_i} \underline{i}(t)\, \mathrm{d}t + \int_0^{t_i} \Delta K\, \delta(t - \sigma)\, \mathrm{d}t =$$

$$= \gamma \int_0^{\infty} \underline{i}(t)\, \mathrm{d}t + \gamma \int_0^{\infty} \Delta K\, \delta(t - \sigma)\, \mathrm{d}t$$

whence we obtain:

$$\overline{C} + \Delta t_i \cdot \underline{i}(t_i) + \Delta K = \gamma\overline{R} + \gamma\Delta K \quad \text{for} \quad 0 \leqslant \sigma \leqslant t_i\,;$$

$$\overline{C} + \Delta t_i \cdot \underline{i}(t_i) \qquad = \gamma\overline{R} + \gamma\Delta K \quad \text{for} \qquad \sigma > t_i$$

where $\Delta t_i = t_i - \underline{t_i}$ and

$$\overline{C} = \int_0^{\underline{t_i}} \underline{i}(t)\, \mathrm{d}t = \gamma\overline{R}\,.$$

Hence, by adding the contributions to the variance arising from all photoelectrons emitted and as

$$\frac{C}{R} = 1 - \exp\left(-\frac{t}{\tau}\right); \quad \underline{i}(t) = \frac{\overline{R}}{\tau} \exp\left(-\frac{t}{\tau}\right)$$

we have:

$$\varepsilon^2_{t_i,\mathrm{em},A} = (1 + \overline{\nu}\varepsilon_{rr}^2 + \varepsilon_A^2) \left\{ \int_0^{t_i} \frac{(\gamma - 1)^2}{\underline{i}^2(t_i)}\, I(\sigma)\, \mathrm{d}\sigma + \right.$$

$$\left. + \int_{t_i}^{\infty} \frac{\gamma^2}{\underline{i}^2(t_i)}\, I(\sigma)\, \mathrm{d}\sigma \right\} = (1 + \overline{\nu}\, \varepsilon_{rr}^2 + \varepsilon_A^2)\, \frac{\tau^2}{R}\, \frac{C/R}{1 - C/R}\,. \qquad \text{(VI-4)}$$

NUCLEAR INSTRUMENTS AND METHODS 4 (1959) 202–212; NORTH-HOLLAND PUBLISHING CO.

ÜBERLEGUNGEN ZUM BAU EINES WENDELLINEARBESCHLEUNIGERS FÜR PROTONEN

W. MÜLLER und J. REMBSER†

Institut für angewandte Physik der Universität Frankfurt (M)

Eingegangen am 20 März 1959

The method of accelerating heavy particles in a helix waveguide as repeatedly suggested in literature has been examined theoretically in detail. The first part of this article deals with the HF-characteristics of the wave-guide that were taken from known investigations based on the Pierce theory. A more accurate examination of the acceleration process for protons shows that the accelerating electric field strength on the axis of the helix is strongly reduced for proton energies larger than ca. 30 MeV, while for proton energies smaller than ca. 0.5 MeV the losses in the wave guide are considerably increasing. An acceleration, therefore, will only be advisable for a medium energy range, but here it is equivalent if not superior to other methods. In the case discussed here (acceleration of protons from 1 to 10 MeV) the optimum vacuum wave length was found to be ca. 1.5 m. With a HF-source output of 0.5 MW such an accelerator would have a length of ca. 12 m, while the diameter of the shield would be 12 cm, the volume being about 0.15 m³.

1. Einleitung

Nach einem Vorschlag von Walkinshaw und Wyllie[1]) sowie unabhängig davon von Johnsen[2]) lassen sich zur Beschleunigung schwerer Teilchen wendelförmige Wellenleiter verwenden, die koachsial von einem zylindrischen Aussenleiter umgeben sind. Ähnliche Konstruktionen haben zur Verstärkung sehr hoher Frequenzen als Wanderwellenröhren grosse Bedeutung erlangt, sodass die Untersuchung ihres allgemeinen elektromagnetischen Verhaltens bereits mehrfach durchgeführt wurde (vergl. [3])). Die Beschleunigungseigenschaften solcher Wellenleiter hat insbesondere Johnsen theoretisch behandelt, wobei sich herausstellte, dass z.B. für Protonen bis etwa 30 MeV der Wendellinearbeschleuniger ein aussichtsreiches und im Vergleich zum Driftröhrenbeschleuniger nach Alvarez durchaus konkurrenzfähiges Gerät darstellt.

Zur Vorbereitung der nachfolgenden Überlegungen, die sich mit einer genaueren Auswertung der Theorie des Wendellinearbeschleunigers beschäftigen, sei zunächst eine kurze qualitative Übersicht über die Feldverteilung im Innern des Wellenleiters sowie über die Wirkungsweise des Beschleunigers gegeben.

Abb. 1 zeigt dazu im Längsschnitt ein

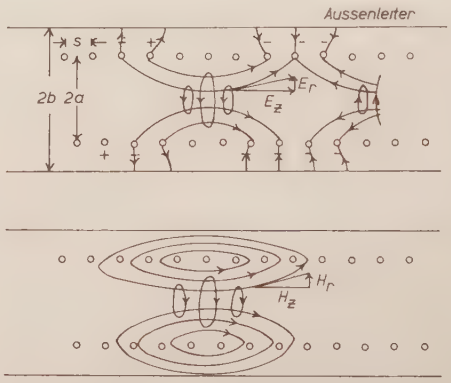

Abb. 1. Kraftlinienbild der beiden Grundschwingungsformen im Innern des Wendelleiters. (Abb. 1a: TM-mode, Abb. 1b: TE-mode.)

Teilstück des Wellenleiters mit dem zugehörigen umhüllenden Aussenleiter. Denken wir uns auf dieser Anordnung eine nach rechts laufende

† Jetzt: Allgemeine Elektricitätsgesellschaft Frankfurt (M), Abt. Kernenergieanlagen.

[1]) W. Walkinshaw und K. Wyllie, Math. Memo **57** (1948).
[2]) K. Johnsen und H. Dahl, Chr. Michelsens Inst. Beretn. **14** (1951).
[3]) K. Johnsen, CERN-PS/KJ 27 (August 1954);
K. Pöschl, A.E.Ü. **7** (1953);
H. Kaden, A.E.Ü. **5** (1951).

elektromagnetische Welle, deren Wellenlänge $\lambda = 2\pi/k$ gross gegen den Windungsabstand sei, so bilden sich auf dem Wendeldraht periodische Ladungsanhäufungen wechselnden Vorzeichens aus. Von diesen Ladungen gehen elektrische Kraftlinien aus, die im Innern abschnittsweise längs der Wendelachse laufen und dann wieder zur Wendel zurückkehren. Die zugehörigen, rein transversalen magnetischen Kraftlinien umschliessen die elektrischen Kraftlinien ringförmig in Form konzentrischer Kreise um die Mittelachse. Das Kraftlinienbild dieser Schwingungsform, die in der Literatur unter dem Namen "transverse magnetic mode" (TM-mode) bekannt ist, geht aus Abb. 1a hervor.

Daneben existiert noch eine zweite Schwingungsform, die ihre Ursache in dem zeitlich veränderlichen Wendelstrom hat, und bei der die elektrischen Kraftlinien ähnlich verlaufen wie die magnetischen Kraftlinien der ersten Schwingungsform. Die zugehörigen magnetischen Kraftlinien treten aber jetzt zwischen den Windungen hindurch und werden erst im Aussenraum geschlossen. Dieser Schwingungstypus, der den Namen "transverse electric mode" (TE-mode) führt, ist in Abb. 1b skizziert.

Wegen des Zusammenhangs zwischen Wendelstrom und Ladung auf dem Wendeldraht sind beide Schwingungsformen in einem festen, von den geometrischen Daten der Wendel und der Betriebsfrequenz ω abhängigen Verhältnis miteinander gekoppelt. Das resultierende Feld bewegt sich mit der Phasengeschwindigkeit der Welle

$$v_{\mathrm{ph}} = \frac{\omega}{k} \tag{1}$$

nach rechts. Wie weiter unten gezeigt wird, kann in erster Näherung für die Abhängigkeit der Phasengeschwindigkeit von den geometrischen Daten der Wendel gesetzt werden:

$$v_{\mathrm{ph}} = \frac{s}{2\pi a} c\,. \tag{2}$$

Hierbei bedeuten s den Windungsabstand, a den Wendelradius und c die Lichtgeschwindigkeit. Der physikalische Sinn von Gl. (2) ist leicht ersichtlich: die nach (2) berechnete Phasengeschwindigkeit entspricht einer mit Lichtgeschwindigkeit längs der Wendeldrahtachse schraubenartig bewegten elektromagnetischen Welle. Die Wellenzahl k auf der Wendelachse ist nach (1) von der Wellenzahl $k_0 = \omega/c$ wohl zu unterscheiden. Im Allgemeinen kann nach (2) angenommen werden:

$$k_0 \ll k\,. \tag{3}$$

Die Beschleunigung der Teilchen im Wendellinearbeschleuniger erfolgt nach dem Wellenreiterprinzip, wobei ein einmal eingefangenes Teilchen an der vorderen Flanke eines Wellenberges mitgeführt wird und dabei kontinuierlich Energie aus der Welle gewinnt. Damit eine feste Phasenlage des Teilchens während der gesamten Beschleunigung beibehalten wird, ist dafür zu sorgen, dass die Phasengeschwindigkeit der Welle bei zunehmender Teilchenenergie stets mit der Teilchengeschwindigkeit übereinstimmt. Dies kann nach (2) durch geeignete Variation der geometrischen Daten erreicht werden.

2. Hochfrequenzeigenschaften des Wellenleiters

Für eine genauere quantitative Betrachtung des Beschleunigungsvorgangs ist es zweckmässig, neben der Phasengeschwindigkeit zwei für den Wellenleiter charakteristische Grössen ξ und η durch die Definitionen

$$\xi = \frac{E^2}{S} \tag{4}$$

$$\eta = \frac{E^2}{p} \tag{5}$$

einzuführen. Dabei bedeuten: E die Amplitude des achsialen elektrischen Feldes auf der Wendelachse, S den durch den Querschnitt des Wellenleiters tretenden Leistungsfluss und p die pro Zeit- und Längeneinheit auftretenden Verluste. Die erste Grösse ξ, die auch als Reihenimpedanz des Wellenleiters bezeichnet wird, liefert bei bekanntem Leistungsfluss S die Amplitude des beschleunigenden elektrischen Feldes, während die zweite Grösse η, die man Parallelimpedanz des Wellenleiters nennt, ein Mass für die im Wellenleiter auftretenden Verluste und damit für den Abfall von S in

Beschleunigungsrichtung darstellt. Beide Grössen hängen nur von den geometrischen Daten des Wellenleiters und von der Betriebsfrequenz ab. Für die Abnahme des Leistungsflusses S auf einem infinitesimalen Wegstückchen dz in Fortschreitungsrichtung der Welle gilt entsprechend der Definition von p

$$dS = -p\,dz$$

und nach Integration über z unter Beachtung von (4) und (5) für S:

$$S = S_0 \exp\left(-\int_0^z \frac{\xi}{\eta}\,dz'\right) = S_0 \exp\left(-\int_0^z \frac{dz'}{l_0(z')}\right). \quad (6)$$

Die hier eingeführte Grösse l_0 gibt die Entfernung an, nach der bei konstanter Geometrie der Anfangsleistungfluss S_0 auf den e-ten Teil abgeklungen ist.

Die Berechnung dieser charakteristischen Grössen unter Zugrundelegung einfacher Modellvorstellungen über den Wellenleiter ist in der Literatur[2,3,4]) bereits mehrfach durchgeführt worden, sodass wir uns im folgenden auf eine kurze Erläuterung der für die Rechnung notwendigen Annahmen und Mitteilung der Ergebnisse beschränken können. Da eine exakte Theorie wegen der komplizierten, durch den Wendeldraht gegebenen Begrenzungsfläche, auf der die Randbedingungen zu erfüllen sind, kaum möglich ist, ersetzen wir in üblicher Weise nach Pierce[4]) die Wendel durch einen unendlich dünnen Zylinder, dessen elektrische Leitfähigkeit in Richtung des Wendeldrahtes unendlich gross, in jeder anderen Richtung dagegen als verschwindend angenommen wird. Die Lagerung der Wendel innerhalb des Aussenleiters kann im Prinzip durch dielektrische Stützen erfolgen, die radial in Winkelabständen von 120° von der Wendel zum Aussenleiter laufen (vergl. Abb. 2). Für die Rechnung kann der Einfluss solcher Stützen auf die Feldgrössen nach Harvie[5]) in guter Näherung erfasst werden, wenn man ein Ersatzmedium anisotroper, komplexer DK zwischen Wendel und Aussenleiter annimmt. Nach Annahme von Zylinderkoordinaten r, φ, z, wobei die positive z-Achse in Beschleunigungsrichtung zeigen möge, gilt für die dielektrische Verschiebung $\boldsymbol{D}$ dieses Ersatzmediums:

$$D_r = \varepsilon_r E_r\,, \quad D_\varphi = \varepsilon_\varphi E_\varphi\,, \quad D_z = \varepsilon_z E_z$$

wobei nach Harvie in den einzelnen Richtungen zu setzen ist:

$$\varepsilon_r = \varepsilon_z = \varepsilon_\parallel (1 + i \operatorname{tg}\delta_\parallel)\,, \qquad \varepsilon_\varphi = \varepsilon_\perp (1 + i \operatorname{tg}\delta_\perp)$$

mit

$$\varepsilon_\parallel = 1 + \alpha(\varepsilon - 1)\,, \qquad \frac{1}{\varepsilon_\perp} = 1 - \alpha + \frac{\alpha}{\varepsilon}\,,$$

$$\operatorname{tg}\delta_\parallel = \alpha \frac{\varepsilon}{\varepsilon_\parallel} \operatorname{tg}\delta, \quad \operatorname{tg}\delta_\perp = \alpha \frac{\varepsilon_\perp}{\varepsilon} \operatorname{tg}\delta$$

ε und δ bedeuten DK und Verlustwinkel des Stützmaterials, während α den Bruchteil des von den Stützen eingenommenen Volumens angibt. Als Lösungen der Maxwellschen Gleichungen für in z-Richtung fortlaufende Wellen

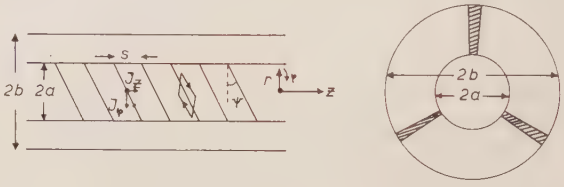

Abb. 2

erhält man unter Beachtung der vorhandenen Zylindersymmetrie in den beiden Teilräumen $r < a$ und $a < r < b$ die Darstellungen:

$$\begin{aligned} E_z &= E I_0(\gamma r) & H_z &= H I_0(\gamma r) \\ E_r &= \frac{ik}{\gamma} E I_1(\gamma r) & H_r &= \frac{ik}{\gamma} H I_1(\gamma r) \\ E_\varphi &= -\frac{ik_0}{\gamma} H I_1(\gamma r) & H_\varphi &= \frac{ik_0}{\gamma} E I_1(\gamma r) \end{aligned} \quad (7)$$

für $r < a$ und

$$\begin{aligned} E_z &= E' I_0(\gamma_E r) + E'' K_0(\gamma_E r) \\ E_r &= \frac{ik}{\gamma_E}\left(E' I_1(\gamma_E r) - E'' K_1(\gamma_E r)\right) \\ E_\varphi &= -i\frac{k_0}{\gamma_H}\left(H' I_1(\gamma_H r) - H'' K_1(\gamma_H r)\right) \\ H_z &= H' I_0(\gamma_H r) + H'' K_0(\gamma_H r) \\ H_r &= \frac{ik}{\gamma_H}\left(H' I_1(\gamma_H r) - H'' K_1(\gamma_H r)\right) \\ H_\varphi &= \varepsilon_\parallel \frac{ik_0}{\gamma_E}\left(E' I_1(\gamma_E r) - E'' K_1(\gamma_E r)\right) \end{aligned} \quad (8)$$

für $a < r < a$.

[4]) J. R. Pierce, Travelling Wave Tubes (Van Nostrand, N.Y. 1950).

[5]) R. B. R. Harvie, Nature **162** (1948) 890.

Der allen Feldgrössen gemeinsame Faktor $\exp\{i(\omega t - kz)\}$ ist hier weggelassen worden. Ferner bedeuten I_0, I_1, K_0, K_1 die modifizierten Bessel- bzw. Hankelfunktionen. Die in die Lösungen eingehenden Konstanten E, H, E', H', E'', H'' werden später durch Randbedingungen festgelegt. Für die im Argument der Zylinderfunktionen auftretenden Grössen γ, γ_E, γ_H, die den radialen Feldverlauf bestimmen, gilt:

$$\gamma^2 = k^2 - k_0^2\,, \quad \gamma_E{}^2 = k^2 - \varepsilon_\parallel k_0^2\,,$$
$$\gamma_H{}^2 = k^2 - \varepsilon_\perp k_0^2\,.$$

Da im vorliegenden Fall $\varepsilon_\parallel$ und $\varepsilon_\perp$ nahe bei 1 liegen, kann wegen (3) für alle weiteren Betrachtungen gesetzt werden:

$$\gamma_E{}^2 = \gamma_H{}^2 = \gamma^2 = k^2 - k_0^2\,. \tag{9}$$

Die Felddarstellungen (7) und (8) stellen die mathematische Beschreibung der in den Abb. 1a und 1b skizzierten Schwingungsformen dar. Die erste, von den Wendelladungen herrührende Schwingungsform (TM-mode) erhält man aus (7) und (8) durch Nullsetzen von H, H', H'' und entsprechend die zweite, mit dem Wendelstrom verknüpfte Schwingungsform durch Nullsetzen von E, E', E'' (TE-mode).

Neben der üblichen elektromagnetischen Randbedingung am Aussenleiter (Verschwinden der Tangentialkomponenten von $\boldsymbol{E}$) sind auf der Wendelfläche ($r = a$) folgende Bedingungen zu erfüllen: Stetigkeit der tangentialkomponenten E_z und E_φ, Verschwinden der elektrischen Feldkomponente in Richtung der Leitfähigkeit und Stetigkeit der magnetischen Feldkomponente in Stromrichtung. Die letzte Bedingung folgt aus $\oint \boldsymbol{H}\,\mathrm{d}\boldsymbol{s} = 0$ für eine infinitesimale Schleife in Stromrichtung (Abb. 2). Die Berücksichtigung dieser Randbedingungen liefert die in Gl. (7) und (8) eingehenden Konstanten als Lösungen eines homogenen, linearen Gleichungssystems. Man findet:

$$H = -i\frac{\gamma}{k_0}\frac{I_0(x)}{I_1(x)}\operatorname{tg}\psi \cdot E$$

$$E' = -\frac{I_0(x)K_0(y)}{K_0(x)I_0(y)}\frac{1}{D_{00}}E$$

$$E'' = -\frac{I_0(x)}{K_0(x)}\frac{1}{D_{00}}E$$

$$H' = i\frac{\gamma}{k_0}\frac{I_0(x)K_1(y)}{K_1(x)I_1(y)}\frac{\operatorname{tg}\psi}{D_{11}}E$$

$$H'' = -i\frac{\gamma}{k_0}\frac{I_0(x)}{K_1(x)}\frac{\operatorname{tg}\psi}{D_{11}}E$$

wobei ψ den Steigungswinkel der Wendel bedeutet und zur Abkürzung die Grössen

$$x = \gamma a \qquad y = \gamma b \tag{10}$$

und

$$D_{00} = 1 - \frac{I_0(x)K_0(y)}{K_0(x)I_0(y)} \qquad D_{11} = 1 - \frac{I_1(x)K_1(y)}{K_1(x)I_1(y)}$$

sowie für späteren Gebrauch

$$D_{01} = 1 + \frac{I_0(x)K_1(y)}{K_0(x)I_1(y)} \qquad D_{10} = 1 + \frac{I_1(x)K_0(y)}{K_1(x)I_0(y)}$$

verwendet werden. Das Verschwinden der Koeffizientendeterminante des homogenen Gleichungssystems liefert ausserdem noch eine Beziehung zwischen der radialen Wellenzahl γ und den geometrischen Abmessungen ψ und a der Wendel.

$$k_0^2 a^2 \operatorname{ctg}^2\psi = x^2\frac{I_0(x)K_0(x)}{I_1(x)K_1(x)}\frac{D_{00}}{D_{11}}\frac{1}{1-(1-\varepsilon_\parallel)\,\frac{1}{2}\pi x\, I_0(x)K_1(x)D_{10}}\,. \tag{11}$$

In der Praxis kann Gl. (11) durch die einfachere Beziehung

$$k_0^2 a^2 \operatorname{ctg}^2\psi = x^2\frac{I_0(x)K_0(x)}{I_1(x)K_1(x)}\frac{1}{\varepsilon_\parallel}\frac{D_{00}}{D_{11}} \tag{12}$$

ersetzt werden†. Die Näherung (2) ergibt sich aus (12), wenn man den Korrekturfaktor

$$\frac{I_0(x)K_0(x)}{I_1(x)K_1(x)}\frac{1}{\varepsilon_\parallel}\frac{D_{00}}{D_{11}}$$

der in der Nähe von 1 liegt, weglässt. Die verbleibende Gleichung geht dann für kleine ψ wegen (9) in (2) über.

Bei der Berechnung von ξ beachten wir, dass der Leistungsfluss S durch den Ansatz

$$S = \frac{c}{8\pi}\int_0^b (E_r H\varphi^* - E\varphi H_r^*)\,2\pi r\,\mathrm{d}r$$

† Die Lösungen γ fallen im Gegensatz zur Theorie der Hohlrohrleitung stets reell aus, sodass nach (9) keine Grenzfrequenz für die Wendelleitung existiert- wenigstens im Rahmen der hier vorausgestezten Pierce'schen Theorie. Der physikalische Grund für dieses Verhalten liegt darin, dass die Tangentialkomponenten von $\boldsymbol{E}$ auf der Wendel nicht verschwinden.

gegeben wird. Nach längerer Rechnung ergibt sich für ξ die Darstellung:

$$\xi^{-1} = c\,\frac{\lambda_0^2}{8\pi^3}\,\frac{\beta^2}{(1-\beta^2)^2}\,\frac{I_0}{K_0}\Big\{2 - \tfrac{1}{2}x\Big[\frac{I_0}{I_1} - \frac{I_1}{I_0} + \frac{K_1}{K_0} - \frac{K_0}{K_1}\Big] + \varepsilon_\parallel\,\tfrac{1}{2}\pi x\, I_0K_0G + (\varepsilon_\parallel - 1)\,F\Big\}$$

mit

$$G = \frac{I_1}{I_0}\Big(\frac{D_{01}}{D_{00}} - 1\Big) + \frac{K_1}{K_0}\Big(\frac{D_{10}+D_{11}}{D_{00}} - 2\Big) + \frac{2}{\pi^2 x}\,\frac{1}{K_0^2 I_0^2(y) D_{00}^2}\Big(1 - \frac{I_1K_0}{K_1I_0}\,\frac{D_{00}}{D_{11}}\,\frac{I_0^2(y)}{I_1^2(y)}\Big) + \tfrac{1}{2}x\Big[\frac{I_1K_0}{K_1I_0}\Big(\frac{D_{01}^2}{D_{00}D_{11}} - 1\Big) - \frac{K_1^2}{K_0^2}\Big(\frac{D_{10}^2}{D_{00}^2} - 1\Big) - \frac{K_1I_0}{K_0I_1}\Big(\frac{D_{11}}{D_{00}} - 1\Big)\Big]$$

$$F = 1 - \tfrac{1}{2}x\Big(\frac{K_1}{K_0} - \frac{K_0}{K_1}\Big) + \tfrac{1}{2}\pi x\, I_0K_1\Big[1 - \tfrac{1}{2}x\Big(\frac{I_0}{I_1} - \frac{I_1}{I_0}\Big)\Big]. \qquad (13)$$

Bei allen Zylinderfunktionen, die ohne Argument auftreten, ist das Argument $x = \gamma a$ zu ergänzen. Die Grösse β ist für das Verhältnis von Phasengeschwindigkeit zur Lichtgeschwindigkeit gesetzt.

Die in Gl. (13) eingehende Funktion G erfasst den Einfluss des Aussenleiters, während F die Korrektur in ξ bei Vorhandensein des dielektrischen Stützmaterials darstellt.

Zur Berechnung der Parallelimpedanz η gehen wir davon aus, dass sich die Gesamtverluste p aus den Ohm'schen Verlusten im Wendeldraht p'_Ω, den Ohm'schen Verlusten im Aussenleiter p''_Ω und den dielektrischen Verlusten p_ε zusammensetzen. Nach Johnsen gilt für die einzelnen Anteile:

$$p'_\Omega = E^2\,\frac{c^3}{4\pi^3}\sqrt{\frac{\lambda_0}{\sigma}}\,\frac{\beta}{\sqrt{1-\beta^2}}\,\frac{\Phi s}{\pi d}\,\frac{\varepsilon_\parallel}{\cos\psi}\,\frac{I_0}{xI_1K_0K_1}\cdot\frac{1}{D_{00}D_{11}}$$

$$p''_\Omega = E^2\,\frac{c^3}{4\pi^3}\sqrt{\frac{\lambda_0}{\sigma}}\,\frac{\beta}{\sqrt{1-\beta^2}}\,\frac{\varepsilon_\parallel}{y}\,\frac{I_0I_1}{K_0K_1}\,\frac{1}{D_{00}D_{11}}\,\frac{1}{I_1^2(y)}\cdot\Big[1 + \varepsilon_\parallel\,\frac{k_0^2}{\gamma^2}\,\frac{I_0K_1}{K_0I_1}\,\frac{D_{11}}{D_{00}}\,\frac{I_1^2(y)}{I_0^2(y)}\Big]$$

$$p_\varepsilon = E^2\,\frac{c\lambda_0}{8\pi}\,\varepsilon_\parallel\delta_\parallel\,\frac{\beta^2}{(1-\beta^2)^2}\,\frac{K_1}{K_0}\,I_0^2(x)x\,\frac{D_{10}}{D_{00}}\cdot\Big[1 + \beta^2\Big(\frac{2}{\pi^2 x}\,\frac{1}{K_1K_0I_1^2(y)}\,\frac{1}{D_{00}D_{10}} + \tfrac{1}{2}x\Big[\frac{K_0}{K_1}\,\frac{D_{00}}{D_{10}} - \frac{K_1}{K_0}\,\frac{D_{10}}{D_{00}}\Big]\Big)\Big] + E^2\,\frac{c\lambda_0}{8\pi}\,\varepsilon_\parallel\varepsilon_1\delta_1\,\frac{\beta^4}{(1-\beta^2)^2}\,x^2\,\frac{I_0I_1}{K_0K_1}\Big\{\tfrac{1}{2}\Big[K_0^2\,\frac{D_{01}^2}{D_{00}D_{11}} - K_1^2\,\frac{D_{11}}{D_{00}}\Big] + \frac{1}{x}\,K_0K_1\,\frac{D_{01}}{D_{00}} - \frac{2}{\pi^2x^2}\,\frac{1}{I_1^2(y)}\,\frac{1}{D_{00}D_{11}}\Big\}. \qquad (14)$$

Im Gegensatz zur Pierce'schen Theorie wird hierbei für den Wendeldraht und Aussenleiter eine endliche Leitfähigkeit σ angenommen, die jedoch als so gross vorausgesetzt ist, dass die in (7) und (8) für unendlich grosses σ errechneten Feldgrössen Gültigkeit behalten. Für die Verluste im Wendeldraht (Durchmesser d) ist ausserdem noch in der ersten Formel (14) durch den Korrekturfaktor Φ, für den nach Johnsen[3]) näherungsweise gesetzt werden kann

$$\frac{\Phi s}{d} \cong 4$$

die ungleichmässige Stromverteilung im Leiter berücksichtigt.

3. Auswertung der Theorie

Der Bau eines Wendellinearbeschleunigers erfordert neben vielen anderen Fragen, die in dieser Arbeit nicht diskutiert werden sollen, die Lösung des sogenannten Wicklungsproblems, bei dem die Frage gestellt wird: wie sind die geometrischen Abmessungen a und s der Wendel als Funktion von z zu wählen, damit ein eingeschossenes Teilchen an jeder Stelle z seine Phasenlage zur Welle beibehält. Daneben werden bei möglichst kleiner Senderleistung N physikalisch und technisch sinnvolle Werte des Aussenleiterradius b und der Betriebswellenlänge λ_0 gesucht.

Wir beschränken uns im folgenden auf eine Teilchenbewegung auf der Mittelachse $z = 0$ bei konstanter Phasenlage, sehen also sowohl von radialen Schwingungen, als auch von Phasenschwingungen in Richtung der Achse ab. Aus

konstruktiv naheliegenden Gründen wählen wir ferner einen konstanten Aussenleiterradius b und berücksichtigen daneben für den Zusammenhang zwischen Windungsabstand s, Steigungswinkel ψ und Wendelradius a die einfache geometrische Beziehung $s = 2\pi a \operatorname{tg} \psi$. Als unbestimmte Variable des Wicklungsproblems treten dann lediglich die Grössen a und s, sowie die Parameter b und λ_0 auf. Ihre Festlegung soll im folgenden behandelt werden.

Zur Lösung des oben formulierten Wicklungsproblems gehen wir von den Forderungen aus, dass in einem beliebig herausgegriffenen Punkt z des Linearbeschleunigers zwei Bedingungen zu erfüllen sind:

Die Teilchengeschwindigkeit v_T muss mit der Phasengeschwindigkeit $v_{ph} = \omega/k$ der beschleunigenden Welle übereinstimmen, und der Zuwachs der Phasengeschwindigkeit muss dem Energiegewinn des beschleunigten Teilchens angepasst sein.

Die letzte dieser beiden Bedingungen lässt sich in der Form

$$T = T_0 + e \cos \phi \int_0^z E(z')\, dz' \qquad (15)$$

schreiben, wenn ϕ die als konstant angenommene Phasenlage auf der beschleunigenden Welle, T die kinetische Energie des Teilchens und e seine elektrische Ladung bedeuten; unter T_0 wird die Einschussenergie an der Stelle $z = 0$ verstanden. Im Falle einer Energierückführung besteht zwischen der bei $z = 0$ eingespeisten Leistung S_0 und der Senderleistung N der Zusammenhang

$$S_0 = \frac{N}{q}$$

wenn q den Bruchteil der vom Wellenleiter bei einem Durchgang absorbierten Leistung bedeutet. In der Praxis kann für S_0 etwa das 3–5-fache von N angenommen werden.

Unter Anwendung der Gleichungen (4) und (5) kann für (15) auch

$$T = T_0 + e \cos \phi \sqrt{S_0} \int_0^z \sqrt{\xi(z')} \exp\left(-\tfrac{1}{2} \int_0^{z'} \frac{d\zeta}{l_0(\zeta)}\right) dz' \qquad (16)$$

gesetzt werden.

Für die weiteren Betrachtungen ist es sehr vorteilhaft, die radiale Wellenzahl γ, welche in der Form $x = \gamma a$ und $y = \gamma b$ in den Grössen ξ und l_0 auftritt, zu eliminieren und durch die Teilchenenergie T zu ersetzen, für die gilt:

$$T = m_0 c^2 \left(\frac{1}{\sqrt{1 - \beta^2}} - 1 \right).$$

In Verbindung mit der Forderung $v_T = v_{ph} = \omega/k$ kann also wegen (9) gesetzt werden:

$$\gamma = k_0 \frac{1}{\sqrt{\left(1 + \frac{T}{m_0 c^2}\right)^2 - 1}}. \qquad (17)$$

Denken wir uns die neue Variable T zusammen mit dem Wicklungsradius a anstelle von γ im Integranden der Gl. (16) eingetragen, so fasst die entstehende Gleichung

$$T = T_0 + e \cos \phi \sqrt{S_0} \int_0^z \sqrt{\xi(T(z'), a(z'))} \exp\left(-\tfrac{1}{2} \int_0^{z'} \frac{d\zeta}{l_0(T(\zeta), a(\zeta))}\right) dz' \qquad (18)$$

unsere beiden Forderungen (15) und $v_T = v_{ph}$ zusammen und die Bestimmung der beiden

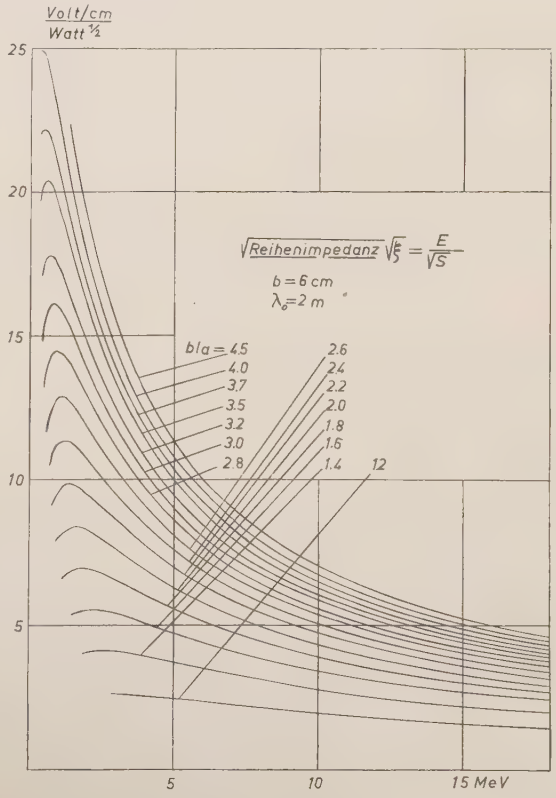

Abb. 3a. Beschleunigende Feldstärke, bezogen auf den Leistungsfluss in Abhängigkeit von der Protonenenergie T mit b/a als Parameter; Betriebswellenlänge $\lambda_0 = 2$m.

Funktionen (Tz) und $a(z)$ nach (18) liefert die gewünschte Lösung des Wicklungsproblems. Die zweite geometrische Grösse, der Windungsabstand s ist für gegebenes T und a durch die Dispersionsbeziehung (12) unter Beachtung von (17) und $s = 2\pi a \operatorname{tg} \psi$ festgelegt.

In den Abb. 3 und 4 sind die beiden charakteristischen Grössen $\xi(T,a)$ und $l_0(T,a)$ graphisch dargestellt, die ein Teilchen der Energie T bei dass bei kleinen Teilchenenergien die Verluste im Wellenleiter stark ansteigen, wodurch der Wirkungsgrad des Beschleunigers, d.h. der Energiegewinn der Teilchen dividiert durch die im Wellenleiter umgesetzte Leistung beträchtlich herabgesetzt wird. Für Protonen wäre es z.B. nicht sinnvoll, mit der Beschleunigung unterhalb 0.5 MeV zu beginnen, weil der apparative und energetische Aufwand für den

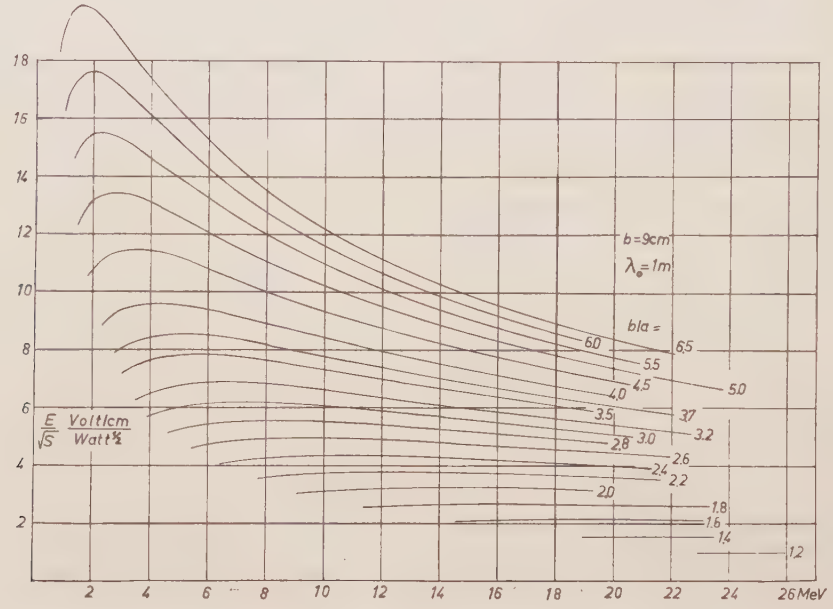

Abb. 3b. Beschleunigende Feldstärke, bezogen auf den Leistungsfluss in Abhängigkeit von der Protonenenergie T mit b/a als Parameter; Betriebswellenlänge $\lambda_0 = 1$ m.

einem Wicklungsradius a vorfindet. Der Aussenleiterradius b wurde mit $b = 6$ cm angenommen; Diagramm 3a zeigt $\sqrt{\xi}$ bei einer Betriebswellenlänge $\lambda_0 = 2$ m, Diagramm 3b für $\lambda_0 = 1$ m.

Man erkennt aus den Abb. 3, die mit $\sqrt{\xi(T,b/a)}$ die Amplitude des beschleunigenden elektrischen Feldes darstellen, dass bei wachsenden Teilchenenergien der Energiezuwachs pro Längeneinheit immer kleiner wird, sodass praktisch eine obere Energiegrenze für den Beschleuniger existiert. Zwar lässt sich die beschleunigende Feldstärke bei höheren Energien durch eine andere Wahl der Betriebswellenlänge vergrössern, doch wird dann wieder der Energiegewinn bei kleineren Teilchenenergien stark herabgesetzt.

Eine nähere Betrachtung der Abb. 4 zeigt, ersten Beschleunigerabschnitt viel grösser als bei anderen Beschleunigungsmethoden wäre†. Wir wollen daher im Folgenden die Beschleunigung von Protonen von 1 auf 10 MeV näher untersuchen.

Wie Gl. (18) erkennen lässt, kann $T(z)$ nur dann eindeutig festgelegt werden, wenn zuvor

† Das starke Ansteigen der Verluste bei kleinen Teilchenenergien macht sich möglicherweise dann bemerkbar, wenn mit einem Wendelleiter noch schwerere Teilchen (z.B. einfach geladene Atomionen) auf mässige Energien beschleunigt werden sollen. Eine Beschleunigung solcher Teilchen im Energieintervall von T_0 bis T_1 würde nach (17) einer Protonenbeschleunigung im Intervall von T_0/M_a bis T_1/M_a entsprechen, wenn M_a die Ruhemasse der Atomionen bedeutet. Die Extrapolation der in Abb. 4 dargestellten Kurven lassen bei diesen kleinen Vergleichsenergien erhebliche Verluste im Wellenleiter erwarten.

a in Abhängigkeit von z bekannt ist. Die Lösung des Wicklungsproblems enthält demnach einen willkürlichen Freiheitsgrad, dessen Festlegung innerhalb der technischen Möglichkeiten vor allem durch die gewünschten Eigenschaften des Beschleunigers bestimmt wird.

Will man z.B. einen gepulsten Beschleuniger hoher mittlerer Strahlintensität bauen, so tritt das Problem der Kühlung des Wendeldrahtes

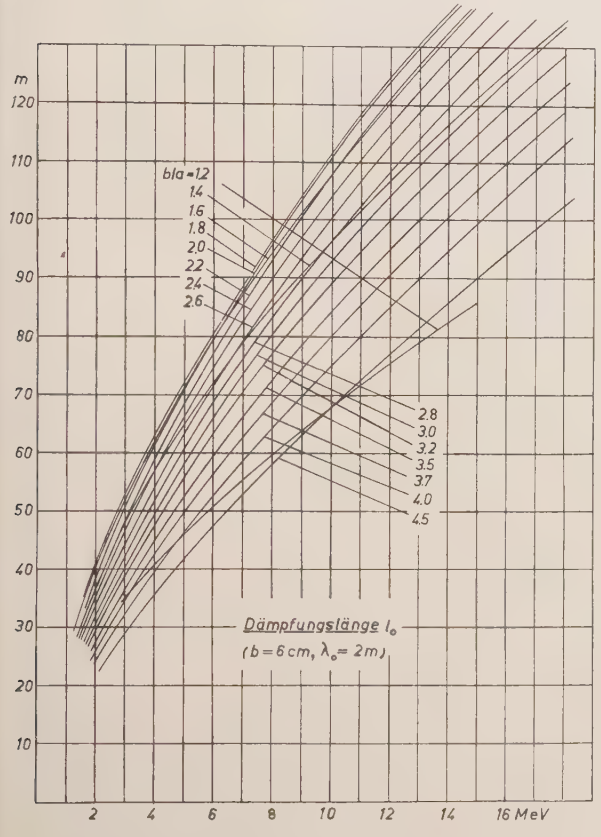

Abb. 4. Dämpfungslänge l_0 als Funktion der Protonenenergie mit b/a als Parameter.

bei der erforderlichen grossen Impulsfolge in den Vordergrund†. Wegen der unvermeidlichen Wasserkühlung muss der Wendeldraht daher eine gewisse lichte Weite aufweisen, sodass der Wendelradius a aus technischen Gründen nur bis zu einer unteren Grenze $a_{\min}$ verkleinert werden kann. Daneben wird zur Vermeidung von elektrischen Überschlägen ein Windungsabstand $s_{\min}$ vorhanden sein müssen. Nimmt man diese Minimalwerte bei einem Drahtdurchmesser von $d = 8$ mm etwa mit $s_{\min} = 10$ mm und $a_{\min} = 20$ mm an, so gibt es für Teilchenenergien T grösser als 1 MeV zulässige Wertepaare von a und s, wie sie in Abb. 5 für einen Aussenleiterradius $b = 6$ mm und eine Betriebswellenlänge $\lambda_0 = 2$ m dargestellt sind. Da nach den vorangegangenen Ausführungen (vergl. Abb. 3) kleine Wicklungsradien a generell grosse beschleunigende Feldstärken liefern, wird man beim Bau eines Wendellinearbeschleunigers versuchen, den Wicklungsradius über die gesamte Beschleunigerlänge so klein wie möglich zu halten. Abb. 5 zeigt nun, dass am Beginn des Beschleunigers ($T = 1$ MeV) der kleinste

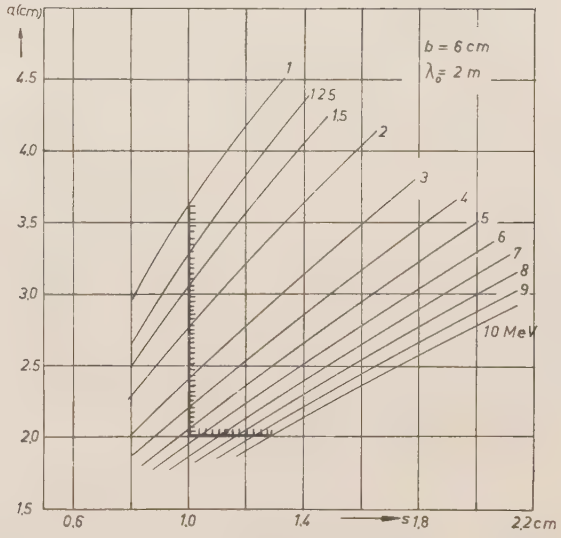

Abb. 5. Variation der geometrischen Daten a, s bei Veränderung der Protonenenergie.

zulässige Radius der zu $s = s_{\min}$ gehörende Wert ist, und dass man auch für den anschliessenden Beschleunigerabschnitt den minimalen Windungsabstand beibehalten wird. Dies ist möglich bis zu einer Stelle z, bei der Wicklungsradius a auf den noch zulässigen Grenzwert $a = a_{\min}$ abgesunken ist ($T = 5.3$ MeV in unserem Zahlenbeispiel). Hier anschliessend kann man nun bei festgehaltenem $a = a_{\min}$ den Windungsabstand gemäss Abb. 5 erhöhen und gelangt für eine Endenergie von 10 MeV

† Rechnet man mit einer Impulsdauer von 1 msec, so würde bei einer Senderleistung von 1 MWatt und einer Impulsfolge von 10 Impulsen/sec eine Verlustleistung von 10 kWatt auftreten, die zum überwiegenden Teil als Joulesche Wärme im Wendeldraht entsteht.

bei den gewählten Daten auf einen Windungsabstand von 12.8 mm Ende des Beschleunigers.

Eine solche Wicklung der Wendel hat den Vorteil, dass die beschleunigende Feldstärke grösser ist, als bei irgend einer anderen Wahl; Daneben bietet sie noch praktische Vorteile, denn eine Wendel mit stückweise konstantem a und s ist mechanisch leichter herzustellen als eine Wendel, bei der sich a und s gleichzeitig ändern.

Sieht man dagegen von einer hohen Strahlintensität ab, so kann der Wendeldrahtdurchmesser so dünn gewählt werden, dass der zulässige Wert von $a_{\min}$ schon am Anfang des Beschleunigers gewickelt werden kann, ohne dass gleichzeitig auch der Windungsabstand schon den zulässigen Minimalwert erreichte. In diesem Fall kann man den zur Verfügung stehenden Freiheitsgrad so festlegen, dass die Verluste im Wendeldraht möglichst klein werden (vergl.[7]).

Die Lösung des Integralgleichung (18) unter den obigen Annahmen über die Wicklungsparameter a und s kann mit Hilfe der Diagramme 3a und 4 und der in Abb. 5 dargestellten Dispersionsbeziehung (12) näherungsweise durchgeführt werden, wenn man die beiden Integrale der Gl. (18) durch endliche Summen approximiert. Für den Energiegewinn auf der Strecke von $n\Delta z$ bis $(n+1)\,\Delta z$ kann für hinreichend kleines Δz gesetzt werden:

$$T(n+1) = T(n) + e\cos\phi\sqrt{S_0}\cdot \Delta z\sqrt{\xi_n}\exp\left(-\tfrac{1}{2}\sum_0^n \frac{\Delta z}{l_0^{(\nu)}}\right) \qquad (19)$$

wenn ξ_ν und $l_0^{(\nu)}$ die Werte von ξ und l_0 an den Stellen $z = \nu\Delta z$ bezeichnen. Ist $T(n)$ bekannt, so wird aus Abb. 5 zunächst der zugehörige Wert von a (oder b/a) ermittelt. Damit sind beide Argumente der Funktionen ξ und l_0 bekannt und die Ermittlung von $T(n+1)$ nach (19) liefert den Anfangswert für den nächsten Schritt. Die Näherung (19), die nur innerhalb der Genauigkeit der Pierce'schen Theorie einen ersten Überblick vermitteln soll, lässt sich natürlich durch genauere numerische Methoden weitgehend verfeinern.

[6]) J. P. Blewett, CERN-Symposium (1956) p. 156.
[7]) R. Servranckx, Diss. Brüssel (1954).

Abb. 6 zeigt den auf diese Weise graphisch ermittelten Verlauf der Teilchenenergie T im Beschleuniger für zwei verschiedene Anfangsleistungen $S_0 = 1$ MWatt bzw. 2 MWatt. Die Betriebswellenlänge λ_0 war mit 1 m, der Aussenleiterradius b mit 9 cm und $\cos\phi$ mit 0.7 angenommen worden. Als Integrationsschrittweite Δz wurde $\Delta z = 0.5$ m gewählt.

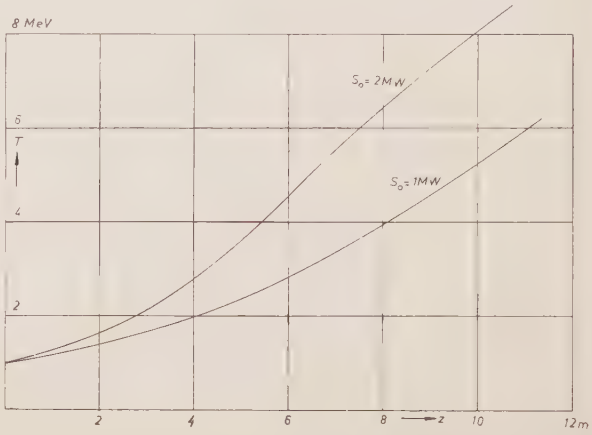

Abb. 6. Protonenenergie T nach Durchlaufen der Strecke z für 2 verschiedene Werte des Anfangsleistungsflusses S_0 ($b = 9$ cm, $\lambda_0 = 2$ m, $\cos\phi = 0.7$).

Es ist von Interesse wie sich der Kurvenverlauf ändert, wenn man zu anderen Betriebswellenlängen oder zu anderen Aussenleiterradien übergeht. Abb. 7 zeigt dazu die Teilchenenergie T in Abhängigkeit von der durchlaufenen Weglänge z für verschiedene Aussenleiterradien b, Abb. 8 die Länge L eines 10 MeV-Beschleunigers als Funktion von b. Wie zu erwarten war, steigt die zur Erzielung einer bestimmten Teilchenenergie notwendige Beschleunigerlänge L bei Verkleinerung des Aussenleiterdurchmessers monoton an, sodass zunächst ein möglichst grosser Aussendurchmesser naheliegen würde. Geht man aber von der Annahme aus, dass die Kosten eines Wendelbeschleunigers im wesentlichen proportional zu seinem Volumen sind, so dürfte, wenn eine vorgebene Teilchenenergie z.B. 10 MeV erreicht werden soll, eine Verlängerung des Beschleunigers innerhalb gewisser Grenzen günstiger sein als eine Vergrösserung des Aussendurchmessers. Ein Beschleuniger für 10 MeV müsste auf diese

Weise bei minimalen Kosten einen Aussenleiterradius von etwa 5 cm aufweisen. In theoretischer Hinsicht dürften allerdings bei eng anliegenden Aussenleitern die Ergebnisse

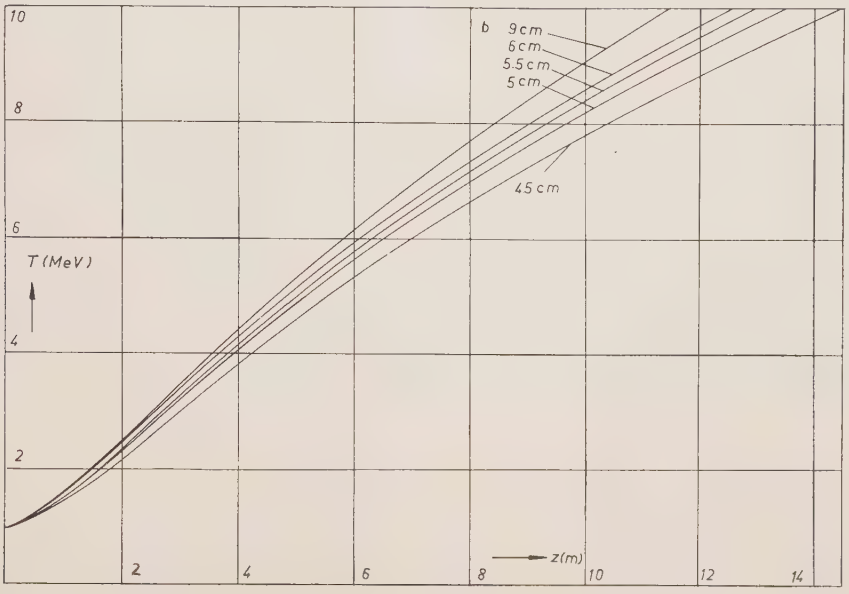

Abb. 7. Protonenenergie T nach Durchlaufen der Strecke z für verschiedene Werte des Aussenleiterradius b ($\lambda_0 = 2$ m, $S_0 = 2$ MWatt, $\cos\phi = 0.7$).

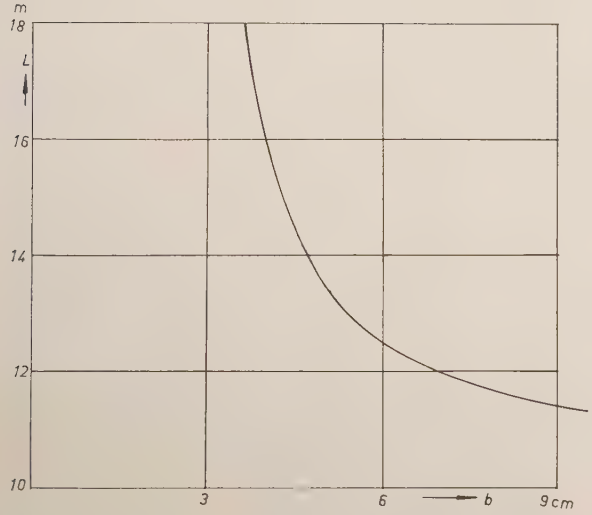

Abb. 8. Länge eines 10 MeV-Protonenbeschleunigers als Funktion des Aussenleiterradius b. ($\lambda_0 = 2$ m, $S_0 = 2$ MWatt, $\cos\phi = 0.7$, Einschussenergie 1 MeV).

der hier zugrundeliegenden Pierce'schen Theorie wegen des endlichen Drahtdurchmessers in Frage gestellt sein.

Abb. 9 enthält den Verlauf der Beschleunigerlänge in Abhängigkeit von der Betriebswellenlänge λ_0. Die Darstellung zeigt, dass zu vorgegebener Einschuss- und Endenergie ein optimaler Wert der Betriebswellenlänge existiert. Im vorliegenden Fall wäre etwa $\lambda_0 = 1.5$ m zu wählen. Ein solcher Beschleuniger würde bei einem Aussenleiterdurchmesser von 12 cm et 12 m lang werden und ein Volumen von ca. 0.15 m³ besitzen. Der Vergleich mit den

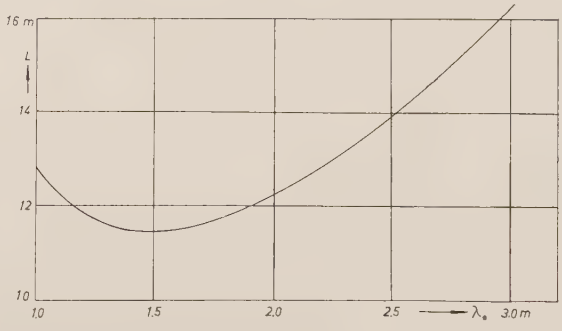

Abb. 9. Länge eines 10 MeV-Protonenbeschleunigers als Funktion der Betriebswellenlänge λ_0 ($b = 6$ cm, $S_0 = 2$ MWatt, $\cos\phi = 0.7$, Einschussenenergie 1 MeV).

entsprechenden Daten eines Driftröhrenbeschleunigers vergleichbarer Anfangs- und Endenergie[6]) zeigt, dass in dem betrachteten Energiebereich der Wendelbeschleuniger eine

praktisch durchaus vertretbare Lösung zur Beschleunigung schwerer Teilchen darstellt.

Zum Schlusse seien mit Hilfe der vorangegangenen Diagramme noch einige kurze Ausführungen über Toleranzen bei der Wicklung sowie über Kühlungsprobleme eines Wendellinearbeschleunigers gemacht.

Abb. 5, die im a,s-Diagramm die Variation der Wicklungsparameter während der Beschleunigung zeigt, kann zu einer Abschätzung der Toleranzen bei der Wendelherstellung herangezogen werden. Betrachten wir als Beispiel den Energiebereich zwischen 8 und 9 MeV, so

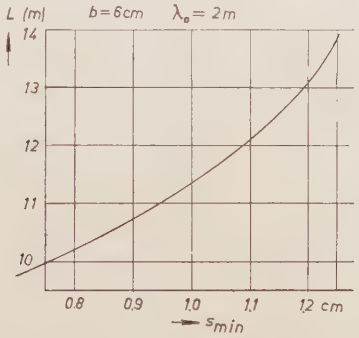

Abb. 10. Länge eines 10 MeV-Protonenbeschleunigers in Abhängigkeit des minimalen Windungsabstandes s_{min}.

gehört dazu eine Änderung des Windungsabstandes s um 6 mm, die nach Abb. 7 auf einem Beschleunigerabschnitt von ca. 1.5–2 m gleichmässig auf etwa 100 Windungen zu verteilen sind. Die Genauigkeit, mit welcher die einzelnen Windungen der Wendel justiert sein müssen, beträgt also einige 1/100 mm, was sich mit mechanischen Hilfsmitteln gerade noch erreichen lässt. Ähnliche Betrachtungen gelten auch für die Genauigkeit bei der Einhaltung des Wendelradius a.

Die im Wendeldraht entstehende Joule'sche Wärme kann, wie oben erwähnt, durch Wasserkühlung abgeleitet werden, wobei zu beachten ist, dass die geeignete Dimensionierung des Wendeldrahtdurchmessers sowohl die erreichbare Intensität des Teilchenstrahls, als auch die Güte der Beschleunigereigenschaft beeinflusst. Wählt man beispielsweise, um die Wärmeabführung zu erleichtern, den Drahtdurchmesser sehr gross, dann wird man den minimalen Windungsabstand s_{min} und nach Abb. 5 auch den minimalen Radius a_{min} vergrössern müssen, sodass nach den vorangegangenen Betrachtungen die beschleunigende Feldstärke durchweg verkleinert und damit der Wirkungsgrad des Beschleunigers verschlechtert wird. Beachtet man andererseits, dass die erreichbare Impulsfolge, soweit sie nicht durch übermässige

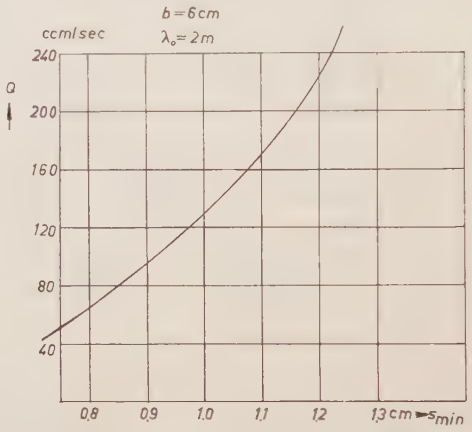

Abb. 11. Wasserdurchfluss für einen 10 MeV-Protonenbeschleuniger in Abhängigkeit des minimalen Windungsabstandes s_{min}.

Erwärmung der dielektrischen Stützen begrenzt wird, praktisch nur von der aus dem Wendeldraht abgeleiteten Wärmemenge abhängt, so kann eine gute Beschleunigereigenschaft nur durch den Verzicht auf hohe mittlere Intensität des Teilchenstrahls erkauft werden. Die beiden Abb. 10 und 11 sollen diesen Sachverhalt anschaulich machen. Abb. 10 zeigt die Länge eines 10 MeV-Beschleunigers in Abhängigkeit von s_{min}. Abb. 11 gibt dazu den Wasserdurchfluss bei einem zugrundeliegenden Wasserdruck von 20 Atm ebenfalls als Funktion von s_{min} an.

Wir danken der Deutschen Forschungsgemeinschaft für die finanzielle Unterstützung bei der Durchfhürung der vorliegenden Untersuchung.

Besonderen Dank schulden wir Herrn Professor Dr. Dänzer, der die Anregung zu dieser Arbeit gab, für sein reges Interesse.

NUCLEAR INSTRUMENTS AND METHODS 4 (1959) 213–220; NORTH-HOLLAND PUBLISHING CO.

AN EXPERIMENTAL STUDY OF THE LINEAR PINCH STABILITY

TAGE SUNDSTRÖM and SVEN SVENNERSTEDT

Institute of Physics, Uppsala, Sweden

Received 5 March 1958

The time to the first bounce of the dynamic pinch has been measured and compared with the formula derived by Rosenbluth. The theoretical dependence on gas pressure and electric field strength is verified. A coil system is described which has been used to detect kink instabilities. When an axial magnetic field of sufficient strength has been applied, it has become impossible to detect the kink instabilities which are shown to destroy the pinch in zero and moderate magnetic fields. Stability observations have been carried over several periods of the discharge. This revealed that the plasma performs a contraction and seems to be stable in the subsequent periods also. Finally an investigation has been made of the pressure dependence of the electro-mechanical oscillation which is performed by the plasma sheath before reaching equilibrium where the axial and azimuthal magnetic fields balance.

1. Introduction

In the field of controlled fusion research, great interest has been paid to pinched electrical discharges, yet still this particular concept is the subject of much scientific work. When a heavy current discharge is initiated in a tube with low pressure gas, the plasma is constricted by the forces of the self-magnetic field. If the plasma conductivity is sufficiently high, the sudden application of an electric voltage produces a thin current layer at the tube wall, and this plasma sheath is accelerated towards the axis of the tube.

However, the lifetime of this dynamic pinch is limited, because it is inherently unstable. The confinement of particles is lost in a very short time. Today a rather exhaustive theory exists, which describes the different modes of instabilities and possible means of inhibiting them. For the present discussion, theoretical references may be found in the works of Kruskal and Schwartzschild[1]), Kruskal and Tuck[2]), Rosenbluth[3]), Tayler[4]), and Shafranov[5]).

[1]) M. Kruskal and M. Schwarzschild, Proc. Roy. Soc. A **223** (1954) 348.

[2]) M. Kruskal and J. L. Tuck, Proc. Roy. Soc. A **245** (1958) 222.

[3]) M. Rosenbluth, Los Alamos Report, L.A. 2030.

[4]) R. J. Tayler, Proc. Phys. Soc. B **70** (1957) 1049.

[5]) V. D. Shafranov, Atomnaya Energya **1**, 5 (1956) 38.

When a small pertubation in the equilibrium state of a pinched discharge grows, the plasma becomes unstable. The normal mode of mathematical treatment of instabilities is based on perturbations which can be described by equations with solutions containing the factor $\exp(ikz + im\theta + \omega t)$. ω is a constant proportional to the rate of growth of an instability where the type of instability is determined by the positive integer m. k is the wave number in the z direction. The $m = 0$ and $m = 1$ modes are the familiar sausage type and kink type instabilities. In a dynamic pinch all wavelengths of these types are unstable with increasing rate of growth for decreasing wavelengths. The modes with $m \geq 2$ have a much lower rate of growth, and accordingly the former types become predominant.

The influence on a plasma of a longitudinal magnetic field combined with a close-fitting cylindrical conductor outside the discharge tube has been thoroughly investigated. Under these conditions the behavior of the pinch is fundamentally changed. If the plasma conductivity is infinite, the axial magnetic flux inside the tube will be trapped within the sheath during the contraction. A sharp boundary is formed between the central region with the axial magnetic field and the outer region with the

azimuthal field. The contraction proceedes until an equilibrium is reached, where the external magnetic pressure equals the sum of the internal magnetic pressure and the plasma pressure. If the latter is neglected, the equilibrium sheath radius, r, is given by

$$r = \frac{2\pi R_0^2 B_{z0}}{\mu_0 I} \text{ (MKSA-units)}$$

R_0 is the tube inner radius, B_{z0} the initial magnetic field, and I the discharge current.

According to the theories referred to above, it is possible to suppress the different m modes of instabilities. It turns out that the $m = 1$ mode is most difficult to stabilize. Once this type is removed the $m \neq 1$ perturbations are inhibited, because they require a lower field strength for stabilization. If the external axial magnetic field strength and the gas pressure are zero, the condition for stability is that the radial compression must not exceed 5:1. For compressions greater than this, no pinch can be stable.

However, so far ideal conditions have been assumed i.e. negligible gas pressure, infinite conductivity, and the formation of an infinitely thin current layer. As far as gas pressure is concerned, the approximation is reasonable. Actually it forms only a small part of the total pressure in strong magnetic fields. The assumed infinite conductivity, of course, is not met in practice. Therefore there will be an amount of axial magnetic flux left out-side the plasma column as it contracts. A further contribution to the external magnetic field strength will also be given in practice by the flux which initially fills the volume between the cylindrical conductor and the tube inner radius. In fact stability depends critically on the absence of axial field outside the pinch. If for example this field strength is half that of the azimuthal field strength at the plasma suffface, the maximum compression permissible is only 1.8:1.

Nor is the assumption of a thin current layer fulfilled in practical experiments. Probe measurements have shown that the current has a certain volume distribution[6,7,8]). Theoretical treatment of a pinched plasma with diffuse boundaries shows that stability is much more difficult to achieve under these conditions[9,10,11]). In the experiments reported in this work, however, it has been impossible to detect kink instabilities when a sufficiently high axial magnetic field has been applied.

2. Apparatus

The experimental set up used in the present work is described earlier[12,13]) but a few modifications have been made. The energy is stored in a condensor bank of 60 μF capacity, and a triggered air spark gap is used as a switch. The discharge tube arrangement is shown in fig. 1. The porcelain tube has a length of 60 cm and an inner diameter of 28 cm. The ratio of the inner radius of the return conductor to the inner radius of the tube is 1.16. The longitudinal magnetic field is generated by a solenoid, which is longer than the tube, so that the difference between the magnetic field strength in the center of the tube and at the electrodes is less than 6%. The solenoid is fed from a selenium rectifier which gives a power of 60 kW. The preionization is obtained by means of a radio frequency generator coupled to the gas by two single turn coils, wrapped around the tube. The preionization, the magnetic field, and the triggering spark are programmed by an electromechanical timer unit.

The coil system for the detection of kink instabilities consists of a ϕ_z-loop around the tube and two diametrically opposite $B\theta$-coils

[6]) L. C. Burkhardt, R. H. Lovberg and J. A. Phillips, Nature **181** (1958) 224.

[7]) S. A. Colgate, J. P. Ferguson and H. P. Furth, The Stabilized Pinch, 1958 Geneva Conference, P/369.

[8]) L. C. Burkhardt and R. H. Lovberg, Field Configurations and Stability Studies of a Linear Discharge, 1958 Geneva Conference, P/2395.

[9]) B. R. Suydam, Stability of a Linear Pinch, 1958 Geneva Conference, P/354.

[10]) M. Rosenbluth, Theory of Pincheffect-Stability and Heating, 1958 Geneva Conference, P/347.

[11]) R. J. Tayler, The Stability of a Constricted Gas Discharge, 1958 Geneva Conference, P/33.

[12]) S. Berglund, R. Nilsson, P. Ohlin, K. Siegbahn, T. Sundström and S. Svennerstedt, Nuclear Instruments **1** (1957) 233.

[13]) P. Ohlin, K. Siegbahn, T. Sundström, and S. Svennerstedt, Nuclear Instruments **3** (1958) 237.

inside the return conductor. The voltage is measured by a resistive voltage divider, and the rate of change of current by a small pick-up coil, placed above the air spark gap.

In the present work we have principally been interested in achieving complete suppression of gross instabilities by means of high magnetic fields. Discharges have been made at 10, 15, 20, and 25 kV initial voltage which correspond to maximum currents from 200 to 500 kA. The gas pressure has been varied between 30 and 150 microns and the maximum axial magnetic field has been 1900 gauss.

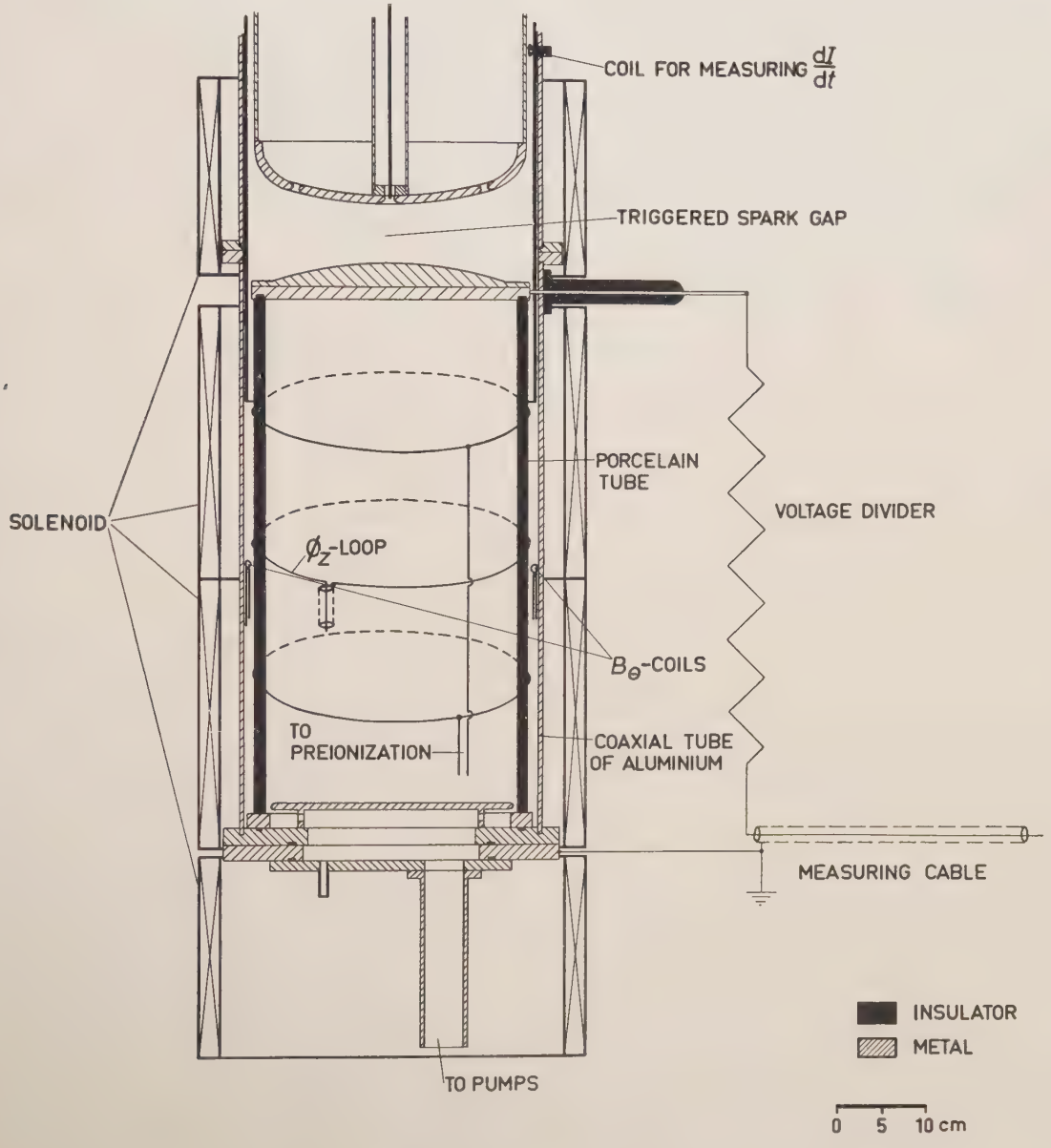

Fig. 1. Drawing to show the discharge tube assembly with the measuring coils and the magnetic field generating solenoid.

3. Experiments and Discussion of Results

The dynamic pinch was the subject of the very first experiments in the field of fusion research in this institute[12]). Also the partly stabilized pinch has been investigated earlier[13]).

However, the dependence of the contraction time of the dynamic pinch as a function of gas pressure and electric field strength is part of the present work. In the theory for the dynamic pinch, Rosenbluth[14]) gives a formula for the time to the first pinch, which is

$$t_p = R_0 \sqrt[4]{4\pi\rho/E^2} \text{ (e.m.u.)},$$

where ρ is the gas density and E the voltage gradient across the tube. In the fig. 2 t_p is plotted against $\sqrt[4]{p_0/V^2}$, where p_0 = initial gas pressure and V = *mean* voltage across the tube. The direct computation of t_p from the formula gives a discrepancy of less than 12%, but the

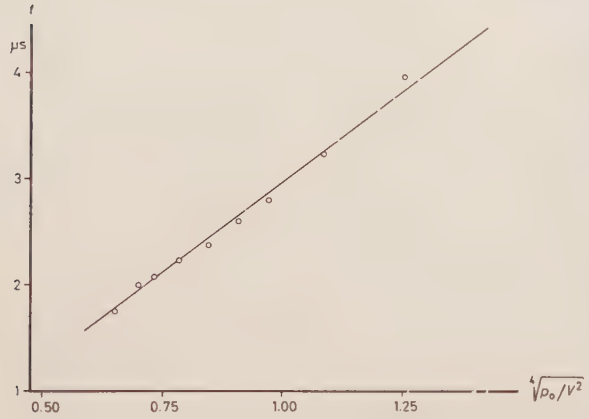

Fig. 2. Time to first bounce of the dynamic pinch as a function of initial gas pressure (in microns) and mean voltage across the tube (in kV).

observed time is always longer than the computed. A calculation of errors shows that it is possible to account for this discrepancy as an addition of uncertainties in the measured quantities. However, as it seems to be a systematic deviation, a further explanation is probably needed. Curran *et al.*[15]) who have obtained the same result (although the amount of discrepancy is not reported) make the suggestion that the rather long, measured time could possibly be due to wall hang up. However, the linearity of the diagram is a check of the theory as far as concerns the dependence of gas pressure and electric field strength.

The summary of the theoretical discussion of hydromagnetic instabilities gives that the $m = 1$ instability is the hardest of all to eliminate, and therefore a criterion of a stabilized discharge should be that no kink instabilities develop. Several investigators have studied this instability. Colgate *et al.*[7]) have detected the kink and also succeded in suppressing it with a sufficiently strong magnetic field. Also the dependence of the B_{z0}-field external to the pinch has been investigated in the same work. The ratio of the inner radius of the conducting shell to the inner radius of the tube, δ, is a measure of the extent to which a B_z-field exists out-side the plasma column. Colgate *et al.* used two different values of δ, viz. 1.3 respectively 1.1. With $\delta = 1.1$, stability was attained at lower field strengths than at $\delta = 1.3$. In Los Alamos[16]) much the same work has been performed. The $m = 1$ instability has been clearly detected, generally at the time of current maximum. However, in these two investigations smaller tubes have been used than in the present, and in fact the tube dimensions affect the growth time of instabilities.

In the coil system used in the present work, the ϕ_z-loop (see fig. 1) measures the rate of change of ϕ_z,—the total axial magnetic flux in the tube. The two small $B\theta$-coils were coupled to a differential amplifier of an oscilloscope and were balanced against one another so as to give no signal for a discharge where the cylindrical symmetry is conserved. The check of that was performed by using a metallic cylindrical conductor instead of the porcelain tube. Thus, as long as the pinch column remains centered along the tube axis, no signal will be displayed on the oscilloscope, while a signal indicates a motion of the pinch proper in the radial direction. The $m = 1$ instability gives a helical shape to the pinch which causes a sudden change in the ϕ_z-flux. Furthermore the $B\theta$-coils will give in most cases a signal at the onset of the kink.

[14]) L. M. Rosenbluth, Los Alamos Report, L.A. 1850.

[15]) S. C. Curran, K. W. Allen, H. A. B. Bodin, R. A. Fitch, N. J. Peacock and J. A. Reynolds, Studies of High Current Gas Discharges at High Rates of Build up. 1958 Geneva Conference, P/1460.

[16]) H. J. Karr, Experimental studies of the pinch effect; The Plasma in a Magnetic Field, ed. by R. K. M. Landshoff.

These pulses have seemed to be less reproducible than the ϕ_z-signals, and this is reasonable because of the violent turbulences which are caused by an instability.

In case of zero magnetic field, kink instabilities are detected usually at about the third pinch, though not with exact reproducibility. Fig. 3 (upper curve) shows an example of a $d\phi_z/dt$ signal for zero magnetic field; the pulse appears at the time of the third contraction. Generally the ϕ_z-pulse is short and the wriggling of the

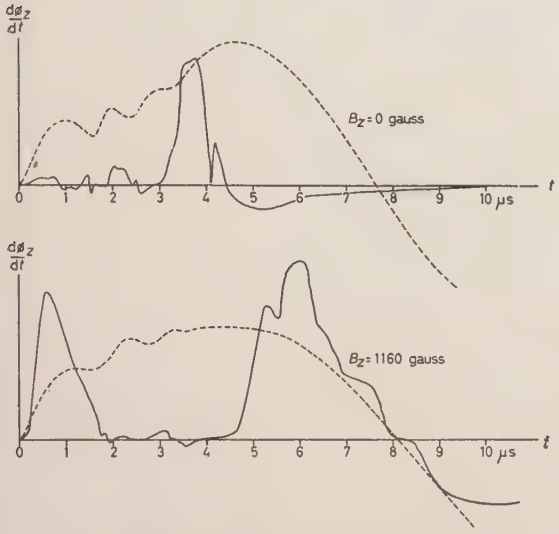

Fig. 3. $d\phi_z/dt$-oscillograms indicating kink instabilities for two different cases. The dashed lines are the corresponding current curves. $I_{max} = 500$ kA; $p = 30$ microns.

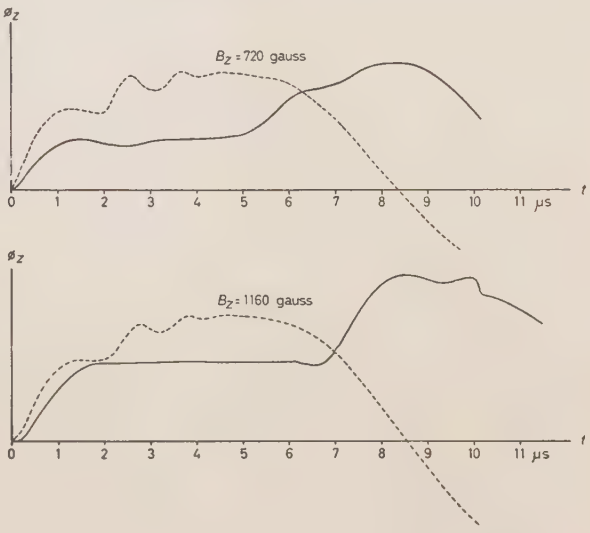

Fig. 4. ϕ_z-curves and corresponding current curves for two different values of B_{z_0}. $I_{max} = 400$ kA; $p = 40$ microns.

pinch seems to be equally probable in both directions. This gives positive and negative signals respectively.

When discharges are made with an axial magnetic field, the appearance of the ϕ_z-signal is changed (fig. 3, lower curve). At the onset of the discharge a pulse is displayed, which indicates an increase of the ϕ_z-flux through the loop as long as the inward motion of the current layer proceeds. During this time the magnetic flux that initially fills the volume between the conductor and the inner tube wall, spreads to the volume between the conductor and the pinch surface. The integral of this pulse increases with increasing field strength, while the length always coincides with the time to the first contraction. After this the ϕ_z-flux through the loop is constant, until—in moderate magnetic fields—a further pulse is displayed, generally after current maximum. The polarity of this second pulse is always the same as that of the first one. This means that the helix prefers a certain direction, viz. so as to further increase the magnetic flux through the loop. As a rule the second pulse is greater than the first one and this leads to a striking change also in the integrated signal. In fig. 4 are shown two integrated ϕ_z-curves for two different B_{z_0}-fields. The height of the signals at the latter part of the curves cannot be explained by an increased flux through the loop from a higher compression —even if infinite—and thus the flux must be created in some other way.

At the same time as the z-flux is suddenly enhanced or a little earlier, a pulse, which indicates the difference between the $B\theta$-coils is often displayed on the oscilloscope. Fig. 5 shows integrated signals for (1) the difference between $B\theta$-coils (upper curve) and (2) the ϕ_z-loop (second curve), together with the current curve. A pulse is displayed on the upper curve after the second contraction, and a little later a sharp increase in ϕ_z-flux is seen on the second curve. This has to be interpreted as a disturbance of

the azimuthal symmetry of the pinch column by a pertubation, which is growing to a kink instability. This one causes the anomalous rise in magnetic flux in the axial direction.

When the magnetic field is increased sufficiently, it is possible to inhibit the large pulse, which indicates an unstable pinch, unless the discharge current is too high. At a discharge current of 300 kA, a magnetic field strength of 1160 gauss is sufficient for achieving stability. If infinite conductivity and sharp boundaries are assumed, an initial magnetic field of 860

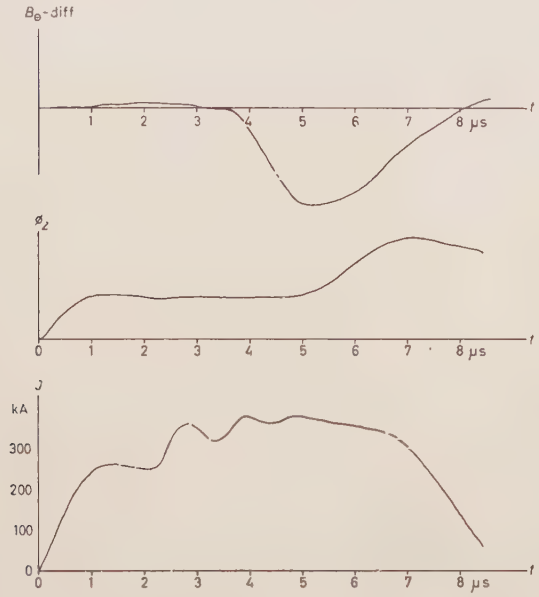

Fig. 5. Oscillograms showing (1) difference between B_θ-coils, (2) ϕ_z-loop signal and (3) total current. $I_{max} = 400$ kA; $p = 40$ microns; $B_{z0} = 1900$ gauss.

gauss should give a compression of 5:1, that is, it should conserve stability. As expected this figure is too small, for as mentioned above there are several reasons for the external axial field not being zero. A field strength of 1900 gauss has prooved to give stability to a discharge with a current of 400 kA, while 500 kA cannot be stabilized with the maximum field available.

At the first stage of the experiments, it was rather confusing to find a pulse from the ϕ_z-loop at about the time of zero current. However, carrying the observations over several periods of the discharge, we found that the pulse was the first half cycle of an oscillation with a frequency equal to twice the frequency of the discharge circuit. The integrated ϕ_z-signal is shown in fig. 6, together with the current curve. The first half cycle of this curve is an example of a ϕ_z-signal, which is *not* subject to the second sharp increase in z-flux, that is, kink instabilities do not develop. Moreover a maximum of z-flux within the loop is found at every current peak, positive and negative. Note on the figure the coincidence between the first maxima on the upper curve and the indications of pinches on the current curve.

The interpretation of this result is somewhat

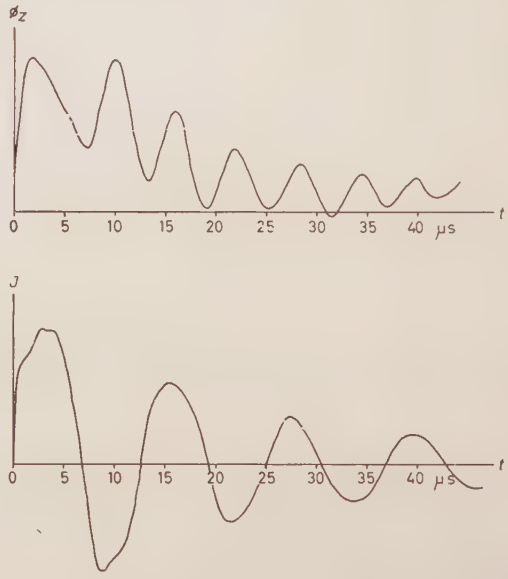

Fig. 6. ϕ_z and total current curves, extended over several periods, $I_{max} = 300$ kA; $p = 40$ microns; $B_{z0} = 1900$ gauss.

delicate, but it seems certain that a trapping of the axial magnetic flux occurs also in the subsequent periods, and consequently the plasma performs a contraction at every current peak. Furthermore the plasma is probably stable in a gross sort of way. If the observed phenomenon is significant to the problems involved in pinch research, the degree of confinement attained is interesting. However, it is precarious to make any statement about this, especially at the time of zero current. In fact it is both predicted[17]) and verified[18]) that at that very moment closed

[17]) S. A. Colgate and H. P. Furth, UCRL Report 5086.
[18]) L. C. Burckhardt and R. H. Lovberg, Nature **181** (1958) 228.

current loops exist within the tube. These represent currents as large as one third of the

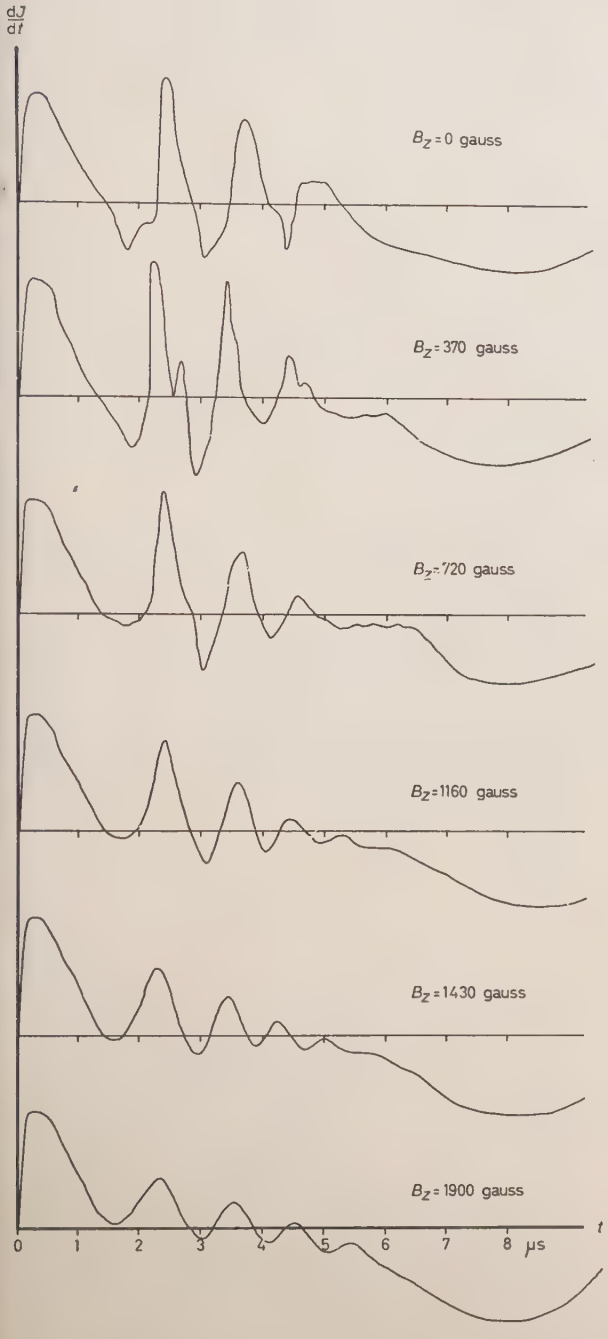

Fig. 7. Sequence of dI/dt oscillograms for increasing B_{z0}, showing the dynamic pinch and the change to the stabilized pinch with the electro-mechanical oscillation. $I_{max} = 400$ kA; $p = 40$ microns.

original maximum current. The fact that the plasma is able to trap the magnetic flux for several periods, suggests a comparatively good conductivity during all this time. An average decrease of z-flux through the loop can be observed on the figure as the oscillation proceeds. This possibly indicates a magnetic field diffusion.

In a stabilized pinch the inward motion of the current sheath is counteracted by a force which increases as the compression proceeds. Before the equilibrium is finally reached, the current sheath performs an electro-mechanical oscillation, the inertia of which is the mass of the gas in the layer. The frequency has been shown to be $\omega = (B_{z_0}^2 R_0^4 / 4\pi r^5 \rho_s)^{\frac{1}{2}}$, where ρ_s is the surface density of the layer.

This type of oscillation has been studied by means of probe measurements at Los Alamos[8]), and the result has been used to evaluate the density. In the present work it has been clearly detected both by the dI/dt-measurements of total current and by voltage measurements. The relatively small inductance external to the tube is a reason why even small changes in the inductance of the tube can appreciably affect the total current and voltage. Fig. 7 shows a series of dI/dt signals for increasing B_{z_0}-fields up to the maximum field, 1900 gauss. The first curves show the behavior of the dynamic pinch and the partly stabilized one with large and irreproducible contractions and expansions, usually two or three bounces. However, when the B_{z_0}-field is increased, the amplitude is decreased and the curves become more smooth,

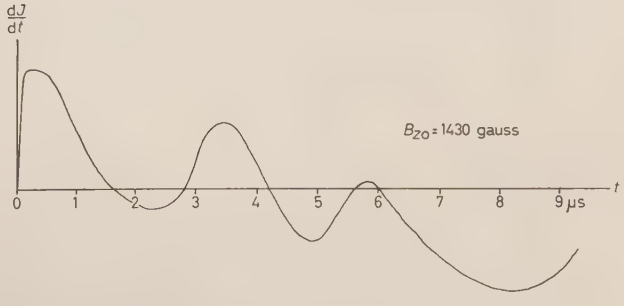

Fig. 8. dI/dt curve of a stabilized pinch showing the oscillation at higher pressure. $I_{max} = 400$ kA; $p = 150$ microns.

that is the amplitude of the plasma sheath motion is decreased. At the two highest field strenghts the stability measurements indicate

stability against kinks. The curve in fig. 8 shows the same oscillation, with a considerably lower frequency, because of the high gas pressure used in this case. The surface density of the current sheath is reasonably proportional to the initial gas density, p_0. The dependence of ω on $1/\sqrt{p_0}$, other parameters being constant, is seen in fig. 9 to be linear and this shows agreement with the formula.

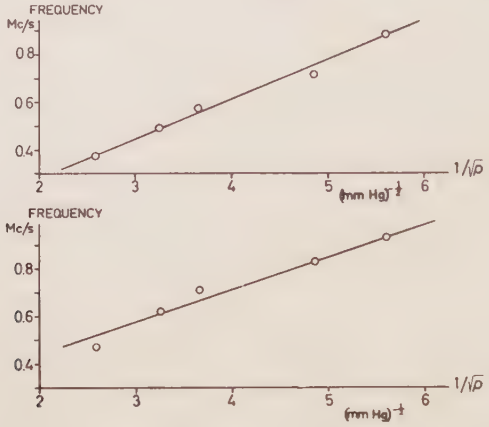

Fig. 9. The frequency of the oscillation of the stabilized pinch as a function of initial gas pressure. $B_{z0} = 1900$ gauss; $I_{max} = 400$ kA resp. 500 kA.

This work was initiated by Professor Per Ohlin and Professor Kai Siegbahn. We wish to express our sincere gratitude for their encouraging interest and support. Furthermore we wish to thank Mr. Lars Gramstad and Mr. Lennart Lang for valuable technical assistance. The work has been sponsored by ARDC through its European office and by the Swedish Atomic Committee, the support of which is gratefully acknowledged.

NUCLEAR INSTRUMENTS AND METHODS 4 (1959) 221–227; NORTH-HOLLAND PUBLISHING CO.

A NEW METHOD FOR TRACK ANGLE MEASUREMENT IN A GRIDDED IONIZATION CHAMBER

U. FACCHINI, E. GATTI † and F. PELLEGRINI

C.I.S.E.'s *Laboratories, Milano*

Received 31 March 1959

A simple method of handling the information at the collector of a conventional gridded ionization chamber is described. This method, based on the evaluation of the maximum of the current at the collector allows us to obtain a direct information on the angle formed by the tracks of the particles with the electric field. This maximum value is independent from the position of the track within the sensitive volume and from the energy of particles of identical mass.

The method allows us to obtain the collimation of the particles, the range-energie study, and possibly, the development of neutron spectrometers based on the energy of gas recoil, and the (n,p) and (n,α) studies in which the angular distribution of the emitted particles is involved.

1. Introduction

In normal ionization chambers, when used for measuring the energy of α particles, protons, etc., only a part of the whole information, delivered by the particle interaction with the gas filling, is utilized. In fact, the energy is measured by the number of ions or of electrons produced by the particles under study. On the other hand, the knowledge of the space distribution of the ion pairs, that is of the whole particle track, would make it possible to obtain the range, the specific ionization, the θ angle which the particles make with the direction of the electric field, and eventually the mass. Generally it is possible to get some of this additional information on the ionization track, because the charges formed drift along the lines of force of the applied electric field, without appreciable diffusion. In this work we shall describe a particularly simple method which allows us to obtain a measure of the angle formed by the particles with the direction of the electric field.

It is interesting to discuss briefly the works carried out by other Authors relative to the angle measurement of particles in ionization chambers, with the aim of comparing different methods.

† Politecnico of Milan and C.I.S.E.

Sherr and Peterson[1]) have measured the curve range-energy and the angle of the particles under study with respect to a direction using a parallel plate ionization chamber with electron collection. As it is known, in a uniform field the current to the electrodes in a parallel plate chamber at any time is:

$$i = \frac{q_+ w_+ + q_- w_-}{a}$$

where q_- and q_+ are the negative and the positive charges present at the time considered in the sensitive volume of the chamber, where a is the plate separation and w_+ and w_- are respectively the ion and electron drift velocities.

Sherr and Peterson have considered negligible the contribution of the positive charges ($w_+/w_- \approx 1/1000$) for which simply:

$$i = \frac{q_- w_-}{a}$$

q_- is equal to Q_0, total charge delivered by the ionizating particle, until the negative charges, corresponding to one extremity end of the track, begin to be collected by the anode, after which, at any time, q_- is equal to the charge distributed along the remaining part of the track, left between the plates of the chamber. Sherr and

[1]) R. Sherr and R. Peterson, Rev. Scient. Instr. 18 (1947) 567.

Peterson observed and photographed the current pulses obtained by differentiation of the voltage pulses appropriately amplified. The current pulse has the shape shown in fig. 1, whose variables

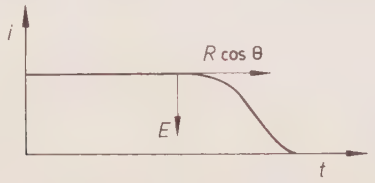

Fig. 1. Current pulse according to Sherr and Peterson.

time and current may be easily interpreted as the variables range-energy. From a number of events caused by identical particles, having the same energy, but different θ angles, pulse shapes of fig. 2 will be obtained; the constant part of the pulse was left out for simplicity in the figure.

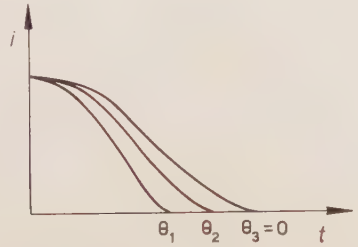

Fig. 2. Current pulse shapes for identical tracks at different angles according to Sherr and Peterson.

The study of a family of such pulses allows us to know those particles corresponding to $\theta = 0°$ and therefore to be able to know the range-energy curve and so also the mass of the particle.

Bochagov and co-workers[2]), J. Ogawa[3]), advised another method for obtaining an electrical collimation of the particles making a particular angle with respect to the lines of force in the electric field.

In a gridded chamber, as shown in fig. 3, and considering a source placed on the electrode at high voltage, the following maxima values of the amplitude of the voltages pulses detectable at the three different electrodes are given by:

$$V_1 = \frac{ne}{C_1}, \qquad V_2 = \frac{ne}{C_2}\left(1 - \frac{\bar{x}}{b}\cos\theta\right),$$

$$V_3 = -\frac{ne}{C_3}\left(1 - \frac{\bar{x}}{b}\cos\theta\right)$$

where by n we indicate the total number of ion pairs produced by the particle, by C_i we indicate the capacity of the electrode under study with respect to all others grounded, by $\bar{x}$ we indicate the distance between the center of gravity of the ions and the beginning of the particle track, by b the space between the grid and the high voltage electrode and by θ the angle between the track and the field.

Considering the pulse on the collector, which gives direct information on the energy of the particle and by comparing it appropriately with the corresponding pulse at the grid or with that

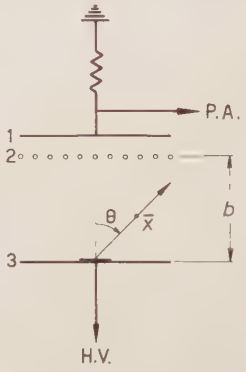

Fig. 3. Schematic drawing for illustrating the method of angle evaluation according to Bochagov and others, Ogawa, Valladas.

of the electrode 3, it is possible to obtain the required collimation.

Valladas[4]) used this method with a parallel plate ionization chamber with the aim of eliminating α particles making an angle θ larger than a certain value.

The work of Bertolini and Bettoni[5]) can be also mentioned: these Authors obtained the values of the range of α particles measuring at the oscilloscope the rise time of the voltage pulses given by collimated α particles parallel and perpendicular to the direction of the electric field.

Lastly we remember the special ionization

[2]) B. A. Bochagov, A. A. Vorob'ev and A. P. Komar, Soviet Physics (Technical Physics) 2 (July 1957) 1458.

[3]) J. Ogawa, Private communication.

[4]) G. Valladas, Rapport C.E.A. 483 (1955).

[5]) G. Bertolini and M. Bettoni, Nuovo Cimento 1 (1955) 644.

chamber of R. W. P. McWhirter and co-workers[6]), used to discriminate between He^3 and He^4 by measuring dE/dx and E.

2. Description of the Method

The method described in the present work is based on the fact that in a gridded chamber the current pulse to the collector is at any time proportional to the charge quantity which is present in the space between the grid and the collector; therefore the instantaneous current is:

$$i = \frac{w_-}{d} \int_x^{x+d\cos\theta} \sigma(x)\, dx \qquad (1)$$

where $\sigma(x)$ is the linear density charge along the track at the point x; x is measured from the end of the track, d is the grid collector spacing and θ is again the angle that the particles make with the direction of the electric field. Eq. (1) is valid at any time in which a constant length $d/\cos\theta$ of the electron track is contained between the grid and the collector (fig. 4).

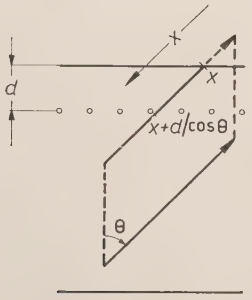

Fig. 4. Schematic drawing for calculating the current pulse at the collector as due to a track forming an angle θ with the electric field.

This current reaches its maximum when the segment track comprised between the grid and the collector is the one which corresponds to the end of the range. Consequently the maximum value of the current is:

$$i_{max} = \frac{w_-}{d} \int_0^{d/\cos\theta} \sigma(x)\, dx\,.$$

We can roughly state the following expression for heavy particles[7]):

$$E = \text{const.}\ R^{2/n} \qquad (2)$$

where E and R are the energy and the range of the particle.

Considering that $\sigma(x) = k(dE/dx)$ we have:

$$i_{max} = \frac{w_-}{d} \int_0^{d/\cos\theta} K \frac{dE}{dx}\, dx = \frac{w_-}{d} K \left(\frac{d}{\cos\theta}\right)^{2/n}$$

K depends on the type of the gas and on the nature of the particle. For α particles of a few MeV we have $n = 3$ for which, lastly, we obtain:

$$i_{max} = \frac{w_-}{d} \frac{Q_0}{(\cos\theta)^{\frac{2}{3}}} \qquad (3)$$

where with Q_0 we have indicated the charge present in a length d at the end of the track.

The determination of i_{max} for a given Q_0, that is for a known particle, is equivalent to an angle measure. This measure results independent from the energy of the particle for an angle θ subject to the following limitation:

$$R\cos\theta \geqslant d\,. \qquad (4)$$

One could choose d small enough to satisfy eq. (4) even for particles with large θ, but in this manner the increased collector capacity involves a lower signal to noise ratio. It is convenient to resort to a compromise solution choosing a filling pressure which making the range sufficiently large allows us to fix a not too small grid collector spacing.

This method, with respect to previous ones, has the following advantages:

(I) The track angle measure, with respect to the lines of force of the electric field, is independent from the position of the track.

(II) The track angle measure, between not very restricted limits, is independent from the energy of the particle, always with identical mass particles.

(III) The track angle and total energy measure are carried out very simply elaborating the information taken on only one electrode, that is on the collector.

[6]) R. W. P. McWhirter, P. Palit and E. H. Bellamy, Nuclear Instruments 3 (1958) 80.

[7]) D. H. Wilkinson, Ionization Chambers and Counters, pag. 14.

3. Experimental Apparatus

We have used a gridded chamber, filled at atmospheric pressure with a mixture of A (98%)–N_2 (2%) which is insensitive to little O_2 contamination[8]).

The gas is made to flow slowly through the chamber itself. The space between the base and the grid is 11 cm, the space between the grid and the collector is 1 cm. The diameter of the electrodes is 14 cm. The grid is made up by tungsten wires having a diameter of 100 μ separated from each other by 3 mm. The inefficiency of the grid is consequently $\sigma \approx 5\%$. The voltages given to the collector and the grid are respectively of 1500 and 1050 volts, by which the grid does not capture electrons. We have used a Po-α source of an intensity of 2.5 μCurie; this source was collimated by means of a capillary tube, having an internal diameter of 1 mm and 2 cm length; thus we had particles collimated with respect to a direction of $\pm$ 3 degrees. The source, as indicated in fig. 5, has

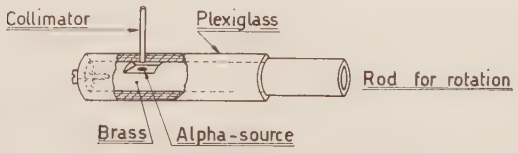

Fig. 5. Rotating collimator N. 1.

been covered with a plexiglass support in such manner that one could handle it without excessive precautions. This source was placed at a distance of 7 cm from the grid and could be rotated of a known angle from the outside.

With this collimator, called N.1, we have studied the precision of the method at many different angles.

To demonstrate the independence of the track angle measure from the energy of the particle, we used a second collimator, called N.2, which is made up by a small plate having a lattice of 200 holes of which 100 are parallel to the electric field and of a diameter of 0.5 mm and 100 with an inclination of 45 degrees with respect to the field, and of a diameter of 0.7 mm. Some of the holes at 0 and 45 degrees have been covered by a thin Al foil having thickness of mg/cm^2 $\approx$ 1.95, in such manner as to have α particles of 3 energies emitted in two different directions with respect to the lines of the electric field.

The thickness of the small plate was 0.5 cm having a square shape of 5 cm sides, the holes were distributed circularly around the center of the small plate.

This last collimator was placed over a Po-α spread source of 0.1 μCurie/cm^2 intensity.

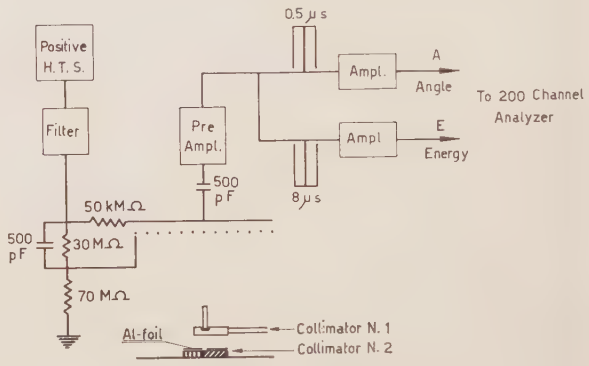

Fig. 6. Block scheme of the device.

The scheme of the electronic device is indicated in fig. 6. We have used only one preamplifier[9]) that gives the signal to two amplifiers, from which the energy and angle measures are obtained. The channel relative to the energy is characterized by the transfer function,

$$\frac{A}{P}\frac{1}{1+p\tau}[1-e^{-pT}]$$

that is by an integration of the current of the chamber on the input capacity of the preamplifier, by a time constant τ (0.1 μsec) and by a reflection T (8 μsec).

The channel relative to track angle measure has a similar transfer function but with T (0.5 μsec).

The observed pulses at the output of the channel corresponding to the energy measure had rise times ranging between 1 to 6 μsec in the experiments with the collimator N.1, shifting this collimator perpendicular and parallel to the electric field.

[8]) U. Facchini and A. Malvicini, Nucleonics **13** (1955) 36.
[9]) C. Cottini, E. Gatti, G. Giannelli and G. Rozzi, Nuovo Cimento **3** (1956) 473.

For the angle measures, the optimum electronic chain would be the same as that studied by Valladas[10]) for Sherr and Peterson's method. Valladas suggests an amplifier having the following response to the step input function, as indicated in fig. 7.

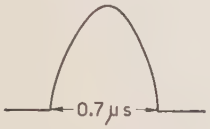

Fig. 7. Response to voltage step of the optimum amplifier according to Valladas.

The response of the amplifier used by us is the one drawn in fig. 8, with a loss in the resolution of 7% with respect to optimum value.

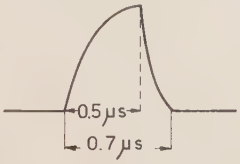

Fig. 8. Response to voltage step of amplifier used in this work.

4. Experimental Results

First we shall discuss the results obtained with the collimator N. 1. The Po-α line is shown in fig. 9; its full width at half maximum is of 3.3% and its independence from the orientation of the collimator has been proved. Attempts to improve the resolution have not been made; we merely ascertain that electronics did not contribute more than with a r.m.s. equivalent to 25 keV.

The current pulse spectra corresponding to different inclinations of the α particles and obtained from the channel indicated as A in fig. 6 are shown in fig. 10; it clearly shows the effect of θ on the current pulses. It is possible to obtain the values of i_{max}, at a given θ, from the position of the various peaks of fig. 10. The dependence of the i_{max} values on the angle θ has been further studied, varying the position of the collimator N.1 in steps of 6 degrees and is shown in fig. 11.

The vertical segment indicates the width of an obtained line at half maximum whilst the horizontal line indicates the spread of the angle due to the collimator, that is ± 3 degrees. Fig. 12 shows the same curve versus $(\cos\theta)^{\frac{2}{3}}$ together with the normalized theoretical curve obtained, substituting in eq. (2) $n = 3$. As can be seen, the agreement is sufficiently good.

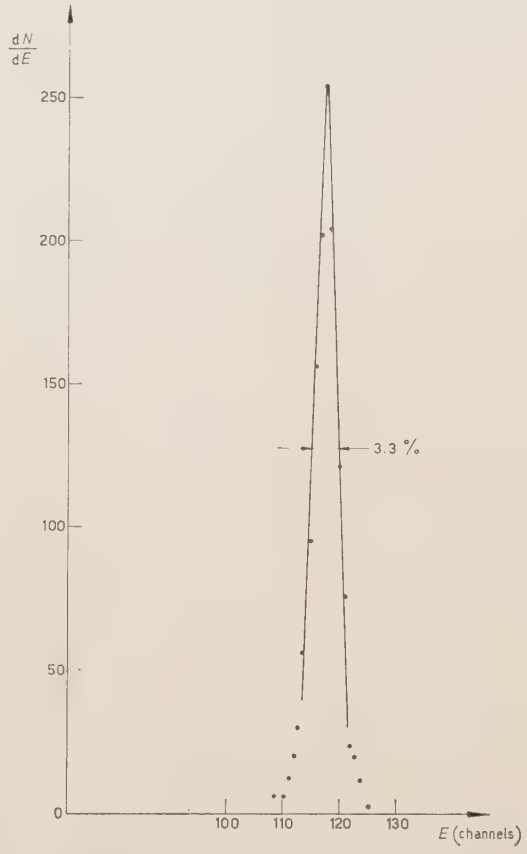

Fig. 9. Energy spectrum of Po-α particles obtained with collimator N. 1 (parallel to electric field).

It is interesting to note that this kind of measurement can be used in order to study the range energy relation for a given type of particles. In fact, using a collimator at various fixed angles θ, the values of i_{max} give, as shown in formula (3), the total charge contained in a length $d/\cos\theta$, i.e. the energy corresponding to such length.

In fact in the case of α particles the curve $n = 3$ is the one which gives the best agreement with experimental results: we may say that this value is comprised between 2.5 and 3.7.

[10]) G. Valladas and A. Levéque, Rapport C.E.A. N. 141 (1952).

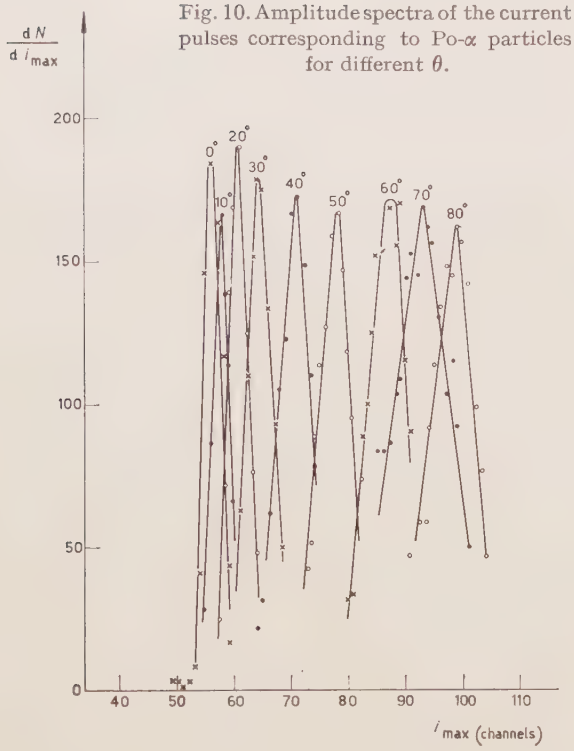

Fig. 10. Amplitude spectra of the current pulses corresponding to Po-α particles for different θ.

Fig. 11. Dependence of i_{max} values versus the angles θ.

Finally we discuss the spectrum obtained with the lattice collimator, called N. 2.

From the graphs, figs. 13 and 14, we see how the information on the angle is independent

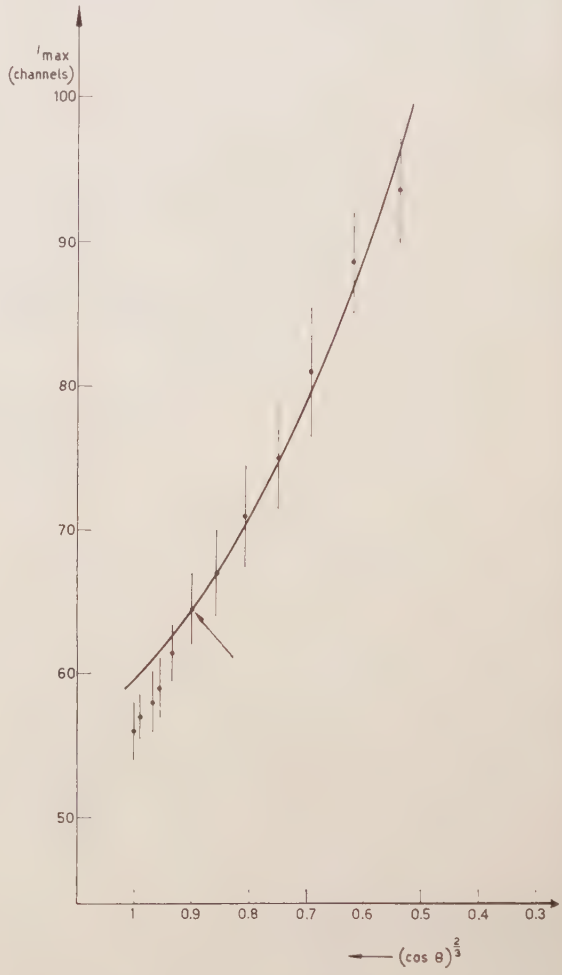

Fig. 12. Dependence of i_{max} values versus $(\cos\theta)^{\frac{2}{3}}$. The full line is the theoretical curve normalized in the point shown by the arrow.

from the energy. Fig. 13 shows the energy α spectrum for the collimator N. 2; the resolution of the three lines, which is respectively 4%, 7% and 13% is due to the loss of energy in the Al foil of the α particles.

Fig. 14 shows that the current pulses are independent from the energy.

With the aim of applying this method we may say how a chamber, used as above, allows us to have fast neutron measures, when the filling

gas is He. In fact, as it is known, the energy of the recoil particle E_r for a nucleus of mass A is:

$$E_r = \frac{4A}{(A+1)^2} E_n \cos^2 \theta$$

where E_n is the neutron energy, and θ is the angle between the neutron and the nucleus in the laboratory system. When the chamber is crossed by fast neutrons with a parallel direction to the electric field, an appropriate current pulse

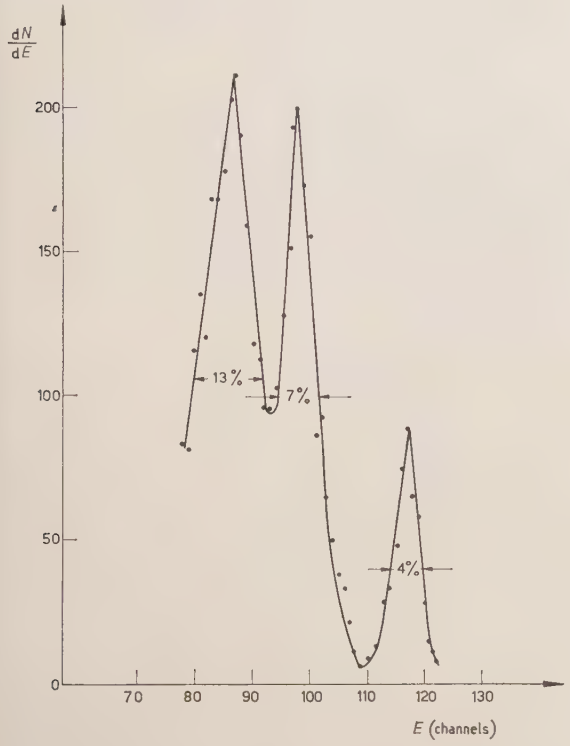

Fig. 13. Energy spectrum of α particles as obtained with collimator N. 2.

measure allows us to measure the energy of the recoil particle at a fixed angle with respect to the electric field, and therefore to the neutrons.

Keeping in mind that the current pulse is independent from the energy, it is quite clear how the chamber is a simple neutron spectrometer with a good efficiency.

It is possible to use a large fraction of the solid angle for the recoil particles considering this appropriate product function of the voltage and current pulse, that is of E and A pulses:

$$E_r\,(i_{max})^3 = \frac{4A}{(A+1)^2} E_n \cos^2\theta \left(\frac{w_-}{d} \frac{Q_0}{(\cos\theta)^{\frac{2}{3}}} \right)^3 = \text{const. } E_n$$

which is independent from the angle.

Another application of the described method is the study of polarized neutrons. In fact the He gas is particularly suitable for this purpose and is one of the most studied polarized neutron analizers.

For example, for polarized neutrons of 3–4 MeV, the polarization results greatest for

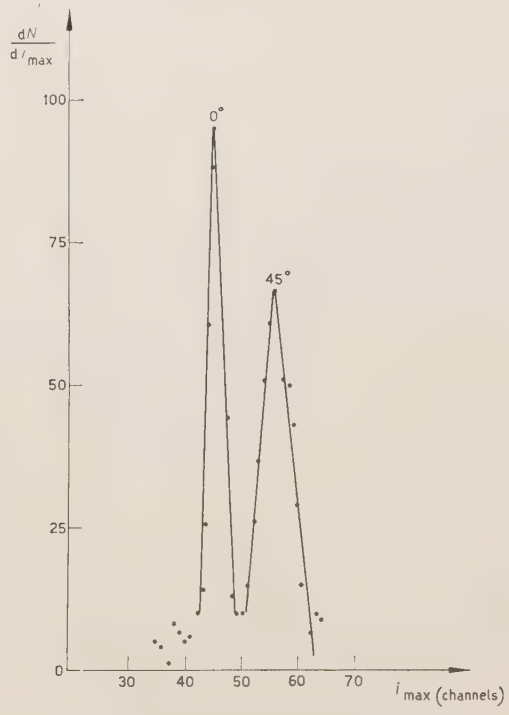

Fig. 14. Angle distribution spectrum of α particles as obtained with collimator N. 2.

$\theta = 22°30'$ and $\theta = 45°$ where θ is the angle between the α particle and neutron in the laboratory system.

To make the current pulse, in the chamber, dependent on azimut, it is necessary that the direction of the incidental neutron is different from that of the electric field E.

The ionization chamber described in this work has been tested as a neutron spectrometer filling it with He and with a mixture of He-A obtaining satisfactory preliminary results.

NUCLEAR INSTRUMENTS AND METHODS 4 (1959) 228–233; NORTH-HOLLAND PUBLISHING CO.

FAST SCALING CIRCUITS

G. W. HUTCHINSON, W. H. WELLS and D. H. WHITE†

Department of Physics, University of Birmingham

Received 29 January 1959

A scaler of 11 mμsec dead time has been designed and built for use at the Birmingham proton synchrotron. This unit is described, and the circuit elements that are used to define the dead time of scalers are discussed.

Several fast scaling circuits, of resolving times down to 25 milli micro seconds, have been produced for counting events produced by fast accelerators, or for coding information in digital form[1–5]). In this paper we report circuits which have been developed in Birmingham for counting experiments on the proton synchrotron. Two types of binary stage have been made: a fast stage with a resolving time $T = 11$ milli microseconds, and a slower stage for which $T = 25$ milli microseconds. The latter has been in use for more than a year with scalers whose total resolving time was limited by their input circuits to 100 milli microseconds. Under these conditions it has proved very reliable and has required practically no attention.

The faster stage has been developed more recently and has not yet been used in experiments. It is combined with two of the slower stages to make up scales of eight which can then be used to drive conventional scalers. No attempt has been made to produce feedback or ring networks to give scales of 10. Usually at the counting rates for which these scalers are needed, eight counts are not statistically significant and the readings of the conventional scalers can simply be multiplied by eight without introducing important errors if an absolute count is required. For experiments in which the counting rate is expected to vary widely, indication of the state of the fast scales has been provided with a resistance network and a meter. The scalers can be coupled directly by hundred ohm coaxial cable to the anodes of the photomultipliers, such as the R.C.A. 6810.A. used with a fast phosphor. A gating circuit is included so that the scaler can be made to count only during a synchrotron pulse.

1. Design Principles

1.1. TRANSIENT RESPONSE

The circuit is made up of symmetrical binary stages, storing information by virtue of the level of the current in the anodes of the valves used. Each stage therefore needs a d.c. coupled positive feedback loop and, in addition, a short term memory which can record the previous state of the system during the period of its disturbance by an incoming pulse. This latter must be supplied by additional components in the feedback loop. These produce signals sufficient to drive the circuit into a determined state at the end of the disturbance from an otherwise symmetrical disturbed configuration. For the fastest operation the signals must be of minimum necessary amplitude. They must maintain this amplitude during the removal of the disturbance, and after that they must return to zero quickly so as not to influence adversely the state of the circuit on

† Now at The University of Pennsylvania, Philadelphia, U.S.A.

[1]) N. F. Moody *et al.*, Rev. Sci. Instr. 22 (1951) 439.

[2]) J. Fischer *et al.*, reported by R. E. Bell, Ann. Rev. Nucl. Sci. 4 (1954) 93.

[3]) H. K. Schoenwetter, Rev. Sci. Instr. 24 (1957) 515.

[4]) M. Nakamura, Rev. Sci. Instr. 28 (1957) 1015.

[5]) B. Collinge and G. B. Huxtable, Nuclear Instruments 3 (1958) 116.

recovery from the subsequent disturbance. Fig. 1 illustrates three ways in which such a signal can be produced, together with typical resulting wave forms. (a) shows the traditional method of R.C. coupling giving a transient pulse decaying exponentially to the final level. (b) shows a damped L.R. coupling in which the back edge of the transient peak may be made to overshoot the final level by making the damping less than critical. (c) shows coupling by means of an electro-magnetic delay line, producing a transient which is symmetrical in back and

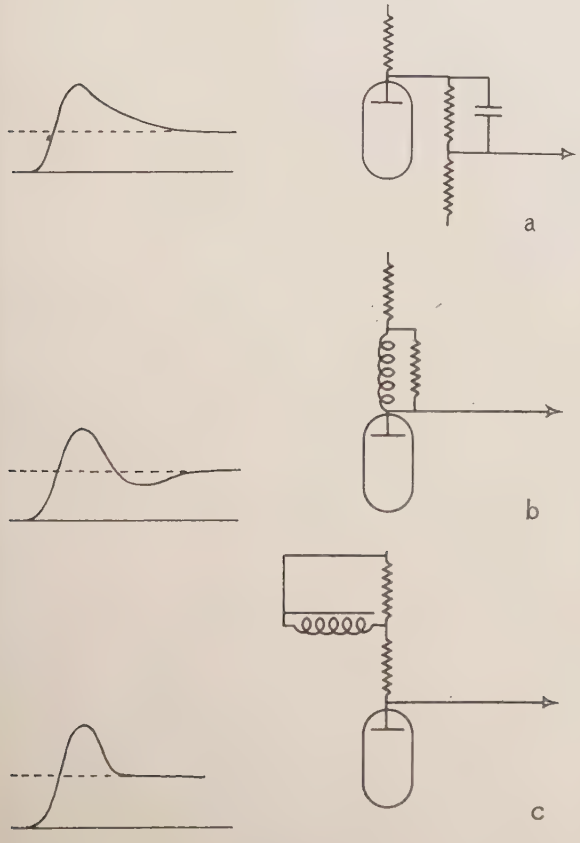

Fig. 1. Shaping networks.

front edges, superimposed upon the d.c. signal. Network B is similar in principle to the transformer coupling used by Chaplin[6]).

The principle of delay line coupling has previously been used by Kandiah (private communication). Clearly networks B and C are both superior to network A for short resolving times. If the end of the circuit disturbance could be considered to take place instantaneously, at the peak of signal B, then signal C would have little advantage over B. The overshoot of signal B would increase rather than decrease the sensitivity of the symmetrical circuit during the second part of the transient. The resolving time would therefore be determined largely by the time of crossover and not by the total duration of the transient. However, the recovery of the circuit is not instantaneous and must be considered to take place during a time comparable to the rise time of the transient when all the components are being used near the limit of their band width. Under these conditions, the flat topped signal of network C is superior. There are, however, some practical disadvantages in delay line coupling. Coaxial delay lines tend to have too low an impedance for use with most valves and lumped impedance lines do not usually give a perfect enough wave form. It is only the first few harmonics of the transient's fundamental frequency which are important and it should therefore be practicable to make use of a simulating ladder network[7]) instead of a delay line. We have preferred to use a coaxial line coupling for the first stage of the scaler since in this stage the valves used have a characteristic which makes a 50 ohm impedance level acceptable as a load, and simple inductance coupling for the following stages in which the speed can be made adequate by this means.

1.2. VOLTAGE SWING LIMITATION

Some fast scaling circuits have used diodes to limit the voltage swings of various circuit points[4]). This can increase the speed of the circuit, but only if (a) the band width of the diodes themselves is high enough, (b) the forward impedance of the diodes is considerably smaller than the load impedance suitable for the valves used, and (c) the reference voltages are provided for the diodes from sources which are low impedance relative to the forward impedance of the diodes themselves at all frequencies from

[6]) Chaplain, Proc. I.E.E. B **103** (1956) 510.

[7]) G. G. Scarrott, W. J. Harwood and K. C. Johnson, Proc. Inst. El. Eng. B **103**, Supp. 3 (1956) 476.

d.c. up to the highest involved in the circuit operation. The complication of providing low impedance reference points could possibly be avoided by some such symmetrical network as that shown schematically in fig. 2, but the advantage likely to be gained would be expected to be small, when using modern valves, because of the difficulty of meeting the first two conditions. We have not therefore used any diode limiters in our circuits, and in this way they have been kept fairly simple.

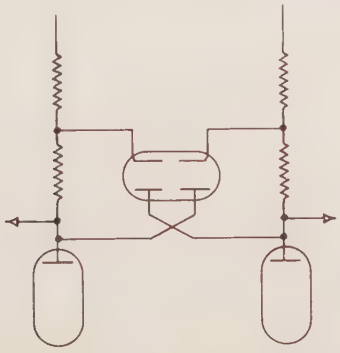

Fig. 2. The use of diodes to limit the voltage swing.

1.3. INPUT CIRCUIT

The disturbance to the first binary stage of the scaler should be produced by a pulse whose amplitude is standardized and whose length is suited to the transient response of the scaler. It is the function of the input circuit to produce these pulses from the signals fed to the instrument. Since these are to be derived directly from a photomultiplier feeding a coaxial cable, it may be assumed that their rise time will be short, compared with the resolving time of the scaler. For this reason, the input circuit is not intended to increase the rise time of pulses, but only to standardize them. If the scaler were to be used to count pulses of rise time slower than its transient response, it would be necessary to use some form of positive feedback in the input circuit. This would be undesirable because the response and recovery time of such a circuit would be limited by the same considerations of valve band width under positive feedback conditions, as is the scaler itself, and this has not been attempted. The scalers are, therefore, only suitable for counting pulses from photomultipliers or pulses with similar short rise time. This is not considered a serious limitation, however, since it is only under these conditions that the resolving time of the scaler is useful.

2. Circuit Description

2.1. INPUT CIRCUIT

It is the purpose of the input circuit to provide a negative pulse of defined width for the first scale of two circuit. The circuit diagram is given together with the fast scale of two in fig. 3. The input circuit consists of valves V_1 to V_4, of which V_2 only is drawing substantial current. Valve V_1 is a Mullard type 180 F wide band pentode normally cut off by a voltage defined by the resistor chain R_2–R_5. The purpose of this valve is to remove overshoots in a negative incident signal and to provide a discriminator bias in the input circuit. Valve V_2 type 3A/167/M is normally conducting and the negative signal applied to the grid is shaped to about 5 mμsec by the shorted line in the anode circuit. The standing current in this valve is sufficient to generate a signal at the anode of amplitude above that necessary to drive the scaler. Large input signals are limited at this point. The clipping line in the anode of V_2 produces a waveform with a negative excursion and it is necessary to remove this. The cascode stage V_3, V_4 type 3A/167/M removes the overshoot by virtue of its normal cut off condition and a negative amplified waveform is produced at the anode of V_4. A cascode stage was used so that the capacitative feed through this stage of the driving pulse was minimised.

The input circuit therefore produces a negative pulse of defined width without overshoots from a negative signal of undefined, but longer, duration at the input. Incoming signals shorter than the clipping time tend to be lengthened at the anode of V_1. A gating facility is provided in the input circuit. The circuit diagram of the gating circuit is given in fig. 3. The grid of V_3 is used to influence the gain of the cascode stage. When the gate facility is used, this grid is held at a voltage well below the voltage of V_3 cathode. The gating signal is

generated by a flip flop and the valves V_{5a} and V_{5b} apply this signal to the grid of V_3. A count switch is also incorporated at this point in the circuit as shown.

negative signal from the input circuit is used to remove current from the circuit for a defined time. Since the circuit is symmetrical it is only necessary to consider one of the two possible

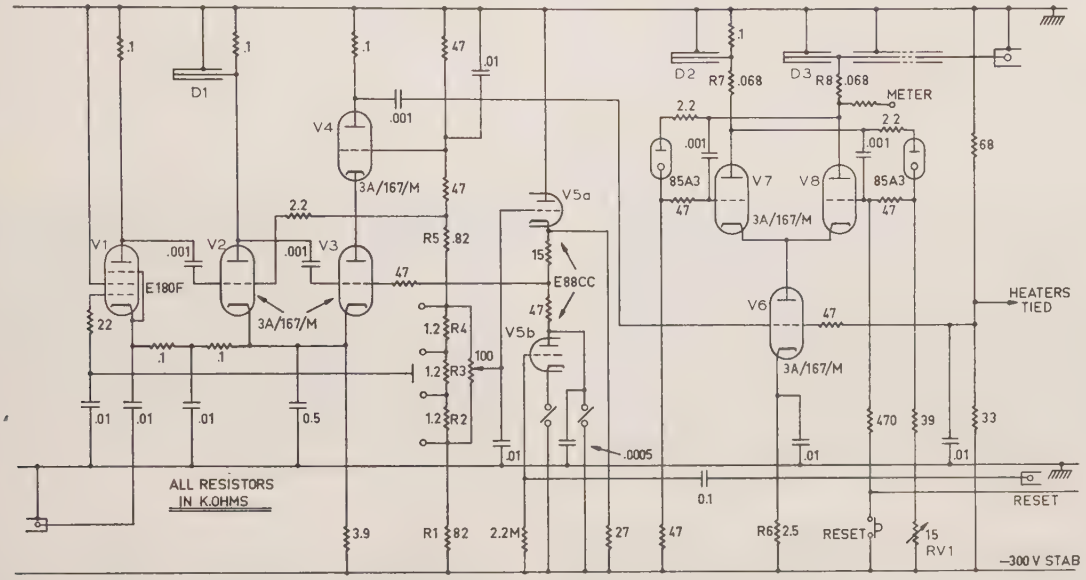

Fig. 3. The input circuit and first scale of two. D_1 — 25 cm; D_2 and D_3 — 85 cm; — semi air spaced, 100 Ω impedance.

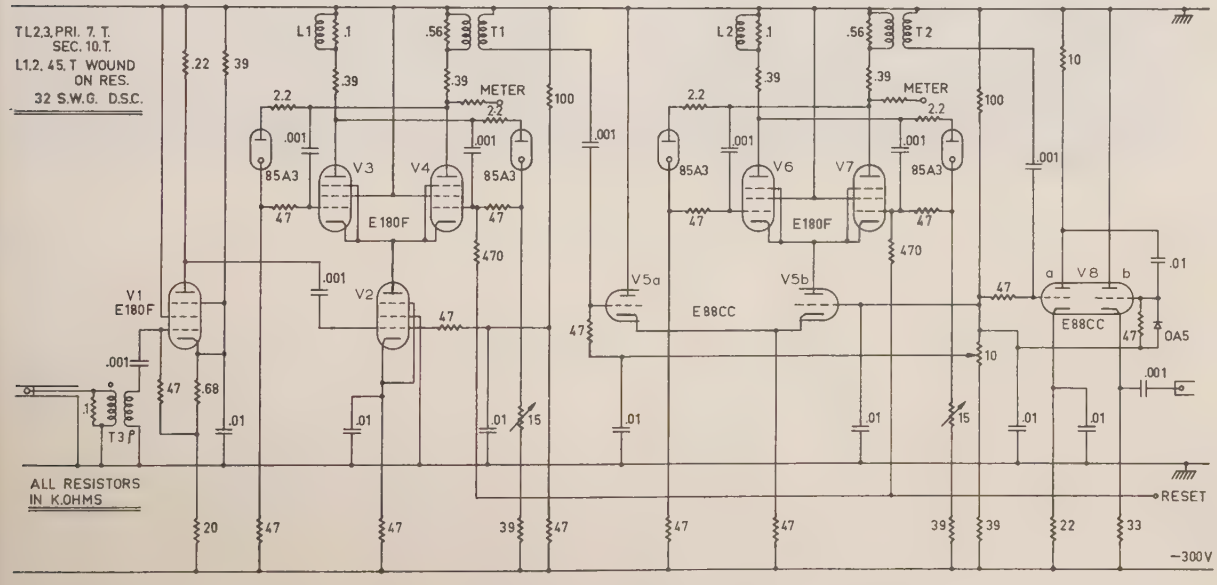

Fig. 4. The scale of four.

2.2. FIRST BINARY STAGE

Valves V_6, V_7, V_8 type 3A/167/M form the active elements of the first binary stage. The current in the stage is defined by the grid potential of V_6 and the cathode resistor R_6. The current conditions. Suppose current is flowing in V_7. V_8 is cut off in virtue of the potential induced by the current flowing in R_7. This potential determines the difference in grid potential of V_7 and V_8 and hence the distribution

in current between the valves. It is made large enough to ensure that less than 1 mA flows in the valve that is cut off. In practice, for this to be true in both states, a slightly larger voltage is necessary than is to be expected from the manufacturers' characteristics, for the potential across the neon tubes is not precisely the same. The potentiometer RV1 is inserted to balance the burning voltages of the neon tubes. An estimate of the time taken to complete the transition may be made from the photograph. It is 5×10^{-9} sec.

From this time, the optimum length of line may be deduced. It is equal to the rise time of the signals at the anodes of V_7 and V_8 giving a maximum amplitude of driving pulse from the line, consistent with the speed of the circuit. In fig. 6, a tracing is given of fig. 5a, together with

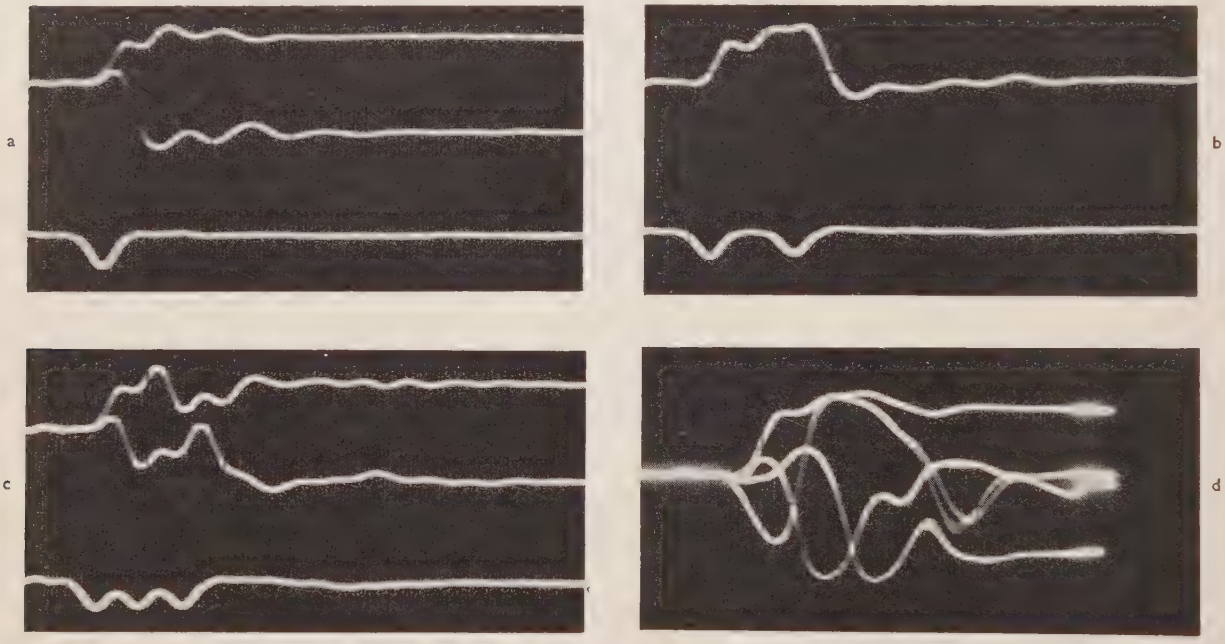

Fig. 5. Waveforms. a. Single pulse operation; b. Double pulse operation; c. Triple pulse operation. The upper waveform appears at either anode of the first scale of two, with the lower waveform as input to the circuit. d. Triple pulse operation, waveform at either anode of second scale of two. In c and d the input pulses occur at 11 mμsec intervals.

Variations in characteristics are then accommodated by a larger value of R_7 and R_8.

When the current is removed from the valves V_7 and V_8 a waveform is induced in the anode circuit of the conducting valve; in the present case V_7. A positive pulse, generated by the shorted line is superimposed upon the rise of the anode of V_7 to ground potential and it is this pulse that raises the grid potential of V_8 above that of V_7. When current returns to the pair of valves it is to V_8 that current begins to flow. The rate of fall of potential at the grid of V_7 determines the minimum length of the clipping lines in the anodes of V_7 and V_8. Oscillograph waveforms are shown in fig. 5. the driving pulses deduced, by subtracting the voltage change induced by the change of current in R_7.

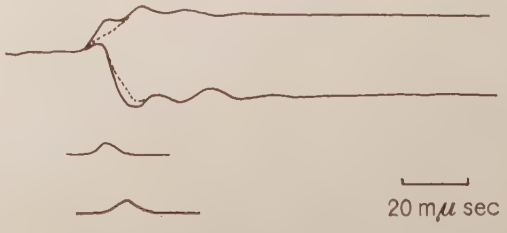

Fig. 6. Tracing of single pulse operation with the driving signals.

2.3. THE SECOND BINARY STAGE

Fig. 4 shows the following scale of four. It is driven from a 100 Ω line terminating the shaping

line in the anode of V_8. The problem of designing the scale of four is considerably eased by the standard waveform supplied by the first scale of two.

V_1 is normally cut off. Its grid receives a positive pulse through the inverting transformer T_3 when the fast scale of two reverts to the "O" condition. It then produces a negative pulse at the grid of V_3 and the operation of the scaling stage is thereafter similar to that of the preceding scale of two, except for an inductance memory in place of the delay line memory.

Coupling between this stage and the next is by transformer in the anode circuit of V_4, in the same way that the last binary scale is coupled to the output circuit. V_{8a} is designed to remove the negative signal corresponding to transference to the "1" condition. V_{8b} is a cathode follower.

3. Experimental Performance

A scale of four similar to the scale of four in fig. 4 has been used at the synchrotron at Birmingham for more than one year. It has proved reliable and the pulse height needed to trigger the scaler has been stable.

The fast binary has been triggered with a mercury relay pulse generator, giving pulses approximately 5 mμsec rise. A delay line network was used to provide multiple pulses with a variable relative delay. In this condition the resolving time has been 11 mμsec. In fig. 5a, the circuit is responding to a single input pulse, in fig. 5c, the pulses are 11 mμsec apart.

With an input circuit delivering pulses of optimum shape, it seems inevitable that a dead time at least as long as the driving signal is induced because of the reflection generated by the clipping line. The use of the limiting valve V_2 implies that, for signals of normal amplitude, the circuit will also be dead for the length of the input pulse. In the unit built in the laboratory, there is a minimum dead time of 10 mμsec.

The minimum input amplitude is 1 volt on approximately 100 Ω (the input impedance at V_1) and the minimum rise time is approximately 10 mμsec.

Coils L_1 and L_2 in the circuits were wound on $\frac{1}{4}$ watt resistors and the transformers on Mullard toroidal ferroxcube cores, type FX1322. The numbers of turns are marked on the diagrams.

Acknowledgment

We should like to acknowledge the help of Mr. K. Kandiah in showing us his own circuits before publication and for useful discussions during early stages of the project.

NUCLEAR INSTRUMENTS AND METHODS 4 (1959) 234–238; NORTH-HOLLAND PUBLISHING CO.

MEASUREMENT OF THE POLARIZATION OF D-D NEUTRONS BY A SOLENOID

P. S. DUBBELDAM, C. C. JONKER and F. J. HEEMSKERK

Natuurkundig Laboratorium der Vrije Universiteit, Amsterdam

Received 10 March 1959

A solenoid is described which turns the polarization vector of D D neutrons over + 90° or — 90°, while the detectors remain in a fixed position. The method avoids the false asymmetries that may be introduced if one turns the detectors over 180° and it allows heavy shielding. This way a good accuracy was obtained. For a thick, golden "drive-in" target the relative left-right asymmetry was found to be $|R_0| = (4.6 \pm 0.2)\%$ at $E_D = 450$ keV and $\vartheta_{1\,lab} = 50°$; $\vartheta_{2\,lab} = 42°$.

1. Introduction

Several authors[1–6]) have measured the polarization of the neutrons from the D–D reaction. The polarization is analysed by scattering the neutrons by a scatterer consisting of some light nuclide with spin zero, generally He^4 or C^{12}. The scattered neutrons show an azimuthal variation of the intensity. A measure for the magnitude of this effect is the relative left-right asymmetry, defined as:

$$R(\varphi) = \frac{N(\varphi) - N(180° + \varphi)}{N(\varphi) + N(180 + \varphi)}$$

$N(\varphi)$ and $N(180° + \varphi)$ are the numbers of neutrons counted by two detectors with equal efficiencies in diametral positions.

For a monoenergetic source, point scatterer and point detectors the following formula applies, according to the theorem of Wolfenstein:

$$R_{th}(\varphi) = P_1 P_2 \cos\varphi \ , \qquad (1)$$

P_1 is the magnitude of the polarization of the initial beam of neutrons which is perpendicular to the reaction plane; P_2 is the magnitude of the polarization that would result if an unpolarized beam of neutrons were scattered by the same nuclide, it is perpendicular to the scattering plane. P_1 is a function of the deuteron energy (E_D) and the angle ϑ_1 between deuteron- and neutron beam. P_2 is a property of the scattering material and depends on the neutron energy (E_n) and the scattering angle ϑ_2.

It is not possible to determine the relative efficiencies of two neutron detectors as accurate as is necessary to measure the (small) polarization effect. Therefore one is accustomed to base the measurement upon one detector that is turned from one position to the diametral one. The second detector remains in use, because it provides an independent measurement of R which serves as a check, and enhances the accuracy. This method requires a very accurate mechanical equipment. This has to be checked regularly by test runs, and sometimes false asymmetries show up. Moreover the variation of the neutron intensity over the scatterer necessitates the computation of a considerable correction.

These difficulties are avoided by a method, due to Hillman and others[7]), which they applied to 100 MeV neutrons. They use the Larmor precession of the neutron magnetic moment in a magnetic field. This field is parallel to the

[1]) R. Ricamo, Nuovo Cimento **10** (1953) 1607.

[2]) R. W. Meier, P. Scherrer and G. Trumpy, Helv. Phys. Acta **27** (1954) 577.

[3]) R. Budde and P. Huber, Helv. Phys. Acta **28** (1955) 49.

[4]) B. M. McCormac, M. F. Steuer, C. D. Bond and F. L. Hereford, Phys. Rev. **104** (1956) 718.

[5]) I. I. Levintov, A. N. Miller and V. N. Shamshev, Nuclear Physics **3** (1957) 221, 237.

[6]) P. J. Pasma, Nuclear Physics **6** (1958) 141.

[7]) P. Hillman, G. H. Stafford and C. Whitehead, Nuovo Cimento **4** (1956) 67.

direction of propagation of the neutrons, and it turns the polarization 90° clockwise or opposite depending on the direction of the field. We applied this method to 3 MeV neutrons because of the apparent advantages; in principle no false asymmetries are introduced and the fixed position of the detectors allows heavy shielding.

2. Data of the solenoid

According to the computation of Hillman the number of ampère-turns needed is given by:

$$NI = \frac{v}{1.46 \times 10^4} \qquad (2)$$

N is the number of turns, I the current, v the velocity of the neutrons in cm/sec.

The energy of the neutrons at $E_D = 500$ keV and $\vartheta_1 = 0°$ amounts to: $E_n = 3.5$ MeV, $v = 2.58 \times 10^9$ cm/sec, which gives: $NI = 1.77 \times 10^5$ ampère-turns. We designed the solenoid for 2×10^5 A-turns.

It consists of 45 disk-shaped sections of wound copper tape, 1 mm thick and 12.5 mm wide and insulated with 0.1 mm oiled paper. The space between the disks is 5 mm, giving a space factor of 65 per cent. The inside diameter of the brass tube on which the disks are mounted is 46 mm, the outside diameter of the disks is 230 mm, the length of the solenoid is 780 mm, the maximum available current is 57 A and the maximum dissipated power about 8 kW. The solenoid is cooled by air.

The electrical current is supplied by a generator and stabilized to about one per cent by regulating the field-excitation of the generator. The main current passes through a resistance of 0.1 Ω and the resulting voltage is fed into a difference amplifier that regulates two pentodes providing the current for the field-excitation.

3. Description of the experiment

Fig. 1 gives a schematic view of the setup. A 500 kV cascade generator, with deflection magnet (installed by N.V. Philips) was used as neutron generator. The reaction takes place in a thick, gold "drive in" target, that gives its maximum yield of a few times 10^8 neutrons per second at an ion current of about 500 μA.

The carbon scatterer is 40 mm in diameter and 40 mm long and can be shifted in and out of the beam pneumatically; $\vartheta_{1\,lab} = 50°$. The distance targetspot-centre of scatterer is 1240 mm. The neutrons are detected by two stilbene crystals, 40 mm in diameter and 20 mm thick, mounted on two E.M.I. 6260 photomultipliers. The angle $\vartheta_{2\,lab}$ is 42°, the distance scatterer-photomultiplier is 208 mm.

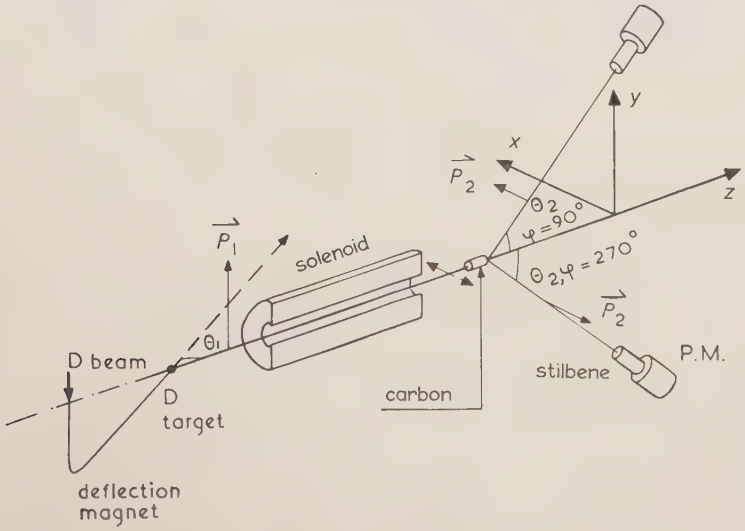

Fig. 1. Schematic view of experimental setup.

The pulses are amplified by a linear amplifier. A channel discriminator cuts off the low energy

background and the background higher than the maximum of the proton recoilspectrum, which is presumably due to capture gamma's from the copper of the solenoid. The detectors are shielded by 90 mm lead and 360 mm paraffin mixed with boric acid. The number of scattered neutrons is about 70 per cent of the remaining background. To reduce the influence of the magnetic field on the photomultipliers two mu-metal cylinders of 2 mm thickness are placed around each of them.

drift of the apparatus is averaged out to a high degree.

Photomultipliers are in general very sensitive to magnetic fields. This introduces a false asymmetry in the measurements, as the pulse-height, and thus the efficiency, changes with the direction of the field. It was necessary to use E.M.I. multipliers, because they have a Venetian blind dynode system, which is less sensitive. The mu-metal shields reduce this influence then to a value that can be treated as a small correction.

TABLE 1

Experimental values of R in %. R_{corr} is the value for R, corrected for the influence of the magnetic field on the PM

I (Ampère)	Upper detector		Lower detector		Weighed average for R_{corr}
	R	R_{corr}	R	R_{corr}	
15	-1.6 ± 0.5	-1.6 ± 0.5	1.6 ± 0.6	1.6 ± 0.6	1.6 ± 0.4
20	-3.3 ± 1.0	-3.3 ± 1.0	2.7 ± 1.1	2.7 ± 1.1	3.0 ± 0.7
25	-2.8 ± 0.7	-2.8 ± 0.7	3.0 ± 1.1	3.0 ± 1.1	2.9 ± 0.6
30	-2.6 ± 0.7	-2.6 ± 0.7	3.75 ± 0.8	3.75 ± 0.8	3.1 ± 0.5
35	-3.6 ± 0.7	-3.6 ± 0.7	4.7 ± 1.1	4.7 ± 1.1	3.9 ± 0.6
40	-3.5 ± 0.7	-3.5 ± 0.7	4.8 ± 0.9	4.9 ± 0.9	4.0 ± 0.55
45	-4.9 ± 0.7	-4.9 ± 0.7	4.3 ± 0.9	4.4 ± 0.9	4.7 ± 0.55
50	-4.2 ± 0.8	-4.15 ± 0.8	3.4 ± 0.7	3.5 ± 0.7	3.8 ± 0.5
55	-5.1 ± 0.7	-5.0 ± 0.7	3.5 ± 1.0	3.6 ± 1.0	4.5 ± 0.6
57.5	-4.7 ± 1.0	-4.6 ± 1.0	4.7 ± 0.7	4.8 ± 0.7	4.7 ± 0.6

To make full use of the fact that the experiment is a relative determination the parameters (position of the scatterer and direction of the current) are changed often. This necessitates mechanization of the measurements.

After a fixed number of monitor pulses from a long counter, during which time (about 20 sec) the scatterer is in the beam and the pulses are registered, the automaton removes the scatterer out of the beam and the background pulses are registered on another scaler. After the same number of monitor pulses the "in" position is restored. This is repeated five times, then the automaton commutates the solenoid current and the scalers are read off or photographed. A new cycle is started and the number of neutrons is measured with the reversed direction of the current. Thus a complete determination of R is made within about seven minutes and possible

To determine this correction we measured the variation in the counted number of pulses from a Co–γ-source, when the current was reversed. From the variation of the efficiency of the detectors for the γ-rays and neutrons with the bias setting one can compute the variation in efficiency of the detectors for neutrons, due to the reversal of the magnetic field. From the measured value of R one has to subtract a certain percentage to obtain the corrected value. The correction is — 0.14 per cent at the highest current for the lower detector, compared with a value of 4.6 per cent for R.

4. Results and Discussion

Table 1 gives the measured and corrected values of R as a function of I, for $E_D = 450$ keV. The formal definition of R is slightly different here. It is no more the relative difference

in counting rate at two positions of the detector, but at two directions of the current: $R = (N^- - N^+)/(N^- + N^+) \cdot N^-$ and N^+ are the counting rates for the two directions of the current.

The sign of R as given in the table agrees with the sign, that follows from $R = \boldsymbol{P}_1 \cdot \boldsymbol{P}_2$, if we derive the direction of $\boldsymbol{P}_1$ and $\boldsymbol{P}_2$ from other sources[1–6]), which agree all in this respect.

Fig. 2 gives a graph of the corrected experimental points. The turning of the polarization vector is proportional to I. The analysing effect

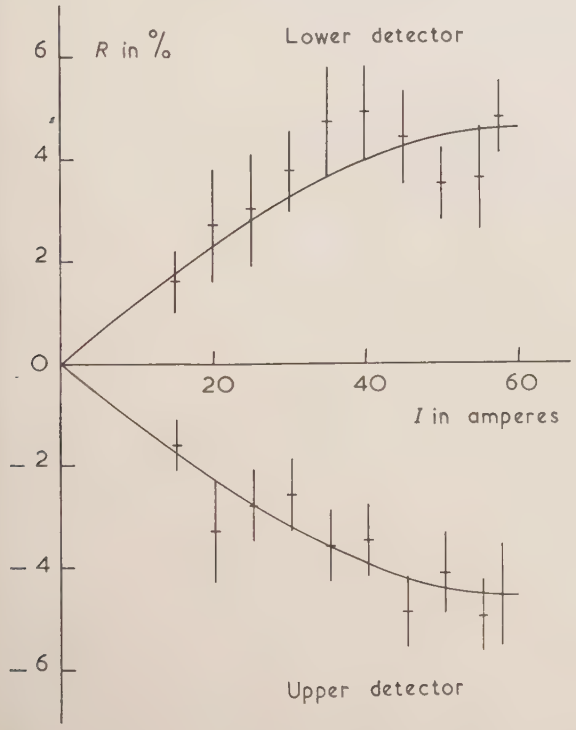

Fig. 2. The relative left-right asymmetry: R_{corr} as a function of the current I. The drawn curves are least squares sinusoids, with the maximum at $I = 60$ A.

of the scatterer is proportional to the projection of P_1 on the scattering plane. Therefore we can write for mono-energetic neutrons: $R = R_0 \sin \frac{1}{2}\pi I/I_0$, where I_0 is the current needed to turn the vector over 90°.

The formula (2) is computed on the basis of the field inside a very long solenoid. We computed the field $H(x)$ on the axis of our solenoid taking into account its finite size, and next evaluated $\int_{x_1}^{x_2} H(x)\mathrm{d}x$, x_1 and x_2 being the positions of target spot and scatterer. This integral is proportional to the angle over which the vector is turned. From this computation we found that we should multiply the current following from (2), with $\frac{4}{3}$ in order to obtain the current I_0 needed in our solenoid. We find then that for the maximum neutron energy in our experiment, $E_n = 3096$ keV, I_0 equals 63 A.

The measured value of R is an average over the R as given in (1). As $E_n = f(E_D)$ all three factors in the right hand side of (1) depend on the deuteron energy at which the reaction takes place. We have made an estimate of the experimental R by averaging numerically over E_D. For $P_1(E_D)$ we took a quadratic fit to the points collected by Pasma[6]) for thin target measurements; for $P_2(E_n)$ we took the values from the graph given by Wills *et al.*[8]) and

$$\varphi = \frac{aI}{\sqrt{E_n}} - \tfrac{1}{2}\pi .$$

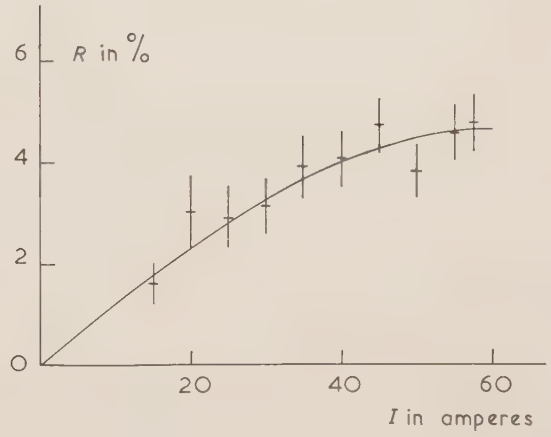

Fig. 3. Weighed average R_{corr} for the two detectors. The drawn curve is the sinusoid: $R = 4.6 \sin \frac{1}{2}\pi I/60$.

We approximated the neutron spectrum by a quadratic dependence on E_D. For the density of deuterons in the metal target increases linearly with the depth, and so roughly with $450—E_D$ (keV) and the cross section for the reaction increases roughly linearly with E_D. We neglected the variation of the efficiency of the detector

[8]) J. E. Wills, J. K. Bair, H. O. Cohn and H. B. Willard, Phys. Rev. **109** (1958) 891.

with E_n and the finite size of scatterer and detector. The computed curve of R versus I cannot be distinguished from a sinusoid within the limits of experimental accuracy; the maximum lies at 60 A and amounts to $R = 1.2\%$.

We computed a least squares fit of the sinusoid: $R = R_0 \sin \frac{1}{2}\pi I/60$ for the corrected experimental points (fig. 2).

This gave for the upper detector $R_0 = -(4.6 \pm 0.3)\%$ and for the lower detector $R_0 = (4.6 \pm 0.3)\%$.

The weighed average of these is: $|R_0| = (4.6 \pm 0.2)\%$.

The computed value $R_0 = 1.2\%$ is considerably lower than the measured value. This discrepancy may be due to a difference between the actual neutronspectrum and our estimate. Another uncertain factor is the P_2, which is very sensitive to small changes in the phase-shifts.

We wish to thank K. Abrahams for his help in preparing the experiments, especially as to the automaton and H. Boersma for his part in the elaborate measurements and computations. Also we express our gratitude to Mr. Jongsma and the technical staff for the construction of the solenoid.

NUCLEAR INSTRUMENTS AND METHODS 4 (1959) 239–242; NORTH-HOLLAND PUBLISHING CO.

MEASUREMENT OF SURFACE DENSITY OF THIN FOILS

K. RAMAVATARAM† and D. I. PORAT

The Physical Laboratories, The University, Manchester, England

Received 23 March 1959

A Po^{210} alpha source is used to measure the surface density of thin foils with a resolution of approximately 1 $\mu g/cm^2$. A calibration procedure is described to convert air equivalents to units of surface density. The mass stopping power of Al, Ni, Ag and Au relative to air, at an alpha energy of 3.72 and 4.33 MeV is reported.

1. Introduction

Many nuclear physics experiments demand an accurate knowledge of the surface density of the target in which the nuclear interaction takes place. Similarly, the thickness of a source may be critical in experiments, demanding high resolution since self absorption and straggling of energy within the source present factors limiting this resolution. The instrument described here was developed in connection with the measurement of the rate of loss of energy of heavy ions (He, C, N, O...) passing through metals[1]).

The following methods of foil thickness measurements are mentioned in literature: gravimetric, colorimetric, photometric, polarimetric, interferometric, X- and beta-ray absorption, radio-activation, electrical conductivity and the change in radio frequency due to presence of a foil of given thickness. A detailed description of the various techniques can be found in the reviews given in ref. [2]).

Weighing and quantitative chemical analyses are the most direct determinations of the number of target nuclei. This quantity rather than foil thickness is mostly sought in nuclear physics experiments. In both methods one assumes an average thickness

$$\bar{t} = (\sum t \cdot \delta A)/A$$

where t is the thickness of a small area element δA. The physical properties of a very thin foil e.g. density and electrical resistivity may differ from the properties of bulk material.

2. Description of the Instrument

The instrument described here measures the air equivalents of foils and a calibration procedure based on simple statistical arguments is shown to convert the air equivalents into units of surface density.

If one counts the number of alpha particles which arrive at the detector as a function of separation between source and detector, one obtains the well known number-distance curve. Consider a foil of thickness ΔX interposed in the path of the alpha particles replacing a thickness, ΔR, of air. The change in surface density is $\Delta R\,(\partial N/\partial R)$ where $\partial N/\partial R$ is the slope of the number-distance curve. Thus a convenient way is obtained for measuring the stopping power of a substance relative to air[3]). The method has to be calibrated with foils of precisely known surface density. The following calibration procedure was adopted in order to obtain accurate stopping powers for various

[1]) D. I. Porat and K. Ramavataram, Proc. Roy. Soc. (London) (1959); to be published.

[2]) P. Cotton and P. Rouard, J. Phys. Rad. **11** (1950) 461; K. M. Greenland, Vacuum **2** (1952) 216; O. S. Heavens, Optical Properties of Thin Solid Films (Butterworth Scientific Publications, London, 1955); L. Holland, Vacuum Deposition of Thin Films (Chapman and Hall Ltd., London, 1956).

[3]) W. C. Barber, Rev. Sci. Instr. **24** (1953) 469.

† On leave from The Physics Department, Osmania University, Hyderabad, India.

metals relative to air. Commercial foils of Al†, Ag†, Au† and Ni†† were cut to accurately measured areas of the order of 100 cm² and weighed on a semi-microbalance. Measurements of relative stopping powers showed variations in thickness up to 30 per cent over the area of a foil, except in the case of Ni, where much better uniformity was observed. The true surface density was found statistically by preparing 30 to 40 targets from each foil and measuring the relative stopping power of each target on the alpha gauge. Thus a mean air equivalent with a small statistical deviation around this mean was obtained. With data from earlier weighing and measurement of area this yielded the mass stopping power, C_m, relative to air. The errors in C_m are governed by the following factors:

(i) Errors in area and weight determination
(ii) Statistics of counting
(iii) Degree of non-uniformity of foil
(iv) Number of targets prepared from each foil
(v) Knowledge of air density.

The influence of conditions (i) and (iii) was minimised by taking large and comparatively thick foils for the calibration.

The air equivalent $\Delta R = \Delta N/(\partial N/\partial R)$ and the error in this quantity due to the statistics of counting is

$$\epsilon_{\Delta R} = \pm \{(N_1 + N_2)/(t \cdot \partial N/\partial R)\}^{\frac{1}{2}}$$

where t is the time interval of counting, N_1 the rate of counts for air only and N_2 the rate of counts after the insertion of the foil in the path of the alpha particles. We see that for maximum sensitivity we require a high slope $\partial N/\partial R$ and for minimum error we also require a long counting time, t. Temperature and pressure corrections were applied in the determination of C_m and a partial pressure P_w corresponding to 80% relative humidity at 20° C was assumed constant being representative of the laboratory atmosphere in the period of this experiment.

It was mentioned earlier that comparatively thick foils were considered for the calibration of the alpha gauge. This procedure may be questioned because C_m is a function of energy. A detailed consideration showed the following limit of foil thickness to be applicable for extrapolation to "zero" thickness.

$$X \leqslant (E_1^{\beta+1})/50\ (\alpha - \beta)\ B \qquad (1)$$

where E_1 is the energy with which the alpha particle leaves the foil and α, β and B are defined from the following relations which express with a good approximation the rate of energy loss of alpha particles over the small energy interval:

$$dE/dR = AE^{-\alpha}\ ; \qquad dE/dX = BE^{-\beta}$$

where dE/dR and dE/dX are the rates of energy loss of alpha particles passing through air and metal respectively, E is the mean energy of the alpha particle in the stopping medium and A, α, B and β are constants. Relation (1) was verified by using foils of various thicknesses and obtaining values of C_m within the experimental errors.

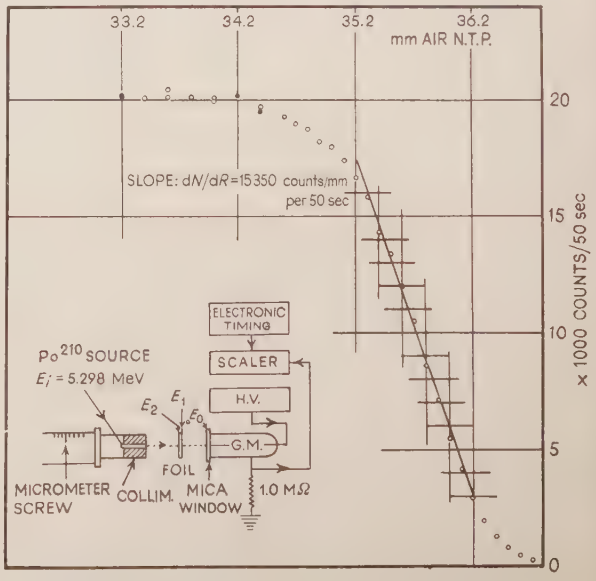

Fig. 1

The alpha gauge consists of a 40 microcurie Po^{210} alpha-source, electro-deposited on a 2 mm diameter dimple in a thin silver disc and covered with a layer of about 10 $\mu g/cm^2$ of VYNS (polyvinyl chloride acetate copolymer) foil[4]), a

† Supplied by Geo. M. Whiley, Victoria Road, Ruislip, Middlesex, England.

†† Supplied by Chromium Corporation of America, Waterbury 20, Conn. U.S.A.

[4]) B. D. Pate and L. Yaffe, Canad. J. Chem. 33 (1955) 15–23.

collimator forming a solid angle of 8×10^{-3} steradians, a Geiger-Muller tube† type MX 113 with a mica window of approximately 2 mg/cm² and a micrometer screw with a resolution of 10^{-3} cm (fig. 1). The strong collimation ensures that the collection of all alpha particles emitted within the solid angle is independent of the position of the micrometer screw. Table 1 shows the minimum thickness of metals which can be measured with the resolution of the micrometer only. The resolution is in fact much greater when one operates on the steep slope.

TABLE 1

Foil thickness equivalent to 10^{-3} cm of dry air.
$\varrho_A = 1.225$ mg·cm^{-3}

Metal	μg·cm^{-2}
Al	1.58
Ni	2.14
Ag	2.96
Au	4.14

A 1.0 megohm resistor is connected between the cathode of the Geiger-Muller tube and earth so that a positive signal is taken to a type 1009A scaler. An electronic timer selects time intervals of 50 sec or more in order to keep the random errors due to counting below 1 per cent.

density was used in conjunction with Bethe's[5]) data on ranges of alpha particles in air—to calculate the energy E_1 of the alpha particle leaving the foil. E_2, the energy of the alpha particles entering the foil, varied according to foil thickness and material. The average energy E_{av} at which values of C_m are reported was taken as:

$$E_{av} = \frac{1}{N} \sum \tfrac{1}{2} (E_1 + E_2)$$

where N is the number of measurements taken for this calculation.

The surface density of the foil as deduced from alpha gauge measurements is:

Surface density =

$$\rho dX = \frac{1}{C_m} \left\{ \Delta R + \frac{\Delta N}{\partial N / \partial R} \right\} \rho_A \text{ gm·cm}^{-2} \qquad (2)$$

where C_m is the mass stopping power relative to air, ΔR the distance travelled by micrometer screw, $\Delta N = N_1 - N_2$ where N_1 and N_2 are counts in the GM counter without and with foil respectively, $\partial N/\partial R$ the slope of the number distance curve of alpha particles in air, the operating point being the maximum value of this slope and ρ_A the density of air corrected for temperature, pressure and humidity.

The calibration of the alpha gauge yielded

TABLE 2

Metal	C_m	Standard error	C_m*	Standard error
Al	0.777	± 1.8%	0.806	± 2.9%
Ni	0.573	± 1.2%	0.585	± 1.4%
Ag	0.415	± 1.5%	0.439	± 1.7%
Au	0.296	± 2.3%	0.306	± 2.7%

3. Results

C_m was determined at 3.72 and 4.33 MeV kinetic energy of the alpha particles. These energies which are averages of all measurements were deduced in the following way: The distance between source and the plane of the foil was conveniently measured by help of the alpha gauge micrometer. The average of the product of these distances times the instantaneous air the stopping powers for alpha particles relative to air at 3.72 and 4.33 MeV. Table 2 summarises the results of 662 measurements for C_m at $E = 3.72$ MeV and of 240 measurements for C_m* at $E = 4.33$ MeV.

An attempt was also made to establish a semi-empirical rule which would enable one to obtain the approximate surface density of a metal for which the alpha gauge has not been

† Mullard Ltd.

[5]) H. A. Bethe, Revs. Mod. Phys. **21** (1950) 213.

calibrated. This could be useful in nuclear physics experiments which do not require a highly accurate knowledge of surface density. We use an expression established by Lindhard and Scharff[6]) who applied dimensional arguments to the Fermi-Thomas model of the atom and by plotting the quantity

$$L(x) = \{mv^2/(4\pi e^2 Z)\}\cdot \mathrm{d}E/\mathrm{d}X \qquad (3)$$

against the parameter

$$x = (v/v_0)^2 \cdot 1/Z$$

they found that experimental data for the stopping power of protons and alpha particles lie on a single curve. In eq. (3) m is the electronic rest mass, Z the atomic number of the absorber, v the velocity of the moving ion and v_0 the Bohr orbit velocity.

At low energies they deduce the relation

$$L(x) = 1.36\, x^{\frac{1}{2}} - 0.016\, x^{\frac{3}{2}} \qquad (4)$$

valid for

$$0.2 \lesssim x \lesssim 5\,.$$

From eq. (4) one can easily obtain the mass stopping power, C_m of a substance relative to air

$$C_\mathrm{m} = \frac{A_1}{A_2}\left(\frac{Z_2}{Z_1}\right)^{\frac{1}{2}} \frac{1 - 0.01176\, x_2}{1 - 0.01176\, x_1} \qquad (5)$$

where A is the mass number and subscripts 1, 2 refer to air and metal respectively. C_m was calculated using relations (5) and is presented in table 3.

The last column of the table lists values of C_m obtained from an empirical rule

$$C_\mathrm{m} = (Z_1/Z_2)^{\frac{1}{2}} \qquad (6)$$

which, at $E = 3.72$ MeV, is seen to yield relative mass stopping powers in fair agreement with experiment.

The fourth column tabulates C_m data as obtained by multiplying eq. (5) by a factor 1.131. It is seen that except in Al—where the statistical model of the atom is not strictly applicable—corrected values of C_m are in close agreement with our experimental data. The correction factor may arise from the fact C_m in our calculations involves a ratio of stopping powers of solid and gaseous substances. Brolley and Ribe[7]) who measured the stopping power of gases for protons and deuterons obtained results of similar trends. They plotted values of $L(x)$ versus (x) for gaseous obsorbers and showed that their points lie on a single curve, which for low values of x falls below a similar curve constructed from data on the stopping power for protons in solids.

The good agreement between the experimental and calculated data (multiplied by the correction factor) suggests a way of obtaining foil surface densities of materials for which the alpha gauge has not been calibrated.

TABLE 3

Values of C_m at $E_\alpha = 3.72$ MeV

Element	C_m (exp.)	C_m (eq. (5))	$1.131 \times C_\mathrm{m}$ (eq. (5))	C_m (eq. (6))
Al	0.777	0.751	(0.849)	0.745
Ni	0.575	0.510	0.576	0.508
Ag	0.415	0.366	0.414	0.392
Au	0.296	0.261	0.296	0.303

Acknowledgments

The authors wish to express their thanks to Professor S. Devons, F.R.S., for his interest, to Dr. A. A. Jaffe for a helpful discussion, and to the University of Manchester and A.E.R.E. Harwell for their support.

[6]) J. Lindhard and M. Scharff, Mat. Fys. Medd. Dan. Vid. Selsk. 27, No. 15 (1953).

[7]) J. E. Brolley and F. L. Ribe, Phys. Rev. 98 (1955) 1112.

NUCLEAR INSTRUMENTS AND METHODS 4 (1959) 243; NORTH-HOLLAND PUBLISHING CO.

LETTER TO THE EDITOR

REGULARIZING ACTION OF SCALERS

J. SANDSTAD

Institute of Physics, University of Oslo, Norway

Received 8 April 1959

Pryor and Klein[1]) have computed the regularizing action of a fast scaler preceding a slow one.

Some time ago I made similar computations, and with the same general result, except for the factor K in the expression for the fraction of input pulses that are lost due to the dead time of the slow scaler. The factor is introduced with the following argument (loc. cit. p. 2): "Since the loss of one output pulse corresponds to the loss of K input pulses, the fraction of input pulses that are not detected will be

$$X = KQ_K(Nt)\,, \qquad \text{i.e.} \qquad NKQ_K(Nt) = NX$$

counts will be lost per second."

Because the average rate of pulses to the slow scaler will be N/K, one pulse that is lost, as well as one pulse which is detected, corresponds to K input pulses. Consequently the factor K drops out of the expression for the relative counting loss, which for small counting losses will be approximately:

$$X = Q_K(Nt) = 1 - \sum_{m=0}^{K-1} \frac{e^{-Nt}\,(Nt)^m}{m!}\,.$$

(If a pulse that is lost in the slow scaler, dont give any extension of the dead time, then the following pulse will have an increased probability of being detected. The real counting loss will therefore be smaller than computed from the above formula, which may be used as an approximation for counting losses up to about 10%.)

Fig. 1 shows the results of numerical computations for different scale factors.

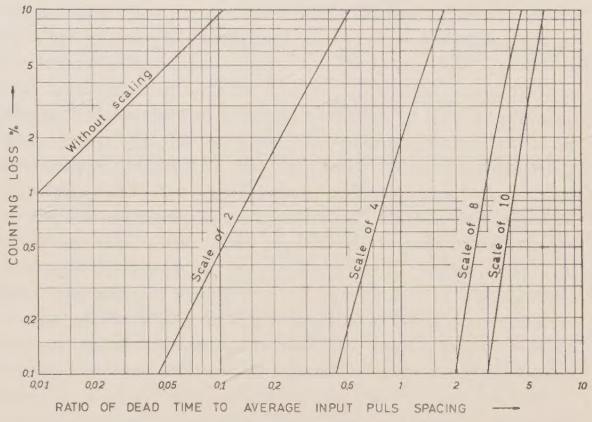

Fig. 1

A counting loss of 0.1% in a scaler preceded by a very fast scale of 10, corresponds to a ratio of dead time to average input pulse spacing of about 2.95 (instead of 2.2 as computed by Pryor and Klein, and used in their numerical examples).

[1]) A. W. Pryor and A. G. Klein, Nuclear Instruments 4 (1959) 2.

ERRATUM

Berichtigung zu: "Eine Apparatur zur Messung der longitudinalen Elektronenpolarisation durch Mott-Streuung" von H. Bienlein *et al.* in Nuclear Instruments 4 (1959) 79.

Die Arbeit enthält einige Druckfehler. Die letzte Zeile der Formel (16) muss heissen:

$$\frac{1 + < S_{Au}\,[\boldsymbol{p}\cdot(\boldsymbol{t}_0 \times \boldsymbol{t}_2)]/\sqrt{1-\xi_2^2} >_2}{1 + < S_{Au}\,[\boldsymbol{p}\cdot(\boldsymbol{t}_0 \times \boldsymbol{t}_1)]/\sqrt{1-\xi_1^2} >_1}.$$

Das Differential $d\Omega$ (1) aus (27) ist zu ersetzen durch $d\Omega(\boldsymbol{t})$. Die vorletzte Klammer $\left(\frac{1}{1-\beta^{\frac{3}{2}}}\right)$ in Formel (30) lautet richtig: $\frac{1}{(1-\frac{1}{2}\beta^2)}$.

BOOK REVIEW

Encyclopedia of Physics, Editor S. FLÜGGE, Volume XL, *Nuclear Reactions I*. Springer-Verlag. DM 128,—

This volume contains four contributions together covering various aspects of nuclear reactions in the more conventional sense, i.e. nuclear reactions caused by charged particles, neutrons and high energy photons. W. E. Burcham (*Nuclear Reactions Levels and Spectra of Light Nuclei*) starts with a brief account of known facts about nuclear forces. Short reviews are given of the nuclear models used for the interpretation of the level schemes of light nuclei. In the following section, the theoretical aspects of nuclear reactions are discussed. A fairly detailed account of experimental methods is given in the third section, this includes studies of radiative transitions from excited states such as measurements of lifetimes of excited states. Coulomb excitation, determination of internal conversion coefficients and angular correlations. In the last two sections, the author has given a comprehensive review of experimental results (up to July 1955) on nuclear reactions in light nuclei. The experimental evidence obtained is summarized in the energy level schemes divided into odd isobars, even isobars of mass 4 n + 2 and even isobars of mass 4 n. More than 100 level schemes are discussed and references are given to current theoretical interpretations.

The second contribution to this volume by B. B. Kinsey (*Nuclear reactions, Levels and Spectra of Heavy Nuclei*) starts with a survey of the theory of compound nucleus formation including direct interactions and the optical model. The following sections are devoted to statistical theory of nuclear reactions direct interactions and the various types of nuclear reactions in heavier nuclei due to charged particles, neutrons and photonuclear effects. Finally, in the last four sections the author presents a systematics of low energy levels. The nuclei are divided into three distinct groups namely deformed nuclei with $N > 90$, nuclei near closed shells and nuclei with $N < 90$. These sections cover a wide variety of subjects, these include the collective model, the Nilsson (not Nillson) model, refinements of the nuclear shell model as well as systematics of alpha-activities and experimental methods like Coulomb-excitation and resonance scattering. These subjects seem to be fairly loosely related to the topics discussed in the first 12 sections. Furthermore, since the last sections to a great extent overlap contributions given in other volumes of the Encyclopedia it would probably have been better to exclude these sections in favour of a more detailed discussion of the experimental techniques used for the study of nuclear reactions. The author has given only brief accounts of experimental methods and instruments though numerous references are given to papers and review articles where the experimental details may be found.

Professor Rainwater's chapter (*Resonance Processes by Neutrons*) begins with a brief survey of various experimental methods for neutron spectroscopy. The importance of high resolution is emphasized. The author shows that experiments with poor resolution can be very misleading. The great achievements in the experimental techniques in recent years is dramatically illustrated. Experimentally determined resonance parameters of nuclei are summarized in an extensive table. In the second half, the theoretical interpretation of the experimental material is discussed by starting with an elementary derivation of the Breit-Wigner one level formula and the Wigner-Eisenbud formalism. Finally, the optical model for scattering (Feshbach, Porter and Weisskopf) and the giant resonance interpretation due to Lane, Thomas and Wigner is discussed. In a note added in the proof, references are given to important results recently obtained by Brueckner *et al.*

The last contribution is written by Albert Wattenberg (*Nuclear Reactions at High Energies*). An attractive feature of Wattenberg's paper is the stimulating general survey of high energy (above 50 MeV) nuclear reactions given in the introduction to his chapter. The author reviews the possibilities to obtain experimental information on some old problems in nuclear physics by making use of high energy nucleons now available in the laboratory, e.g. problems like energy dependence of nuclear forces, the existance, or non-existence, of many-body forces and the saturation of nuclear forces in complex nuclei. By direct quotations from Serber's paper, a very simple picture of the basic principles of high energy nuclear reactions is sketched. In the following sections, a more quantitative analysis is given. The experimental methods are discussed in three sections which deal with high energy machines, sources of particles and detection techniques. An interesting comparison of photographic emulsions, bubble chambers and cloud chambers of different types is given. The experimental results obtained on nucleon reactions are presented. A special section deals with the work on high energy electrons by Hofstadter and his associates at Stanford. Finally, X-ray scattering and photonuclear reactions are reviewed. The last section, dealing with meson-reactions, is, of course, already greatly outdated due to the rapid development in this field.

TOR RAGNAR GERHOLM

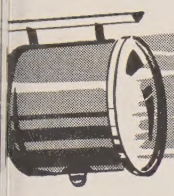

Spotlight on Industry

This section appears each month and features various happenings of interest in the nuclear industrial world and objective information on products of the nuclear manufacturers. It is offered entirely as a service and all nuclear manufacturers are cordially invited to submit clearly objective and descriptive material on their endeavours and product developments for consideration for use in this section.

TAYLOR MULTIRANGE UNIVERSAL METER MODEL 100 A

Tayloy Electrical Instruments, Ltd., Montrose Avenue, Slough, England

Sensitivity

100 000 ohms per volt DC. 5 000 ohms per volt AC.

Ranges

Volts DC 0.5, 2.5, 10, 25, 100, 250, 1 000, 2 500 V (25 000 volts by means of an external adaptor—Model 400).

Volts AC: 10. 25, 100, 250, 1 000, 2 500 V.

DC Current: 10μA, 50μA, 250μA, 1 mA, 100 mA, 1 A, 10 A.

Ohms: 0–2 000 ohms (20 Ω centre scale); 0–200 kΩ (2 000 Ω centre scale); 0–20 MΩ (200 kΩ centre scale); 0–200 MΩ (2M Ω centre scale). All the resistance ranges are with self-contained batteries.

Decible Ranges: —10 db to +15 db (reference level 6 mW in 500 ohms); —2 db to +23 db; +10 db to +35 db; +18 db to +43 db; +30 db to +55 db.

Output Ranges: 0–10 V; 0–25 V; 0–100 V; 0–250 V; 0–1000 V.

Accuracy

DC ranges 2% of Full Scale Deflection. AC ranges 3% of Full Scale Deflection. Ohms ranges 5% Centre Scale.

Meter. The instrument incorporates a 8 μA Moving Coil Taylor Centre Pole Meter precision engineered for reliability and accuracy. It is also inherently magnetically shielded and can withstand a momentary overload of up to 10 000%. The meter is fitted with a Knife-Edge Pointer.

Scale. The scale is 5″ long clearly marked in three colours to facilitate easy reference and maximum readability. An anti-parallax mirror arc is incorporated for better reading accuracy.

AN ELECTRONIC VOLTMETER WITH HIGH IMPUT IMPEDANCE AND BROAD FREQUENCY RANGE

Metronix, Inc., Chesterland, Ohio

Input impedance of 5 megohms, paralleled by 25 micro-microfarads, is several times the customary level for PMEV's. This feature enlarges the special ability of such instruments to measure voltage without loading the circuit being metered.

Frequency range of Model 311 is 20 cps to 250 kc/s, extending approximately 150 kc/s higher than that of previous models. Accuracy is plus or minus 2 per cent of full scale deflection over the whole frequency range.

A multi-voltage-range instrument, Model 311 is comparatively unaffected by line voltage variations. A change of plus or minus 10 per cent in the line voltage causes a readout error of no more than 1 per cent of full scale deflection.

Full scale sensitivity begins at 10 millivolts and goes up to 300 volts r.m.s.

The large 6-inch meter provides easy readability and the built-in power supply makes the instrument self-contained.

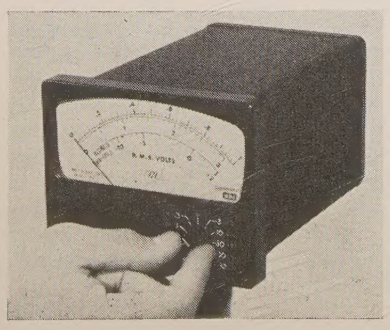

URANIUM AND THORIUM FOIL

M & C Nuclear, Inc., P.O. Box 898, Attleboro, Massachusetts, U.S.A.

Typical specifications

Continuous coils of thin gauge are available in lengths of hundreds of feet.

Camber (slit to width) 0.013″ in any 12″ of length.

Camber (blanked to 24″) 0.004″ in any 12″ of length.

Flatness to suit individual requirements.

Foil may be 100% coated with a plastic meeting nuclear requirements in coating thicknesses from 0.0002″ to 0.0005″ for corrosion protection and health physics purposes.

Enriched, normal and depleted uranium, thorium, and special materials such as Reactor Grade Zircaloy II are available in the following dimensions:

Thickness
0.0005 to 0.0029 ± 0.0002″
0.003 to 0.0069 ± 0.0003″
0.007 to 0.0099 ± 0.0004″
0.010 to 0.0149 ± 0.0007″

Width
0.1875 to 8.000 ± 0.005″
0.1875 to 8.000 ± 0.005″
0.1875 to 8.000 ± 0.005″
0.1875 to 8.000 ± 0.005″

Length
1 to 12 feet ± 0.1875″
1.00″ to 12.00″ ± 0.031″

ACCURATE LIQUID LEVEL MEASUREMENT

Sunvic Controls, Ltd., Crown House, Aldwych, London, W.C. 2.

Five different types of constant differential relay made by Sunvic Controls Ltd., Harlow, Essex, are now available with built-in variable area flow meter (Rotameter) and needle valve. These relays can be used to ensure a constant bubbling rate of purging air or gas in air reaction systems for liquid level measurement.

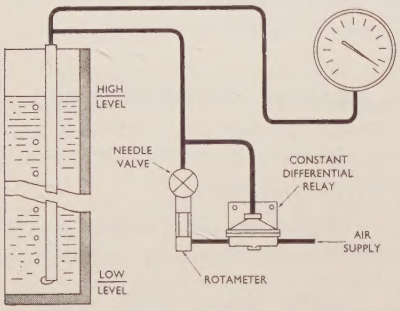

Highly precise flow control of the purge medium is necessary if measurement accuracy is not to be affected by variations in bubble size or by variable kinetic heads across the dip tube. Sunvic model 62A and 63A series relays meet this requirement. They enable flow rates to be regulated accurately within wide limits simply by adjustment of the needle valve.

No liquid whatsoever is used in the purge flow controller and so no maintenance is required. An accurate flow meter, with easily read calibrations is provided. The unit is rated at 50 p.s.i. static pressure and tested at 100 p.s.i. static pressure.

Model 62A relays uses a high-precision bleed-type regulator which has the advantage of releasing any surge from downstream. The body is of brass with neoprene diaphragm and stainless steel valve and spring.

Model 63A relays are non-bleed type and are therefore ideal for use with liquids as well as expensive purge media such as helium or CO_2 or with inflammable gases. Two versions are available: one for use when up-stream pressure can be held constant, one for constant downstream pressure. Construction materials are as for Model 62A. Both versions are also available in a stainless steel body with Teflon diaphragm.

MODEL CS-11 CURRENT GOVERNOR

Ad. Auriema, Inc., Exporters, 85 Broad Street, New York, 4 N.Y., U.S.A.

An unique programmable constant current source of unusual accuracy and stability has been introduced by North Hills Electric Co., Inc. Designed especially for supplying ultra stable precision current, the Model CS-11 Current Governor furnishes currents from 1 μA to 100 mA in steps of 1 μA at load voltages from zero to 50 volts.

Current is set to five places by decade knobs arranged to provide a digital inline readout. Accuracy at any current setting is 0.02% + 0.1 μA short term stability 0.001%, line regulation is better than 0.0005%, and load regulation better than 0.002%.

The CS-11 Current Governor is ideal as a gyro torquer current source which may be programmed by a command signal.

COIL WINDING MACHINE

Avo Limited, Avocet House, 92-96 Vauxhall Bridge Road, London, S.W. 1

An entirely new Coil Winding Machine, is announced which is capable of winding almost perfect layer wound coils without the use of any medium of interleaving. The normal mechanical coupling between the headstock and the traverse of the Machine has been dispensed with and both are driven by independent motors, whose relative speeds are electronically controlled by a sensing head which monitors the wirefeed angle so as to ensure that as far as practicable each turn is laid precisely beside the preceeding turn. The greatly improved space factor of coils produced by this machine ensures maximum electro-magnetic efficiency—a factor of particular importance for such components as relays and solenoids, especially the miniature types, whilst the far more precise rectilinear configuration of coils thus wound, opens up many possibilities of the use of self-supporting coils where formers were previously necessary.

NEW CARBON-14 TRITIUM COUNTING SYSTEM

Baird-Atomic, Inc. 33 University RD., Cambridge 38, Mass.

A new carbon-14 and tritium liquid scintillation counting system was presented. With the combination of a compact Detector, B-A Model 845, and a specially developed ultra-high speed Amplifier, B-A Model 245 counting system can be assembled.

Exhaustive tests have shown that this new instrumentation system is accurate with or without a freezer, and is capable of performing the most sensitive C^{14} and H^3 counts with speed and precision.

Also included in the system are an advanced optical system which features coated optics and a double shutter system that eliminates all ambient light. "Metalvial" container was designed for optimum photon conservation, minimum fluorescense and maximum blue transmission. Triple shielding keeps all background interference at a minimum.

The use of a freezer is optional. It can be operated successfully at room temperature with high detection efficiency.

13-CHANNEL PROGRAMER

Ad. Auriema, Inc., 85 Broad Street, New York 4, N.Y.

A new 13-channel tape Programer, the MLPR-13, is announced by Beattie-Coleman Inc. The new model has tape storage capacity, up to 160 feet of 35 mm Mylar tape, giving a program duration of 10.6 min at a transport speed of 3″ per second.

The MLPR-13 is an electro-mechanical device designed to control up to 13 functions at precisely timed intervals. It operates by providing electrical pulses at pre-determined, controlled intervals through 13 independent channels. A sensing device reads pulses through slots punched in a 35 mm insulating tape (Mylar) which is drawn past the sensing device.

Operating from 151 V 400 cycle current, the entire unit is housed in a dust proof metal case, only 8″ long, 5″ high and 3″ deep. It weighs less than 5 lbs. and is easily removed from panel for loading.